Design of a Helicopter Hover Test Stand

A Major Qualifying Project Report
Submitted to the Faculty of the
WORCESTER POLYTECHNIC INSTITUTE
in Partial Fulfillment of the Requirements for the
Degree of Bachelor Science
in Aerospace Engineering

by

Bror Axelsson

Jay Fulmer

Jonathan Labrie

March 6, 2015

Approved by:

Professor Maria Chierichetti, Advisor
Aerospace Engineering Program
Aerospace Engineering Department, WPI

Professor Anthony B. Linn, Co-Advisor
Aerospace Engineering Program
Aerospace Engineering Department, WPI

Abstract

The development of helicopter test stands allows for the testing and improvement of various components of helicopter rotor head and blade designs. The goal of this project is to design, build, and test a fully articulated helicopter rotor head system for future implementation on a hover test stand. The stand will be used to measure the forces and moments at the blade roots and the strain along the blades. The design of the rotor head is modular, allowing for the type and number of blades to be changed as desired without major disassembly of the test stand. The design is based on a fully articulated, four bladed rotor head with a custom fabricated swashplate and driveshaft. Additionally, a safety system was designed to ensure the safe operation of the hover test stand and protect the users in the case of failure at maximum rotor speed. The recommended data acquisition system for measuring stresses and strains is a light based system that uses fiber optic technology to accurately collect and transmit data from the rotating blades to data analysis equipment in the stationary frame.

Authorship

Section	Primary Author
Abstract	Bror
Chapter 1: Introduction	Bror
Chapter 2: Background	Jay
2.1 Rotor Test Stands	Jon
2.1.1 Principles of Operations	Jon
2.1.2 Scaling	Jay
2.2 Helicopter Rotor Head Systems	Bror
2.2.1 Flybar Rotor Heads	Bror
2.2.2 Solid Articulated Rotor Heads	Bror
2.2.3 Fully Articulated Rotor Heads	Bror
2.2.4 Bearingless Rotor Heads	Bror
2.2.5 Hinges and forces	Bror
2.3 Motor and Motor Drives	Jon
2.3.1 Alternating Current (AC) Motor	Jon
2.3.2 Direct Current (DC) Motor	Jon
	Jay
2.4.1 Slip Rings	Jay
2.4.2 Wireless Sensors	Jay
2.4.3 Wireless Data Acquisition	Jay
2.4.4 Fiber Optics	Jay
2.4.5 Bragg Grating	Jay
Chapter 3: Methodology	Jay
3.1 Hover Test Stand Design	Bror
3.1.1 Design Specifications	Bror
3.1.2 Test Stand Design	Jay
3.1.3 Engine Design	Jon
3.1.4 Engine Mount and Belt Tensioner	Jay
3.1.5 Power Transfer System	Jay
3.1.6 Driveshaft Design	Jon
3.1.7 Driveshaft Analysis	Jon
3.1.8 Support Bearing Design	Jay

Table of Contents

Table of Figures

Table of Tables

Chapter 1: Introduction

The development of helicopter test stands for industry and academia allows for the testing and development of various components of rotor heads. This is important because full scale flight testing is expensive and dangerous when unproven designs are being evaluated. The test stand gets around this by, in most cases, using scale models in a controlled environment to test quantities of interest. This is beneficial because scaled testing significantly reduces cost and improves safety.

The goal of this project is to design, build, and test a helicopter rotor head test stand that can be used to simulate hovering situations. The primary function of the test stand is to measure the forces and moments at the blade roots and the strain along the blades for new blade designs. Other functions can include, but are not limited to, the testing of new rotor hub systems, control optimization, vibrations testing, and structural dynamic studies.

This projects rotor head is scaled down from a full sized helicopter in order to fit in a lab on the Worcester Polytechnic Institute (WPI) campus. It is modular and interchangeable, allowing for the number and type of blades to be modified as desired. The users could therefore test different numbers of blades and configurations without major disassembly of the test stand. Additionally, a preliminary safety system was designed to ensure the safe operation of the test stand and protect the users in the case of failure.

The test stand is designed to accept any type of rotor head as well as any number of rotor blades. This would be accomplished through the design of new rotor heads. Our design will incorporate a fully articulated, 4 bladed rotor head. This allows the rotor head to accurately simulate the response of the blades to a wide range of control inputs. The inputs include the full range of cyclic and collective control inputs that would be available on a full sized helicopter.

The stand is powered by an electric motor that is controlled by a variable frequency drive (VFD). This allows for variable rotational speeds which are required in order to successfully scale different rotor head and blade number combinations.

Measurement of the forces on the rotor head will be accomplished via a data acquisition system capable of measuring strains at multiple points along each blade. The data acquisition system for measuring stresses and strains is a light based system that uses fiber optic technology to accurately collect and transmit data from the rotating blades to data analysis equipment located in the stationary frame. The design is such that adaptions can be made to the data acquisition system for the analysis of different components without major modifications.

.

Chapter 2: Background

2.1 Rotor Test Stands

This section discusses the background research we preformed to obtain a higher understanding of the designs and the mechanics behind current helicopter rotor test stands. It details specifications of other test stands and provides information on rotor head scaling. It goes into the different types of rotor heads and motors as well as various types of data acquisition and transfer systems.

2.1.1 Principles of Operations

Prior helicopter test stand designs were used to perform various tests, including blade balancing, blade de-icing, and verification of experimental blade designs. They range in size from full scale models such as the Sikorsky Bi-Directional Whirl Tower to small scale models that have rotor diameters comparable to model radio controlled helicopters (Sikorsky, 2012). Since preliminary testing of new rotor head designs and new main and tail blade designs on a full scale helicopter is generally impractical and dangerous, helicopter test stands are used to achieve comparable results without endangering an entire helicopter and its crew at a much lower cost. Components common to nearly all documented test stands included a safety enclosure system, a stand to elevate the rotor system, and an electric drive motor.

Most safety system designs utilized either a solid wall enclosure, net, or metal curtain to contain potential projectiles. Some enclosures, especially the AERTS Penn State test stand, are designed to simulate extreme flight conditions. The Penn State facility features internal spray nozzles which create icing clouds which produces ice buildup on the spinning blades, allowing researchers to develop effective countermeasures (Palacios).

Each rotor hub is attached to an elevated stand in the center of the safety enclosure. The distance from the ground helps create a more realistic hovering situation by reducing ground effects. Ground effects occur when a helicopter is close to the ground, where a larger thrust is produced because the induced air velocity pushes against solid ground instead of ambient air creating a cushioning effect. A publication by the US Army noted that a test stand was within the ground effect region when the rotor head is at 0.78 times the rotor diameter above the ground (Fulton, Gold, Nielsen, Mansur, & Tischler, 2012). Because of this most test stands position the rotor blades between 1 and 1.5 times the rotor diameter above the ground to overcome ground effects.

To power the rotor head, each researched test stand used an electric motor. The types of motors used included AC, DC brushless, and DC permanent magnet. Motor size varied greatly due to the range of rotor diameter sizes used. Even the test stands closest to our application of approximately one meter in diameter had a large range in motor size. For example, a 1.0m rotor diameter was powered by a 9 kW (12 hp) motor, while an approximately 1.5 m diameter rotor was powered by a 2kw (2.7 hp) motor (Lee, Byun, Kim, & Kang, 2011; Sirohi & Lawson, 2012).

For stands which measured stress and strain along the blades, data transfer from the rotating system to the stationary frame was performed by a slip ring (Palacios; UM Aerospace Engineering, 2014). Slip rings and their function are explained in section 2.4.1. While investigating highly flexible blades, the test stand at the University of Texas at Austin used a system of cameras and lasers to measure blade characteristics (Sicard & Sirohi, 2013).

2.1.2 Scaling

Importance

Full scale helicopters have large rotor diameters, denoted as δ, which allow them to produce significant lift at relatively low rotor speeds. For example, for the Blackhawk family of military helicopters, δ is equal to 16.36m (53.67ft) (Leishman, 2006). The Bell 206 Jetranger, a common corporate helicopter, has a δ equal to 11.28m (37.1ft) (Leishman, 2006). In both these cases, the rotor diameter is far too large for small scale lab use. This means that for rotor head and blade designs to be tested in a small lab, both the size and rotor speeds must be scaled appropriately. It is also important to note that scaling a rotor head down reduces the power required to spin the blades to a level that can be achieved with a common electric motor and electrical supply. Scaling therefore significantly reduces the mechanical complexity of the rotor head as well as the required maintenance through the elimination of complex power systems and the overall reduction in the total number of parts. Additionally, the reduction in mechanical complexity provides flexibility for rapid blade and main hub modifications or changes.

Six Parameters for Scaling

When scaling a rotor head there are six important parameters which must be scaled using appropriate scaling factors. Lambda, equivalent to $\lambda = \frac{Model\ Value}{Full\ Scale\ Value}$, represents the ratio of characteristic length between the model and full scale helicopter rotor. The six parameters to be scaled are Reynolds number, Mach number, the Froude number, two force ratios, and the advance ratio, as displayed in Table 1. Another important parameter not included is the rotor speed, measured in revolutions per minute (rpm) (Cansdale, 1974).

The Froude number, $\frac{V^2}{g\delta}$, is a dimensionless ratio that relates the centrifugal force to the force of gravity. The force ratios $\frac{\rho}{c}$ and $\frac{E}{\rho V^2}$ are material matching equations that relate the density of air to the material density of the blades and the elastic modulus of the blades to the dynamic viscosity of air respectively. Finally, the advance ratio $J = \frac{V}{\Omega\delta}$ relates the forward velocity of the aircraft to the tangential tip speed of the blades (Cansdale, 1974).

Table 1: Parameters Required for Helicopter Scaling (Cansdale, 1974)

Scaled Parameter	***Units***	***Amount Scaled***
Reynolds number	$\frac{\rho V_{forward}\delta}{\mu}$	$\lambda^{3/2}$
Mach number	$\frac{V_i}{a}$	$\sqrt{\lambda}$
Froude number	$\frac{{V_{forward}}^2}{g\delta}$	1
Force Ratio 1	$\frac{\rho}{c}$	λ^3
Force Ratio 2	$\frac{E}{\rho {V_i}^2}$	λ^3
Advance Ratio	$\frac{V_{forward}}{\Omega\delta}$	
Rotational Speed	Ω	$\frac{1}{\sqrt{\lambda}}$

Hovering vs. Forward Flight

The Froude number, advance ratio and Reynolds number can be disregarded in the considered design because the test stand simulates a helicopter in a hovering situation, for which the forward velocity V is zero. The Mach is number accounted for due to the fact that it is a

function of the rotor speed, measured in rpms, which is also being scaled. The force ratios can also be disregarded because the blades that will be tested are not scale models of current helicopter blades, meaning that the materials for the scaled blades do not need to have the same material characteristics. The final parameter that needs to be scaled is the rotating speed of the rotor. This is scaled by a factor of one over the square root of the scaling factor. This leads to the equation $\Omega_{scaled} = \Omega_{full} \frac{1}{\sqrt{\lambda}}$ giving the required rotor speed as an angular velocity, Ω_{scaled}. Table 2 has a number of sample scaled rotor speeds and the scaling factors for a scale test stand with a rotor diameter of 1.2m (3.94ft) (Cansdale, 1974).

Table 2: Rotor RPM of an H-60 and a JetRanger Scaled 1.2 m Rotor Diameter

Full Scale Helicopter	*Full Scale Rotational Rate (RPMs)*	*Scaling Factor*	*Scaled Rotational Rate (RPM)*
H-60 Hawk series	258.000	0.073	952.3
Bell JetRanger	400.000	0.113	1189.4

Based on the data in Table 2, the test stand will be designed to rotate at a maximum rotational velocity of 1500 revolutions per minute.

2.2 Helicopter Rotor Head Systems

In order to replicate the blade dynamics of a full scale helicopter the design of the rotor head is paramount. Helicopter rotor heads are complex mechanical systems which serve many simultaneous purposes. These include rotating the blades, adjusting the blade pitch, and executing control inputs from the pilot. The rotor head and swashplate system to use a full range of cyclic and collective controls. Collective control move the swashplate up and down, which increases and decreases pitch equally for all of the blades. Increasing the collective increases the angle of attach of the rotor blades which generates more lift. Cyclic controls tilt the swashplate, which changes the blade pitch at specific locations round the rotor head. This creates a dissymmetry of lift, causing the helicopter to pitch away from the high lift side.

During a hovering situation fine adjustments of the collective and cyclic controls are required to maintain precise and stabile hover. For our rotor head system, we selected to uses a swashplate and rotor head that enables complete cyclic and collective control. This allows the test stand to better model real world conditions. Several of the reasons for including cyclic and collective controls are the ability to replicate multiple hovering situations and the possibility of forward flight testing in the future.

After choosing a rotor head that allows a full range of control inputs the design parameters were further narrowed through the selection of a specific type of rotor head. There are a number of different types of rotor heads, however the most common designs are flybar which are used on small helicopters, solid articulated or hinge-less which are used on most large modern helicopters, and fully articulated which due to mechanical complexity at large scales have become uncommon (Leishman, 2006).

2.2.1 Flybar Rotor Heads

Flybar rotor head designs employ weighted flybars which act like gyroscopes, stabilizing the rotor. As the relative momentums of the flybar and blades change, the pitch of the blades also changes, stabilizing the helicopter in flight regardless of attitude. This means that the blade pitch is passively controlled, rather than actively controlled by the pilot. It doesn't mean the pilot has no control over the pitch, it means that instead of direct control of the rotor blade pitch the pilot has control of the flybar. By changing the flybars pitch the pitch of the blades are changed giving the pilot control over the aircraft. Additionally, in the case of a model helicopter the flybar dampens the inputs from the swashplate controls and reduces the forces that servo motors need to apply. The main advantage of a flybar rotor head in a model helicopter is stability, especially when electronic stability control is undesirable or impractical. Most flybar systems do not require onboard accelerometers and electronic stability control.

Figure 1: This figure depicts a Flybar Rotor Head (Salt, 2014)

2.2.2 Solid Articulated Rotor Heads

Solid articulated rotor heads allow active control of the blade pitch via the use of a feathering hinge and swashplate controls. Solid articulated heads do not have flapping hinges, because of this the blades need to include damping rods to absorb the forces and moments that would normally be dissipated by a flapping hinge. The majority of model helicopter rotor heads

are solid articulated rotor heads since the blades are typically very flexible and the applied loads are relatively low.

2.2.3 Fully Articulated Rotor Heads

The third common type of rotor head is a fully articulated rotor head. Very similar to the solid articulated rotor, the fully articulated design includes a flapping hinge, lead-lag hinge, and feathering hinge. This design is the most complex, allowing the blades a full range of motion based on the applied cyclic and collective controls.

Utilizing the collective controls, the pitch of all the blades can be simultaneously changed. As the swashplates moves along the main shaft, the pitch of the blades is adjusted by pivoting about the feathering hinge, increasing or decreasing the angle of attack of the blades collectively. Cyclic control follows a similar process except that pitch of the blades are adjusted only at specific locations around the rotor head.

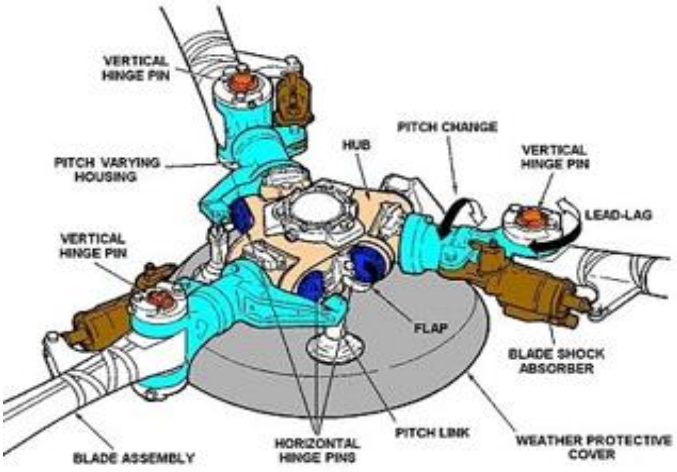

Figure 2: A Fully Articulated Rotor Head (Lewis & Darbo, 2006)

2.2.4 Bearingless Rotor Heads

Bearingless rotor head designs do not utilize hinges, like the previous examples. Rather, bearingless rotor heads are mechanically the simplest rotor head design. Instead of incorporating

lead-lag, flapping, and feathering hinges, the blade is attached to a flexible root which allows the blade to articulate. Different dampers within the root perform the same functions the hinges would perform on a fully articulated rotor head design.

2.2.5 Hinges and forces

The various rotor head designs incorporate different types of hinges and pins which allow different levels of articulation. When a helicopter is flying, it is subject to a number of different forces, which include active forces from the pilot's controls and passive forces from the surrounding environment. In addition, these hinges also mitigate the forces applied to the blade roots by allowing the blades to passively articulate based on the lift, drag, and centrifugal forces acting on them.

Coning

When a helicopter rotor is spinning, the main forces acting on the blades are lift, centrifugal acceleration, and gravity. The magnitude of the lift force is determined by the speed of rotation, the area of the blades, and the pitch of the blades.

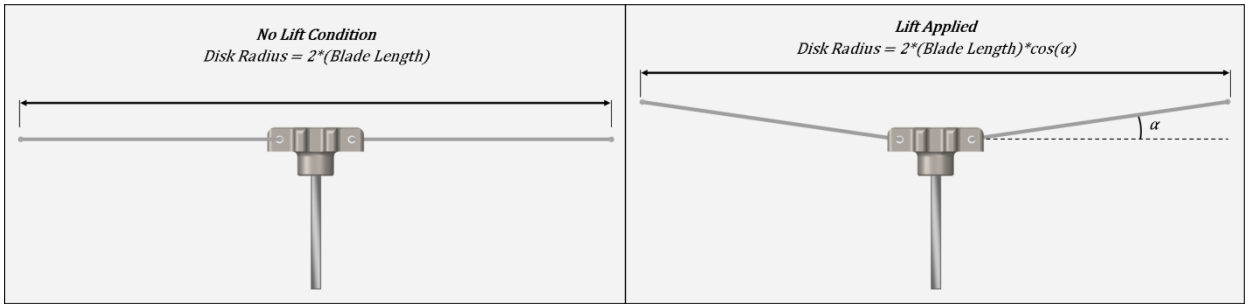

Figure 3: The effects of centripetal force and lift on helicopter blades during flight.

The centrifugal acceleration is primarily dependent on the rotational velocity of the blades, and the gravitational force is a function of the blades' weight. The centrifugal acceleration acts along the length on the blades. As the blades are spun up from zero angular velocity with

zero pitch, the centrifugal acceleration on the blades increases, and the blades can be assumed to be parallel to the ground. As the pitch increases and the blades begin to produce lift, the magnitude of the force vector increases, the direction of which is perpendicular to the length on the blade. The resultant force vector between the centrifugal acceleration and the lift will cause the blades to flap upwards slightly from the horizontal. The resulting angle the blades form to the horizontal plane is known as coning. As the angle the blades rise increases, the blade disk area decreases since the distance between the blade tips also decreases, decreasing the diameter of the disk. Reduction in the disk area leads to a proportional loss in lift (Leishman, 2006).

Flapping Hinge Function

The flapping hinge allows individual blade grips to pivot in the vertical direction, relieving the moments exerted on the blade grips and rotor head when the blades are pitched using the cyclic controls. When the cyclic controls are used to tilt the swashplate, the lift dissymmetry exerts different moments on each blade root. For example, if the cyclic is used to bank the helicopter to the left, the direction of the lift force angles to the left proportional to the amount of cyclic applied. To achieve this, the swashplate increases the pitch of the blades on the right side of the helicopter, creating more lifting force on the right side of the rotor disk. Consequently, the increased lifting force causes the blades on the right side of the helicopter flap upwards while the blades on the left side remain more level. This flapping of the blades helps eliminate the moments that would otherwise be translated to the blade roots and into the rotor hub (Leishman, 2006).

Feathering Hinge Function

In order to create vertical lift, helicopters employ collective control, which moves the swashplate vertically along the main rotating shaft. As the swashplate moves, the control arms

attached to the blades rotate the blades along the axis of their length, changing the angle of attack of the blades collectively. The feathering hinge is what allows the blades to rotate in this way, creating lift proportional to the pitch of the blades. Similarly, when collective is used to bank the helicopter, the feathering spindle again allows the blades on one side of the helicopter to increase their angle of attack and produce the necessary lift (Leishman, 2006).

Lead-lag Hinge Function

The lead-lag hinge, also known as the drag hinge, works in conjunction with the flapping hinge and cyclic controls. Similar to the flapping hinge, the lead-lag hinge reduces the moments exerted on the blade roots when cyclic controls are applied. When the cyclic is used to bank in one direction, the blades will flap accordingly in order to evenly distribute the lifting force across the rotor head. The blades that flap upwards slow down as they reach the top of their arc, while the blades at the bottom of the arc accelerate. The lead-lag hinge allows the blades to pivot horizontally with the corresponding changes in angular velocity along their arc. This pivoting motion is similarly affected by the Coriolis Effect, which is the deflection of a rotating object in the direction opposite to its rotation. For example, if the helicopter blades are rotating counter-clockwise, the Coriolis Effect dictates that the blades will deflect clockwise to the right. The magnitude of the deflection will be proportional to the angular velocity of the blades and the resulting centrifugal force (Leishman, 2006).

2.3 Motor and Motor Drives

Typical model helicopters may use a variety of engine types including nitro, gasoline, miniature turbine, and DC electric motors. However for our application, we need to be able to precisely control motor speed, both within a single trial, and across multiple trials. For this level of control and the ability for the user to directly specify a speed, an electric motor is required. Other requirements include having the ability to rotate the rotor blade assembly at speeds up to 1500 RPM.

2.3.1 Alternating Current (AC) Motor

Alternating current motors are commonly used for industrial applications. Because they use high voltage, they are able to provide high torques. Unlike DC motors, which are easily

Figure 4: AC Motor with variable frequency drive. (Variable Frequency Drives)

controlled by adjusting the applied voltage, AC motors are more complicated to control. Because of the structure of AC current, a constant voltage can be applied to the motor, but the frequency of the alternations can be changed to control motor speed. Adjusting the frequency of the alternating current is done with a device known as a variable frequency drive (VFD). Depending on the VFD configuration, it accepts regular 60 Hz single or three phase voltage, then outputs three phase power at the desired frequency. VFDs are usually programmable with a simple

display which allows the user to specify a frequency or a ramp up/ramp down cycle. External control of the VFD is also possible. These devices are commonly used in industry to provide soft start-ups and to optimize power consumption.

2.3.2 Direct Current (DC) Motor

Direct current motors run on DC voltage and are used in a variety of industrial and consumer applications. Control is performed by limiting the voltage supplied to the motor, usually by a variable resistor. Precise control can be performed using specially designed control units which utilize a series of variable resistors along with an external input.

Figure 5: Variable speed DC motor control unit.

This particular DC motor control unit shown in Figure 5, used as an example, has additional resistor circuits to more precisely control motor performance. On the front panel it features the main variable resistor which changes the voltage supplied to the system. Inside the circuitry box are four more variable resistors, which control minimum speed, maximum speed, speed regulation, and current limit. The maximum speed adjustment prevents the user from directing too much voltage to the motor, and the minimum speed adjustment allows for

calibration of the main speed control knob. Speed regulation will change the rate of motor loading, or the aggressiveness of the ramp up and ramp down stages. Lastly, the current limit adjustment adjusts the amount of current delivered to the motor, adjusting the maximum torque output of the motor. Additional add-in boards can be purchased to control the DC motor control from a 0-5 VDC voltage from a data acquisition box (AutomationDirect.com Inc., 2014).

2.4 Sensors and Data Acquisition

In order to obtain experimental data on stresses, strains, forces, and moments, sensors must be mounted in the rotating frame on the blades and rotor hub. Each type of measurement must have its own type of sensor meaning generally each sensor needs its own connection to the data acquisition (DAQ) box. For example, if a four bladed rotor has four strain gauges on each blade, as well as three force and three moment sensors, then the DAQ box needs a minimum of 40 channels. This is because each conventional sensor needs an input and output channel. The high rate of rotations that characterize a small-scale rotor head create a very difficult environment for conventional sensors and data acquisition systems to work in. In order to transfer the measurements from the rotating frame of the rotor head to the non-rotating frame where the measurements are processed, an appropriate data acquisition system is required. These include the use of slip rings, wireless sensors, a wireless data acquisition box or a light based system.

2.4.1 Slip Rings

The most straight forward option for transferring data from the rotating frame to the stationary frame is a slip ring.

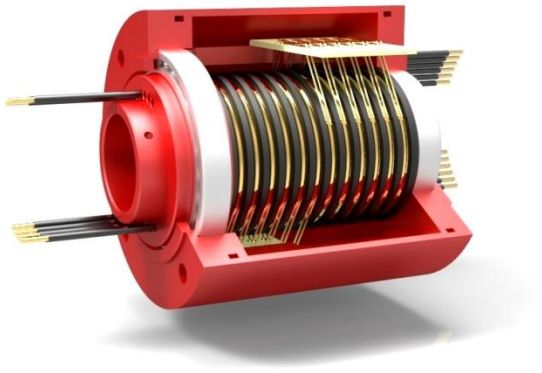

Figure 6: Cut away view of a multichannel slip ring (Rotary Systems Inc.)

Slip rings work through a combination of rotating and stationary rings that are connected by a conductive brush. This allows electrical signals to be passed from the rotating ring through the conductive brush to the stationary ring. One disadvantage of slip rings is that each channel requires a ring set, meaning that the number of channels depends directly on the number of rings. Another disadvantage of slip rings is that the brush systems limits the maximum rpms because an increase in rpms increases the internal temperature of the slip ring. This may lead to failure unless a cooling system is incorporated into the slip ring design.

Figure 7: Moog Inc. AC3757 slip ring (Commercial - Industrial Slip Rings)

Slip rings are common on many types of aircraft, including helicopters. They are used in blade and propeller anti-ice systems, as well as in data transfer applications. Although full scale helicopters use slip rings specifically designed for aerospace applications, the rotational speeds that these slip rings operate at are much less than those of small-scale helicopters. This leads to the need for slip rings specially designed to operate with a high rate of rotation. One example is the AC3757 made by MOOG Inc. The AC3757 has 36 channels and a maximum rpm of 4000 uncooled, with nitrogen cooling the AC3757 can achieve a maximum of 6000 rpms (Commercial - Industrial Slip Rings).

2.4.2 Wireless Sensors

Another option to transfer data from a rotating environment is wireless sensors. In this case, instead of using wired sensors connected to the rotating half of the slip ring, the sensors

would be completely wireless. A wireless transmitter is built into the sensor package that transmits the data directly to a data acquisition box located in the stationary frame. The advantage of this type of system is the elimination of wires that can possibly get tangled and break. One drawback, however, is these sensors are significantly more expensive than their wired counterparts and generally require specialized equipment to receive and process the wireless data. Wireless sensors also tend to be larger than their wired counterparts, this can lead to problems due to spatial constraints and the sensor weight effecting the rotor blades (Lecklider, 2008).

Figure 8: An example of a wireless strain gauge. (Lecklider, 2008)

2.4.3 Wireless Data Acquisition

Another option for transferring data from the rotating frame into the stationary frame is a wireless data acquisition box. This type of system works by placing a wireless data acquisition box in the rotating frame, allowing for the use of wired sensors.

Figure 9: National Instruments Wireless DAQ Box (National Instruments Corporation)

The sensors transmit directly to the wireless data acquisition box which processes the information it receives and transmits it wirelessly out of the rotating frame to the stationary frame. These types of data acquisition boxes often take advantage of the built in wireless capabilities of computers by transmitting their data directly to the computer's wireless internet cards. This eliminates the need for specialized receiving equipment in the stationary frame. One of the advantages of wireless data acquisition boxes are the fact that they can be paired with relatively inexpensive wired sensors. The down side to wireless data acquisition boxes is the fact that the tend to be limited by physical and battery size, therefore the number of channels they can support are less than those of a standard wired data acquisition box. The wireless data acquisition box has to also be designed to operate in a frame that rotates at high speeds. One example of a wireless data acquisition system is the TorqueTrak 10k manufactured by Binsfeld Engineering Incorporated (Binsfeld/engineering).

2.4.4 Fiber Optics

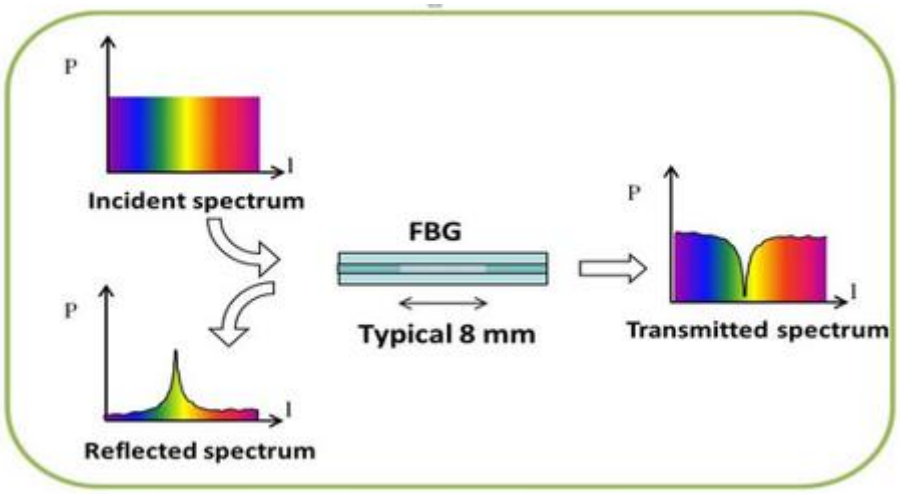

Figure 10: Schematic showing how Bragg Gratings change the reflected spectrum. (Fiber Bragg Grating Principle, 2014)

The final option is a light based fiber optic system. The system works using a combination of five main components. They are the light source, the coupler, the Bragg gratings, the receiver and the fiber optic cable. The light source, which is generally a battery powered light emitting diode (LED), eliminates the need for wires physically connecting the rotating and stationary frames by transmitting a pulse of light down the fiber optic cable. The light then passes through the coupler to the test section of the fiber optic cable. In the test section each Bragg grating allows all but a certain wavelength of light to pass though. The wavelength that does not pass through the given Bragg grating is reflected back to the coupler and sent to the receiver. At the receiver there can be a small gap between the end of the fiber optic cable and the receiver, allowing the receiver to be located in the stationary frame while the cable can be rotating. This eliminates the need for expensive and complicated slip rings and wireless sensors. This light based system also has the advantage of being modular, meaning that if more than one sensor is needed, one can simply add sensors to the fiber optic cable. The number of sensors that can be mounted on one cable is limited by the length of the cable and the sensitivity of the

receiver to different wavelengths. Another added benefit of fiber optics is they are immune to electro-magnetic interference (Fiber Bragg Grating Sensors, 2014).

Since fiber optic cables are flexible, the path and orientation of the fiber relative to the blade can record different types of strain. For example, the fiber may run lengthwise along the blade which would measure longitudinal strain, or if the cable is turned by 90 degrees, the system can measure strain along the width of the blade. The flexibility of the cable would allow for multiple turns, along the length of the blade, which would measure strains at multiple positions and orientations.

2.4.5 Bragg Grating

A Bragg Grating is a type of a fiber optic cable that can be used to measure strain or temperature.

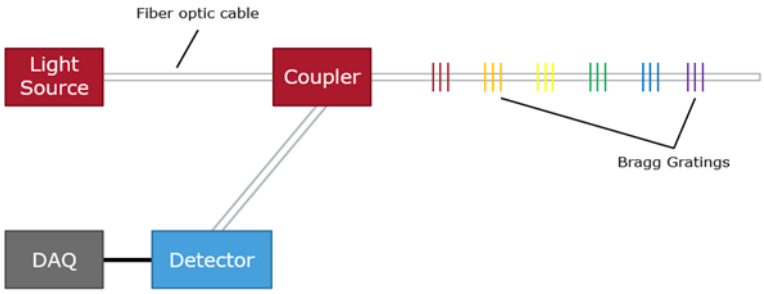

Figure 11: A basic schematic of a Bragg Grating strain gauge.

Bragg gratings work similarly to the fiber optic systems discussed above, except the individual gratings have different indices of refraction than the fiber housing them. Consequently, when the light is transmitted through an unstrained Bragg grating, a small portion of the transmitted spectrum is reflected back due to the change in the refractive index. The reflected wavelength of the unstrained Bragg grating is then used as the reference wavelength for measuring strain or temperature.

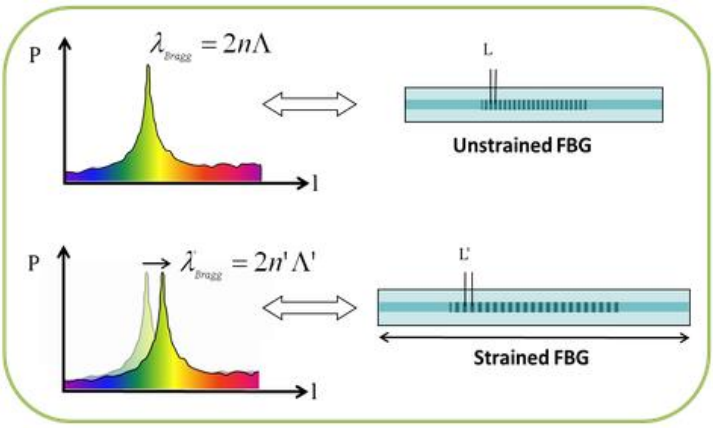

Figure 12: The shift in reflected wavelength corresponds to the strain or temperature of the material (Fiber Bragg Grating Principle, 2014)

In order to measure strain or temperature, fiber optic cables with Bragg gratings are affixed to the material of interest. As the material is strained or heated, the fiber optic cable is either stretched or compressed, changing the refractive index of the Bragg gratings. This change causes a shift in the reflected wavelength versus the reflections when unstrained. The resulting difference in reflected spectrums is registered as the magnitude of the strain or temperature change of the material being tested.

Chapter 3: Methodology

3.1 Hover Test Stand Design

This section is a comprehensive review of the design of our test stand. It discusses each assembly in detail, explaining each design choice we made. It includes our budget and how we designed each part for machinability. It details how to assemble the test stand, how to test it, and finally the theoretical use of the data acquisition system.

3.1.1 Design Specifications

Rotor head selection began by analyzing the advantages and disadvantages of various rotor head designs. The following parameters for the design were established:

1. The diameter of the rotor would be approximately one meter
2. The rotor head should be fully articulated
3. The blades must be easily interchangeable to test different designs
4. The number of blades should be variable

These parameters were met by the final design, which was built based on a fully articulated rotor head. Changing the total number of blades can be accomplished by removing the blade grip assemblies and reattaching them to a different hub built for the appropriate number of blades. Individual blades are changed by disconnecting them from the blade grip and attaching the new blade.

3.1.2 Test Stand Design

The stand was designed to support the entire rotor assembly, the engine, the control system, and the safety system. In order to do this successfully the stand had to be able to remain

stable during the operation of the rotor hub. Additionally, the stand was designed to keep the rotor hub out of significant ground effect and remain simple enough to maintain mobility.

In order to keep the rotor head out of ground effect, the rotor head must be mounted at a distance equal to 125% of the rotor diameter off the ground. This allows the air to exit below the rotor freely, meaning that lift force generated by the rotor head doesn't increase. In the case of our design, the rotor head must remain at least 1.25 meters, or 4.1 ft., above the ground.

3.1.3 Engine Design

Previously documented helicopter hover test stands have no supporting calculations to justify the engine size selection. Large power output requirements typically lead to large, expensive engines and more expensive motor drives.

Effective use of the limited budget provided mandated that the minimum power required to spin our rotor head system at the desired angular speed had to be determined. Accurate calculations allowed our team to determine the motor and drive system which could power our test system while preserving as much of the budget as possible.

Using equations derived from helicopter momentum theory, a minimum power requirement was found based on the parameters shown in Table 3 (Leishman, 2006).

Table 3: Required power calculation parameters and values

Symbol	Parameter	Value	Symbol	Parameter	Value
A	Rotor disk area	1.131 m^2	κ	Induced power factor	1.25
C_{do}	Zero lift (avg. profile) drag coefficient	0.02	ρ	Flow density	1.2 $\frac{kg}{m^3}$
R	Rotor blade radius	1.2 m	σ	Rotor solidarity	0.1016 m^2
T	Rotor thrust	76.9 N	Ω	Angular velocity	125.66 $\frac{rad}{s}$

The values in Table 3 are based on physical conditions such as blade dimensions, the ambient environment, or on approximations of physical phenomena. For blade dimensions, we assumed a rotor disk diameter of 1.2 m, blade length of 1.0 m, and blade width of 0.05 m. Blade dimensions affect A, R and σ. The induced power factor κ, is a coefficient which accounts for the inefficiencies of a non-ideal system which was found to range between 1.15 and 1.25 (Leishman, 2006). For our calculations we used κ = 1.25 to find the maximum power required.

Rotor thrust was indirectly calculated by finding the force due to gravity on a comparably sized model helicopter. Coefficient of drag at zero lift, C_{do}, was approximated from a NACA 0012 airfoil. To determine the thrust created by the rotor system, blade element theory was applied to find the lift along each blade.

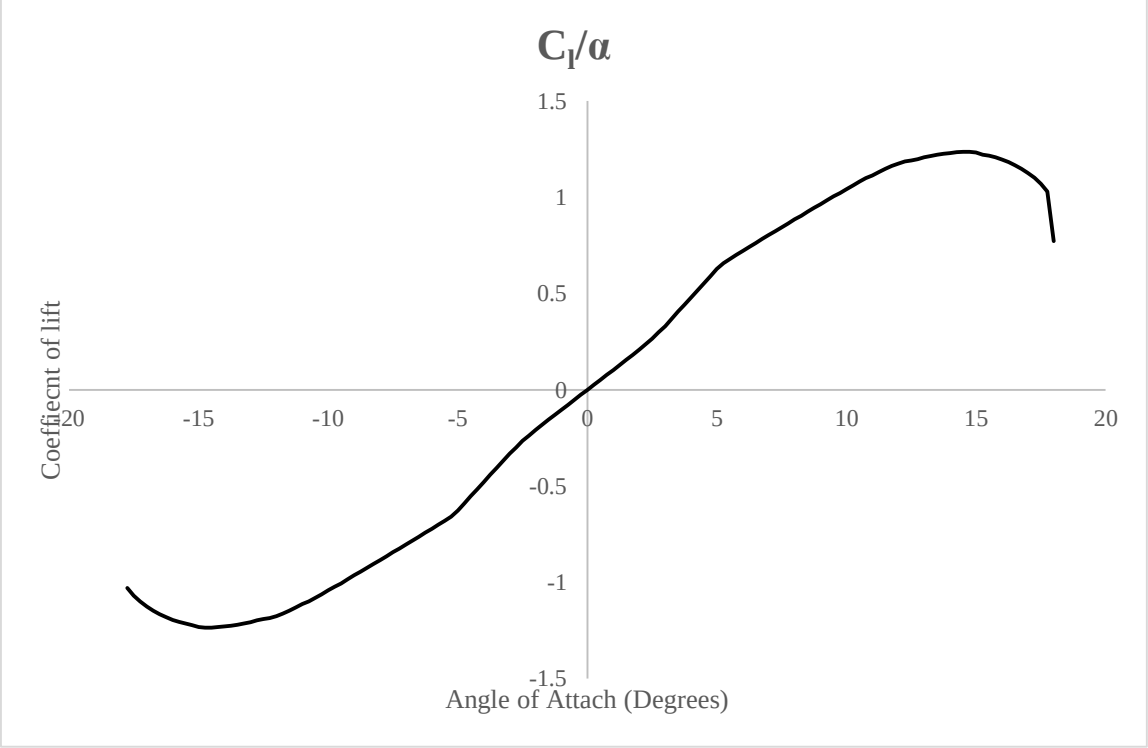

Figure 13: A plot of the lift coefficient versus the angle of attack for a NACA 0012 airfoil

The maximum thrust will be produced at the critical angle of attack, which by using Figure 13, is found to be approximately 12 degrees. Then by approximating the lift curve slope as 2π and

assuming thin airfoil theory, the maximum lift coefficient was calculated to be approximately 1.3. By integrating the angular velocity and coefficient of lift along the length of the blade, the lift force per blade was found. Finally the thrust produced is equal to the lift force created by each blade multiplied by the number of blades.

Equation 1 was modeled in MATLAB with the above parameters and a four bladed rotor configuration, yielding a minimum required horsepower of 0.96 Hp.

$$P = \frac{\kappa T^{3/2}}{\sqrt{2\rho A}} + \rho A(\Omega R)^3 \left(\frac{\sigma C_{d0}}{8}\right) \quad 1$$

Based on the minimum power requirements and the steep cost increase of motor and drive systems with increased power, we recommend the purchase of a 1 horsepower drive system. One option we looked at was the 1 horsepower iron horse motor offered by MSC. A 1 horsepower system will allow for the correct rotational velocity and will allow the user to operate at the maximum angles of attack without significant motor lag. Should longer blades need to be tested, the power requirement should not increase significantly. The longer blades will allow a decrease in the required angular velocity because the required velocity to scale the system will decrease. There for the use of a 1 horsepower motor allows for flexibility in future applications.

3.1.4 Engine Mount and Belt Tensioner

In order to attach the engine to the frame of the hover test stand an engine mounting plate was designed using the engine blue prints provided by the manufacturer. The plate was designed to allow the engine to slide back and forth in the lateral direction so that the drive belt could be tensioned properly.

To achieve this we choose to hang the engine below the engine mounting plate using the 4 factory 3/8”-16 bolts holes. By loosening the 4 bolts the engine may slide back and forth easily while keeping the engine’s output shaft parallel to the driveshaft. The 4 3/8” bolt holes and the 1” hole for the engine output shaft are slotted to a length of 2” so that the belt can be tensioned and changed if needed. The plate is mounted on 4 spacers each positioned concentrically with the bolt holes. The spacers offset the surface of the plate by 0.16 inches, which alleviates the need for a relief on the back of the plate, allowing for a thinner plate and saving manufacturing costs.

3.1.5 Power Transfer System

Drivetrain flexibility was accomplished by using an indirect drive system consisting of belt pulleys on both the motor driveshaft and the rotor shaft. This system will allow for variable gearing, easy maintenance, and possible motor changes. Due to the required costs, we elected to use a belt and timing pulley system over a chain drive or gears.

A timing belt pulley system was chosen since they eliminate the slippage usually present in other belt designs, such as v-belts or flat belts. In order to keep the motor rotating at the same speed as the rotor a gear ratio of 1:1 was chosen. This ratio will allow the motor to operate near its maximum speed, providing maximum power to the rotor. It also allows the operator to change the rotation rate by adjusting the motor through the use of the VFD. By using a motor with a maximum speed close to the required speed of the rotor, the need for complex gear ratios was eliminated allowing more flexibility when changing the speed of the rotor.

3.1.6 Driveshaft Design

The driveshaft design is a critical part of the hover test stand because it transfers the engine’s power from the drive pulley to the rotor hub and allows data from sensors mounted on the rotor hub to be transmitted to the DAQ box. In order to do this, the driveshaft must be hollow

to allow for fiber optic cables and other wires to pass through the middle while remaining strong enough to withstand the forces exerted on it by the motor and aerodynamics.

Due to budgetary constraints the bearings selected were those that were readily available to us, therefore some of the driveshaft dimensions were constrained from the start of design. The bearings available were two Timken 206K light duty Conrad ball bearings with an inner diameter of 1.1811" (30mm). On the other end of the driveshaft, we determined the swashplate bearing and rotor hub bore should be no larger than 0.75". The different bore sizes of the bearings and swashplate required the design of a stepped driveshaft. The preferred starting stock for this part is seamless tubing, however because of the large step and small internal hole, a tube with sufficient wall thickness was unavailable.

Without a tube, we were required to start from solid bar stock and drill a through hole. This presented its own set of challenges due to the extreme hole depth. The overall driveshaft length is a sum of all the heights and clearances of the jesus nut, rotor hub, swashplate, bearings, and drive pulley. This results in a minimum total length of approximately 15 inches.

After weighing the different options a design compromise was achieved. The compromise was to manufacture the driveshaft as two separate sections. The upper smaller section is the mounting point for the Jesus nut, rotor hub, swashplate, and scissor linkage. The outside diameter of this section is limited by the inside diameter of the swashplate, which is 0.75 inches because of the limited selection of readily available spherical bearings. In order to prevent the rotor hub from sliding down the driveshaft a pin is passed through the base of the rotor hub and driveshaft. The pin passes through a 0.25" hole located 2.200" below the top face driveshaft. This has the added benefit of transmitting the rotational force of the driveshaft directly into the rotor hub. As an added security measure the Jesus nut is used. This nut secures the top of the

rotor hub as shown in Figure 14 and transmits the lift force from the rotor head into the driveshaft.

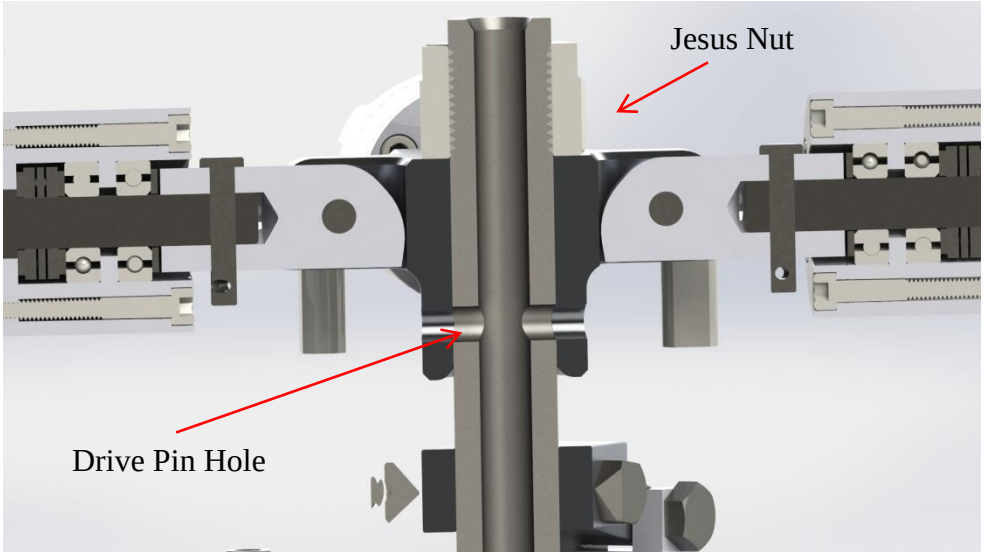

Figure 14: A cut away view of the upper driveshaft showing the locations of the Jesus Nut and drive pin hole.

The outer diameter of the lower section is limited by the inside diameter of the bearing used to mount it. This means the outside diameter of lower driveshaft must be equal to the bore of their mounting bearing which leads to a lower driveshaft diameter of 1.1811 inches (30 millimeters). The two driveshaft sections are coupled together using two flanges, one on each section. The flange on the lower section is thicker than that of the upper section so that it can be tapped to allow for the use of bolts to connect the sections.

Eight bolts are used to connect the sections at the flange in order to spread the force out as much as possible and keep the centers of the sections aligned. The bolts are ¾" #10-32 button head screws. To maintain concentricity between the two shafts, there is a cylindrical male and female connection. This connection is shown in Figure 15 along with the bolts and flanges.

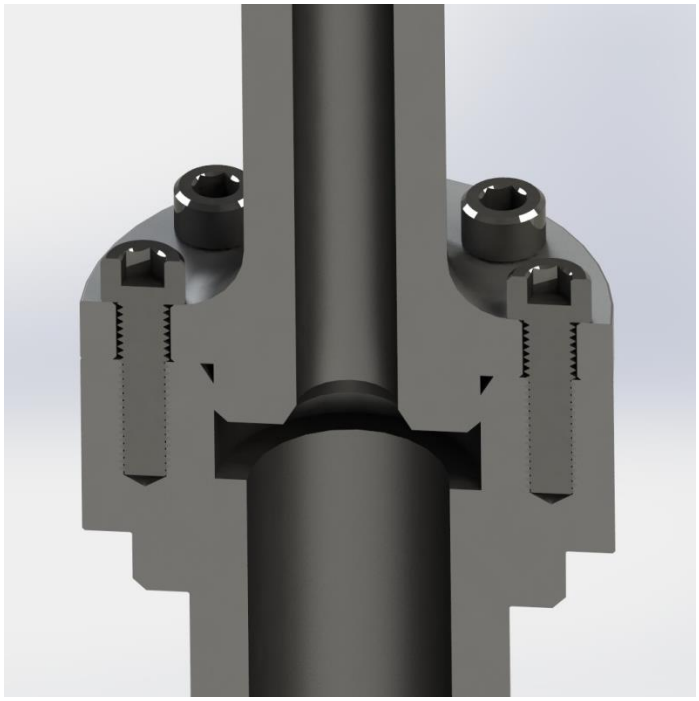

Figure 15: A cut away view of the connections between the driveshafts

The upper section has an inside diameter of 0.375 inches which allows for wires and fiber optic cables to be threaded through the middle of the first section. The lower section has an inside diameter of 0.75 inches, which is larger than that of the first for ease of manufacturing. This allows wires to pass from the upper driveshaft down through the lower driveshaft to the stationary frame. The larger inside diameter of the second section is possible because the size of the stock allows the use of a larger drill. Since the larger section will be easier to machine, this section will be the longer of the two. It measures 9 inches long compared to the 8.25 inch length of the upper section.

3.1.7 Driveshaft Analysis

The driveshaft sections must be able to withstand a series of combined loadings. Stresses due to torsion, tension, and bending moments will all be present in the drive shaft. Analysis of each type of loading was performed separately and subsequently combined to determine the total

resultant force on the driveshaft. Stresses in the driveshaft were analyzed at the point where the highest stress concentrations are most likely to occur. This is the point where the upper driveshaft expands from a diameter of 0.75” to one of 1.97” via a R.25” fillet in order to meet the connecting flange.

Stress Concentrations

The fillet at the base of the upper driveshaft creates a stress concentration. Stress concentration factors are found using experimentally tabulated values bases on part geometry. The industry standard for obtaining these values is Peterson’s Stress Concentration Factors, Second Edition, by Walter D. Pilkey. Pilkey’s resource was used for the calculations and the graphs used are included in Appendix D.

Stress concentration factors were found for torsion, tension, and bending using the driveshaft geometry. Each stress concentration was then multiplied by its respective forces before continuing with the fatigue analysis. The details and results of these calculations can be found in

Appendix E.

Torsion Calculations

Based on the inside and outside diameters stated above the torsion on each section was calculated to ensure that the driveshaft sections were manufactured from a material strong enough to withstand the torsion.

The torsion was calculated using the formula, shown by equation 2

$$\tau_{max} = \frac{Tc}{J} \tag{2}$$

where T is the torque on the shaft and c is the distance from the center of gravity to the point where the torsion is being calculated. Finally J is the polar moment, defined by equation 3

$$J = \frac{\pi}{2}(c_o^4 - c_i^4) \tag{3}$$

where c_o is the distance from the center of gravity to the outside edge of the shaft and c_i is the distance from the center of gravity to the inside edge of the shaft. This results in equation 4

$$\tau_{max} = \frac{Tc}{\frac{\pi}{2}(c_o^4 - c_i^4)} \tag{4}$$

In the case of the upper driveshaft, $T = 15$ Nm which is the maximum torque the motor can provide, $c = c_o = 0.01905$ meters (0.75 in) and $c_i = 0.009525$ meters (0.375 in) leading to a $\tau_{max} = 1.61$ MPa.

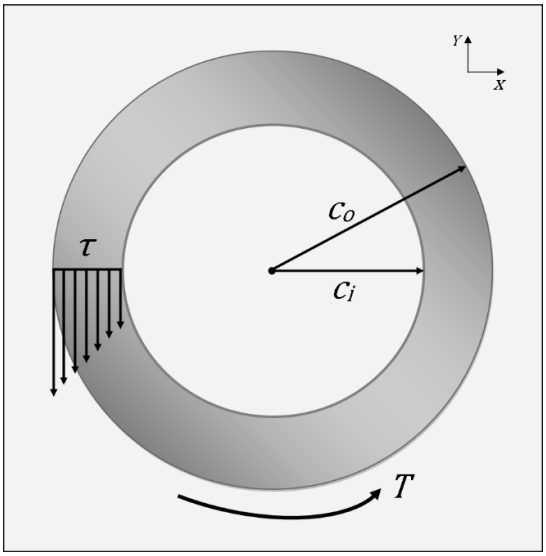

Figure 16: Cross section showing in-plane forces and geometry.

Force Due to Lift

When the device is in motion, the lift force will be transmitted to the shaft. In most cases, when there are no cyclic pitches commanded, the lift vector is purely vertical. However, with the integration of cyclic controls, the resulting lift vector will shift from vertical to some angle as demonstrated in Figure 17. As a note, these non-vertical lift forces are the forces which cause forward flight.

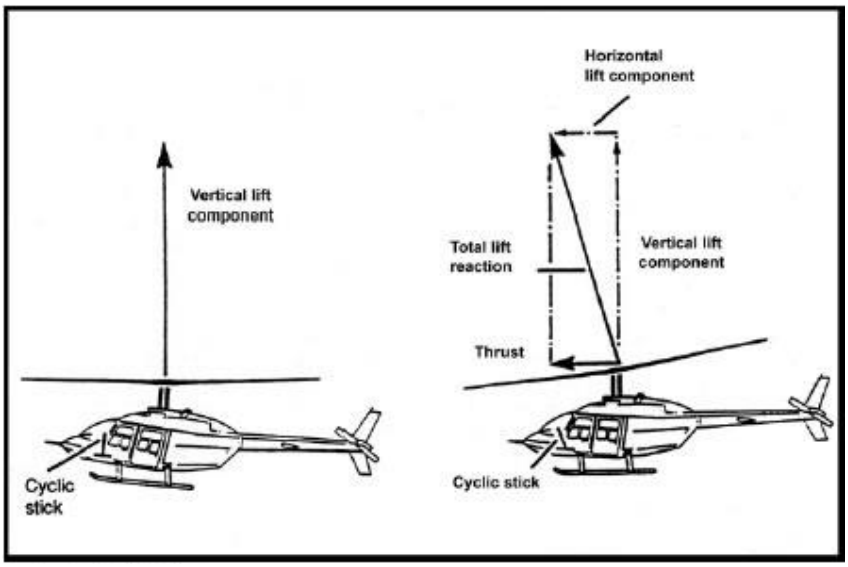

Figure 17: Total Lift Vector and Decomposition (Helicopter Flight Training Manual, 2010)

As shown in the decomposition on the right in Figure 17, the total lift force now has two components, the vertical lift component and the horizontal lift component. The vertical force will create a pure tensile stress on the driveshaft. With the addition of the horizontal lift force, a bending moment will be created at the critical areas of the shaft.

This bending force is calculated first decomposing the total lift vector, given as:

$$F_{Lift,x} = F_{Lift} sin(\beta) \quad 5$$

where β is the angle between the axis of rotation and the total lift vector. Because the lift vector acts at the center of rotation, the moment arm l, is simply the distance from point A to point B (see Figure 18). The bending moment at point B due to lift is then given as:

$$M_{Lift,x} = F_{Lift,x} \times l \quad 6$$

The stress created on the cross section is

$$\sigma_{Lift,x} = \frac{M_{Lift,x} \times c}{J} \quad 7$$

where $c = c_o$ for maximum stress and J, the polar area moment is equal to $\frac{\pi}{2}(c_o - c_i)^4$. For reference geometry see Figure 19.

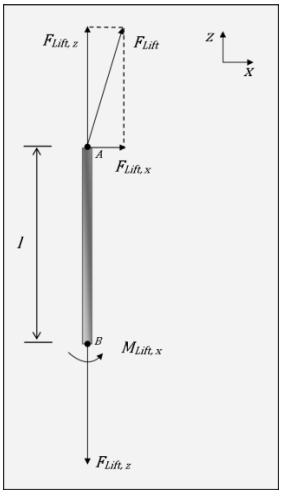

Figure 18: Free Body Diagram of forces due to lift.

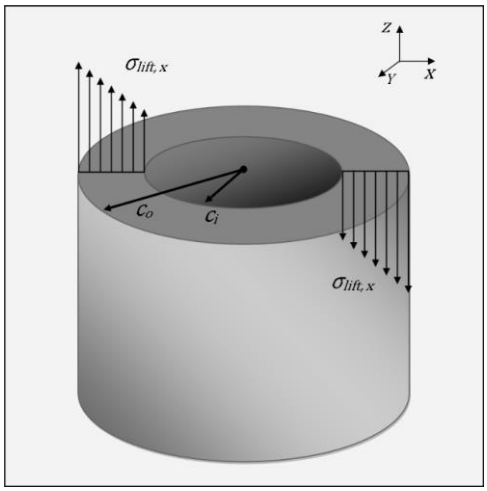

Figure 19: Stress due to horizontal lift

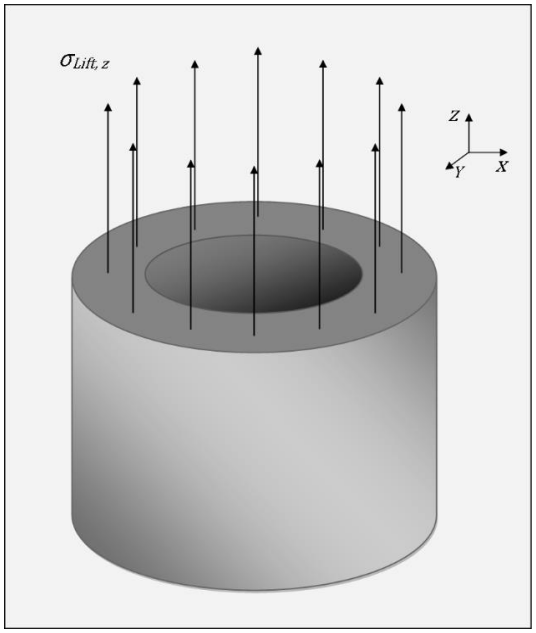

Figure 20: Stress due to vertical lift force.

Next, the tensile force created by the vertical lift vector component is

$$F_{Lift,z} = F_{Lift}cos(\beta) \tag{8}$$

where β is the angle between the axis of rotation and the total lift vector. The tensile stress created on the driveshaft cross section is then given as

$$\sigma_{Lift,z} = \frac{F_{Lift,z}}{A_{pipe}} \tag{9}$$

where $A_{pipe} = \pi(c_o^2 - c_i^2)$. For reference geometry see Figure 20.

From the calculations, found in detail in Appendix E, we found that the stress in the z direction is 0.135 MPa and the stress in the x direction is 0.1175 MPa. These stress values includes the stress concentration factors required by the fillet on the upper drive shaft.

Force Due to Imbalance

A significant bending moment may occur in the driveshaft due to any imbalance of the rotor head and driveshaft system. An unbalanced rotating mass creates a force in the plane of the

rotation due to an imbalance in centrifugal force. In the case of a rotor head, this force will act in the plane of the center of gravity of the rotating rotor hub. Using a force-body diagram shown in Figure 21, the resultant bending force is found at point B.

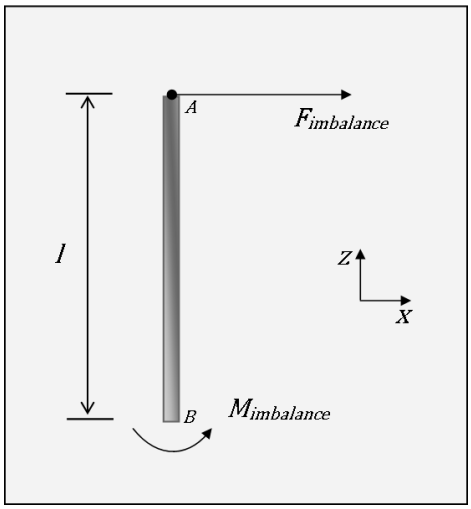

Figure 21: Free Body Diagram of Imbalance Force Equilibrium.

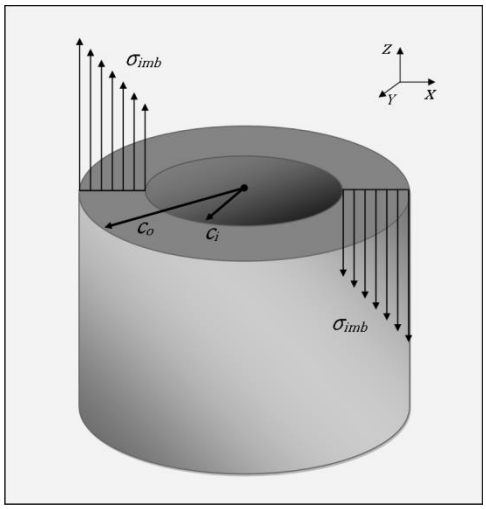

Figure 22: Stress due to Mass Imbalance.

To model this imbalance, the center of mass of the rotor head system was offset by 0.125 inches. This creates a centrifugal force, calculated as

$$F_{imbalance} = \frac{M \times V^2}{r} \quad (10)$$

where M is the mass of the rotor head and blades, $V = r\Omega = \frac{2\pi r}{60} \times RPM$, and r is the distance from the rotation axis to the center of gravity of the rotor head. Through substitution and simplification, the imbalance force can be calculated as:

$$F_{imbalance} = \frac{4\pi^2}{3600} Mr \times RPM^2 \quad (11)$$

Multiplying by the moment arm gives the bending moment at point B:

$$M_{imbalance} = \frac{4\pi^2}{3600} Mr \times RPM^2 \times l \quad (12)$$

The stress created at point B can be found using the following equation

$$\sigma_{imb} = \frac{M_{imbalance} \times c}{J} \quad (13)$$

where $c = c_o$ for the maximum stress (Figure 16), and $J = \frac{\pi}{2}(c_o - c_i)^4$, the polar area moment. As calculated in Appendix E, the stress due to imbalance σ_{imb} was 11.43 MPa.

Cyclic Loading

In addition to the series of combined loadings, the drive shaft will also be subjected to a cyclic loading. At the critical areas of the shaft, there will be a constant cycle of tensile and compressive loadings due primarily to the bending moments.

Imagine the shaft rotating at a constant velocity with a certain imbalance. As shown in Figure 23 and Figure 24, this creates a force $F_{imbalance}$ which becomes a moment $M_{imbalance}$ at point B. Because the force $F_{imbalance}$ is rotating with the drive shaft, the moment also rotates, causing a constant state of tension/compression on the corresponding areas of the shaft. Adding the horizontal lift force due to cyclic pitch, $F_{Lift,x}$, will cause a reaction moment $M_{Lift,x}$ at point B. Contrary to the imbalance force, the lift force does not rotate with the shaft, but instead acts in a fixed direction. The most important instances to analyze are when the two forces act in the

same direction and in opposite directions. The resulting case of minimum bending moment is shown in Figure 23 and the case of maximum bending moment is shown in Figure 24**.** Both Figure 23 and Figure 24 are shown with a reference frame attached to the driveshaft so that the sign convention of the resulting forces and moments will be consistent.

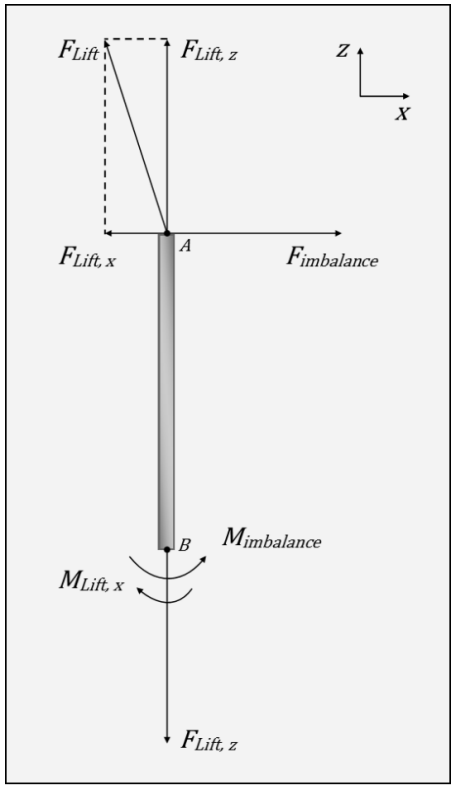

Figure 23: Minimum net moment FBD

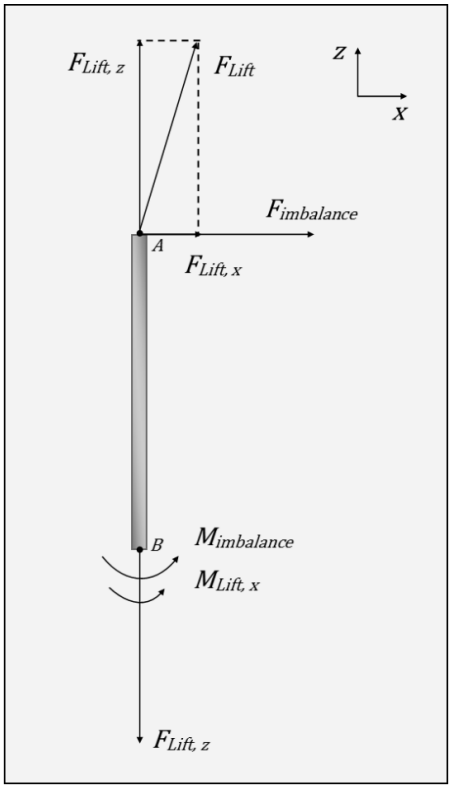

Figure 24: Maximum net moment FBD

At point B, the combination of the lift and imbalance forces results in two bending moments and one force. For the maximum case, these forces sum to

$$\sigma_{max} = \sigma_{imb,max} + \sigma_{lift,z} + \sigma_{lift,x\,max} \quad (14)$$

For the minimum case the stresses sum to

$$\sigma_{min} = \sigma_{imb,max} + \sigma_{lift,z} - \sigma_{lift,x\,max} \quad (15)$$

This combined stress field results in a tensile force which varies in magnitude along the cross section of the shaft. Toward the outer edges of the shaft the tensile stresses are increased in a

linear fashion. Depending on the direction of the lift vector, one side of the shaft will have a higher stress than the other. The stress field is illustrated in Figure 25, with σ_{max} and σ_{min} shown. From the calculations detailed in Appendix E, σ_{max} and σ_{min} were found to be 11.82 MPa and 11.59 MPa respectively.

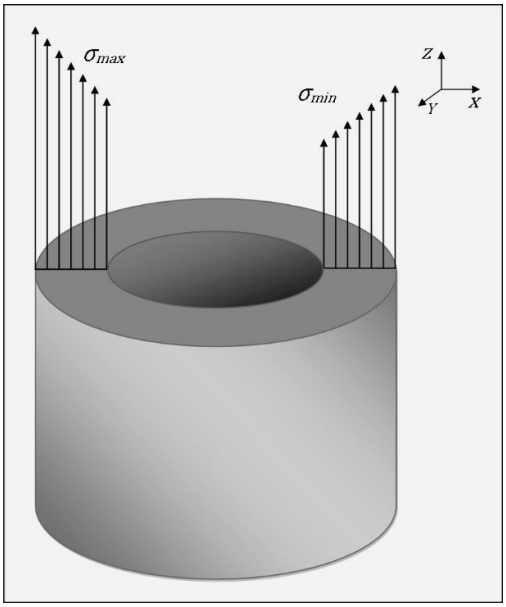

Figure 25: Combined stresses due to lift and imbalance forces

Differential Element Stress Analysis

Because the torsional and bending forces act on the same point, they cannot be analyzed separately. In order to determine the single force resulting from their combination an elemental analysis must be employed. Figure 26 shows the stresses on a differential element located in the plane of interest.

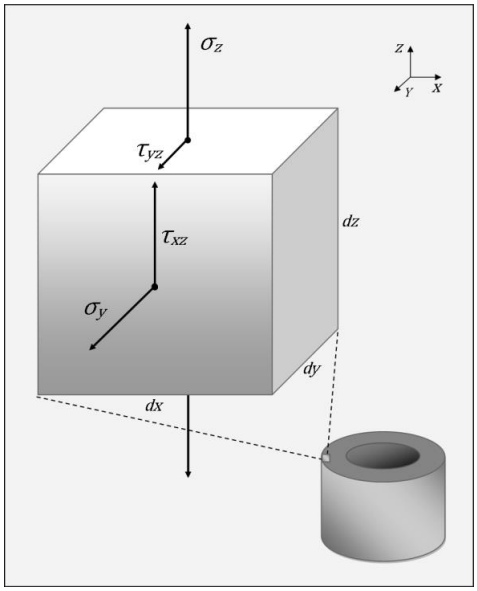

Figure 26: Stress on a differential element.

The maximum normal stress occurs when the element is set at an angle where there is no shear stress applied. The normal stress resulting from this case is called the principal stress. There are two principal stresses σ_1 and σ_2, where $\sigma_1 > \sigma_2$ as found using the following equation:

$$\sigma_{1,2} = \frac{\sigma_z + \sigma_y}{2} \pm \sqrt{\left(\frac{\sigma_z - \sigma_y}{2}\right)^2 - {\tau_{yz}}^2} \quad 16$$

The value σ_1 was used for the rest of the analysis since it is greater in magnitude than σ_2.

The maximum shear stress was found in a similar manner using equation 17

$$\tau_{max,in\ plane} = \sqrt{\left(\frac{\sigma_z - \sigma_y}{2}\right)^2 - {\tau_{yz}}^2} \quad 17$$

The physical significance of each term in Figure 26 and equations 16 and 17 are now presented. The vertical normal stress, σ_z, is a result of the forces due to lift and bending, shown in Figure 26. The shear stress, τ_{yz}, is a result of the torsion, shown in Figure 16. The second shear stress shown on the y face, τ_{xz}, is required to maintain equilibrium within the differential

element. The second normal stress, also on the y face, is shown for reference to equations 18 and 19. However, for this loading, $\sigma_y \approx 0$, so equations 16 and 17 simplify to

$$\sigma_1 = \frac{\sigma_z}{2} \pm \sqrt{\left(\frac{\sigma_z}{2}\right)^2 - {\tau_{yz}}^2} \quad (18)$$

and

$$\tau_{max,in\ plane} = \sqrt{\left(\frac{\sigma_z}{2}\right)^2 - {\tau_{yz}}^2} \quad (19)$$

where σ_z is σ_{max} or σ_{min}.

Equation 18 yields a maximum tensile stress of 11.8 MPa, and Equation 19 yields a maximum shear stress of 5.7 MPa. Using an 1144 stress proof low carbon steel with a yield stress of 620 MPa gives a safety factor of 52 for tension and 109 for shear.

Fatigue Calculations

In order to assess the life cycle of our drive shaft design, a fatigue analysis was performed at the flange on the upper driveshaft, the point most likely to fail. The mean stress and stress amplitude at this location were calculated using equations 20 and 21

$$\sigma_{mean} = \frac{\sigma_{1,max} + \sigma_{1,min}}{2} \quad (20)$$

and

$$\sigma_a = \frac{\sigma_{1,max} - \sigma_{1,min}}{2} \quad (21)$$

Once the values of the stresses at the flange were calculated, the fatigue life was extrapolated from a fatigue cycle analysis graph, depicted in Figure 27. Using a stress of 1.7 ksi

as calculated, this resulted in an expected fatigue life of unlimited hours due to the fact that stress is below 1144 steels fatigue limit.

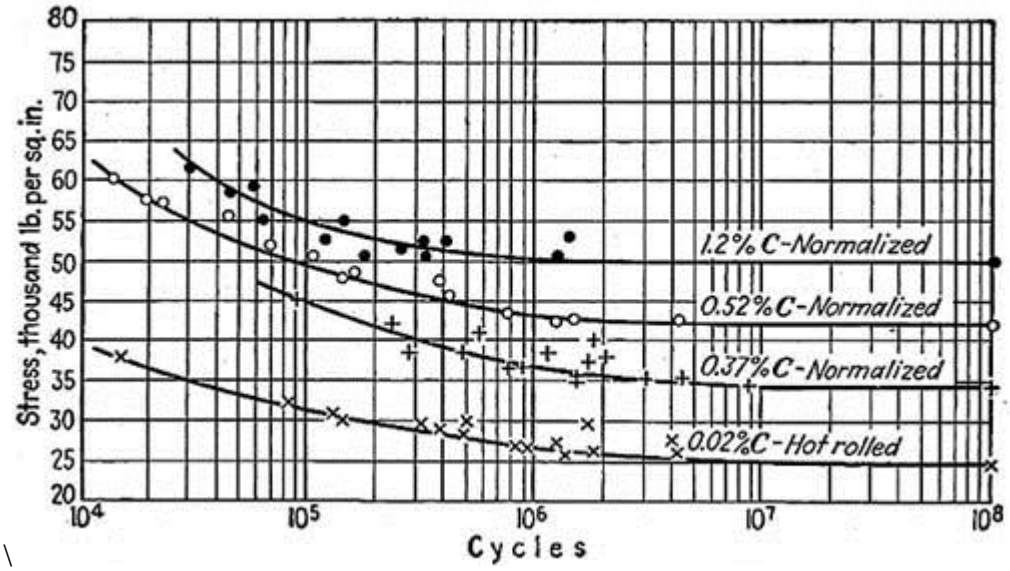

Figure 27: An S-N curve for mild steels. We are using 1144 steel which is .44% carbon (Lienhard)

3.1.8 Support Bearing Design

Supporting the lower driveshaft is a pair of Conrad type ball bearings. These bearings serve two purposes: first, to allow the driveshaft to rotate freely, and second, to support the driveshaft axially, i.e., transmit vertical forces to the test stand frame. The two bearings will be spaced along the shaft to provide better resistance to moments applied at either end of the shaft.

The bearing type we will use is Fafnir 206K light duty bearing. We chose these bearings because they were available to us for no cost and their internal and external diameters of 30 and 62 millimeters respectively met our design requirements for the driveshaft.

After choosing these bearings we performed a life cycle assessment on them to get a clear picture of how long they would last. We did this by using the life cycle formula depicted in equation 22

$$L_{10} = 1500\left(\frac{C_N}{R_E}\right)^3 \quad (22)$$

Equation 22 was provided by Fafnir where C_N is the radial load rating at the operating speed and R_E is the equivalent radial load. More specifically

$$C_N = n_f \times C_B \quad (23)$$

where n_f is the speed rating read from a Fafnir chart (Timken, 2015) and $C_B$is the basic radial reference load provided by Fafnir. The value R_E is found using the greater of the following equations 24 and 25:

$$R_{E1} = X_1 VR + Y_1 T \quad (24)$$

$$R_{E2} = X_2 VR + Y_2 T \quad (25)$$

where R is the radial load in lb., T is the thrust load in lb.,

$$V = 1.2,\ X_1 = 1,\ Y_1 = 0,\ X_2 = .56, \text{ and } Y_2 = \frac{T}{nd^2}.$$

After substitution and using a T of 30 lb., an R of 50 lb., an nd^2 of 1.32, an n_f of .28 and a C_B of 3570, this leads to

$$R_{E1} = 60,$$

$$R_{E2} = 715.42,$$

and

$$C_B = 999.6$$

meaning that R_{E2} and C_B will be plugged into the L_{10} equation. This resulted in a life expectancy of 4,091 hours, or about 170 days of continuous operation, before the bearings fail.

The upper and lower bearings are pressed into aluminum plates and separated by an aluminum spacer tube. The bearings are slip fit onto the driveshaft, which has its vertical motion restrained by a locknut on one side and the flange of the lower driveshaft on the other.

3.1.9 Swashplate Design

The purpose of the swashplate is to transfer pitch control inputs from the stationary frame to the rotating frame. The sensitivity of the input and transfer controls, or the amount of travel required, is determined by the required change in pitch of each blade. A typical helicopter operates at blade angles of attack between -5 and 15 degrees. Negative angles of attack may be necessary to achieve zero lift if the blades have axial twist.

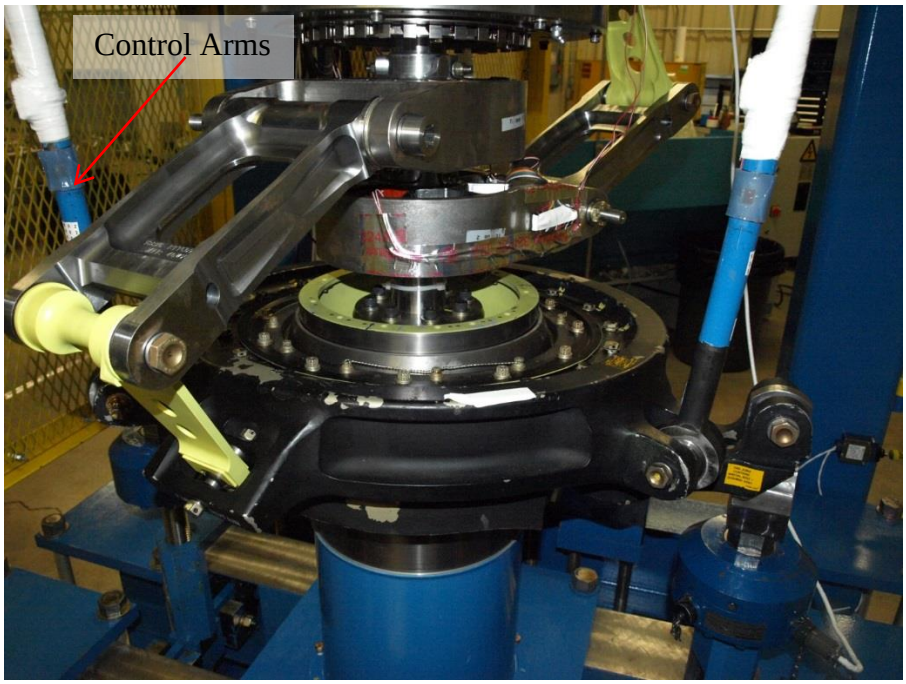

Figure 28: The scissor link from the University of Dayton Research Institute (University of Dayton Research Institute, 2014).

The length of the lever arm created by the offset of the control arm, shown in Figure 28, and the angle of pitch required for the blades means that the control rod needs approximately 0.5 inches of travel. From this, the swashplate also needs to be able to travel 0.5 inches vertically along the driveshaft. This must be combined with the swashplates ability to tilt relative to the horizontal axis, allowing cyclic control for simulating forward flight.

Because of the mechanical complexity of a swashplate and the difficulty of manufacturing a custom system, we initially elected to purchase a prefabricated swashplate designed for a model helicopter. After the outside diameters of the driveshafts were established we released that there were no commercially available swashplates that met our design requirements.

The size of our rotor head system meant that a custom swashplate was necessary to control the rotor hub. All the swashplates examples that we found in our preliminary research used two separate bearings as shown in Figure 29.

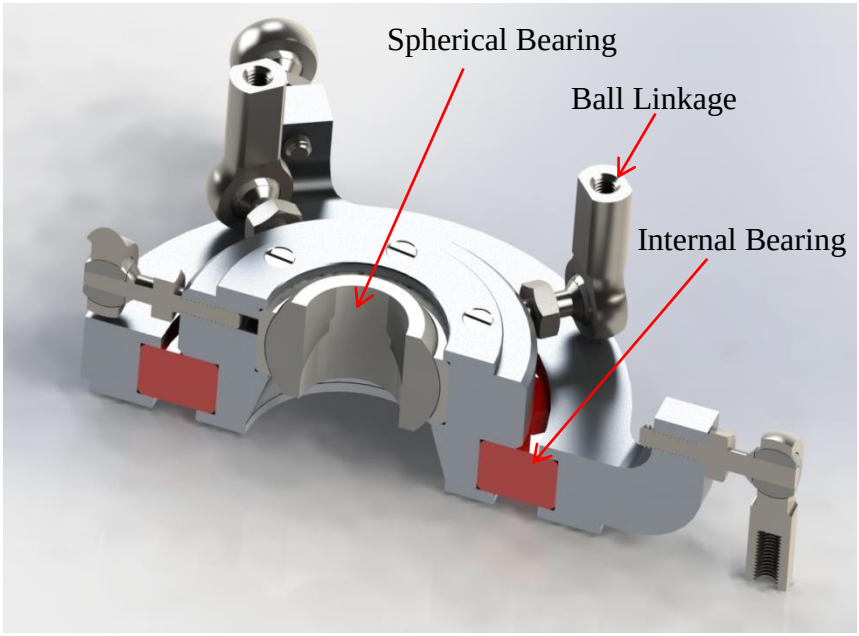

Figure 29: A cut away view of the swashplate

The first bearing, a spherical bearing, allows the swashplate to tilt and travel vertically with respect to the driveshaft. An Igus® plastic spherical bearing was initially selected based on the ¾ inch bore size and tilt angle. After contacting Igus® a similar ¾ inch bore McMasterCarr® bearing was selected. The change was due to the fact that the McMasterCarr® bearing was readily available. With the spherical bearing mounted on the top half of the upper swashplate, the bottom half was designed to allow for the maximum angle of tilt. The spherical bearing is

mounted in the upper swashplate by a press fit. This is backed up by the use of a retaining ring which is mounted on the upper swashplate using 6 $^{3}/_{8}$ inch #4-40 flat head machine screws.

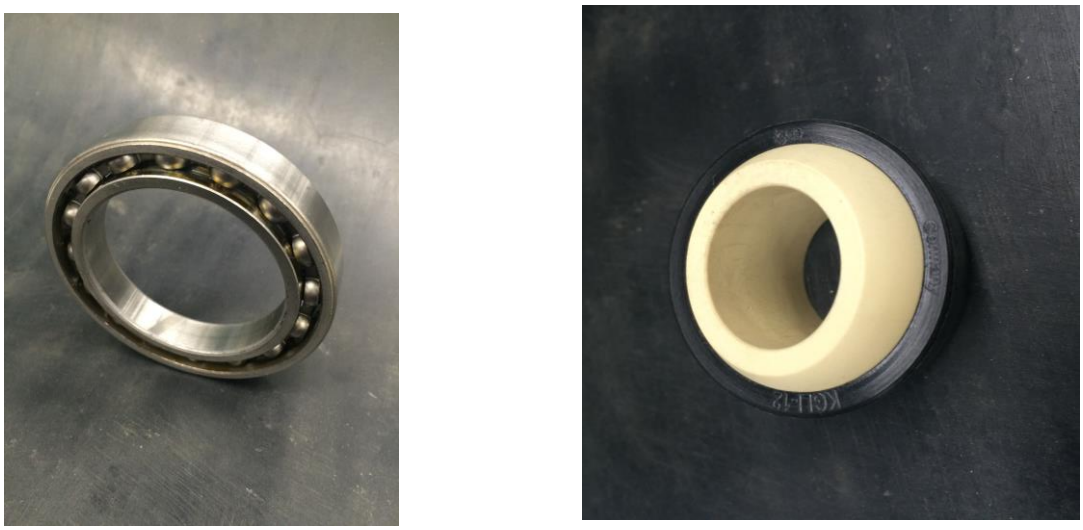

Figure 30: The two bearings used in the swashplate

The second bearing, a ball bearing, allows the upper and lower swashplate sections to rotate independently. For this internal bearing we initially selected a thin section, x-type 4 point contact, bearing by Silverthin®. This bearing had a thickness of only .25 inches, but again due to time constraints in manufacturing and shipping another bearing was chosen. The bearing that is in the final iteration of the swashplate is a Timken Ultra-Light series 9310K. This bearing has a bore of 50 millimeters, an outside diameter of 72 millimeters and a thickness of 12 millimeters. Because of the change in the thickness of the internal bearings the overall thickness of the swashplate increased to accommodate the larger size of the new bearing. The bearing is pressed fit into both the upper and lower halves of the swashplate and in both cased the press fit is backed up by a retaining ring that is fastened to each respective half of the swashplate using 6 $^{3}/_{8}$ inch #4-40 flat head machine screws.

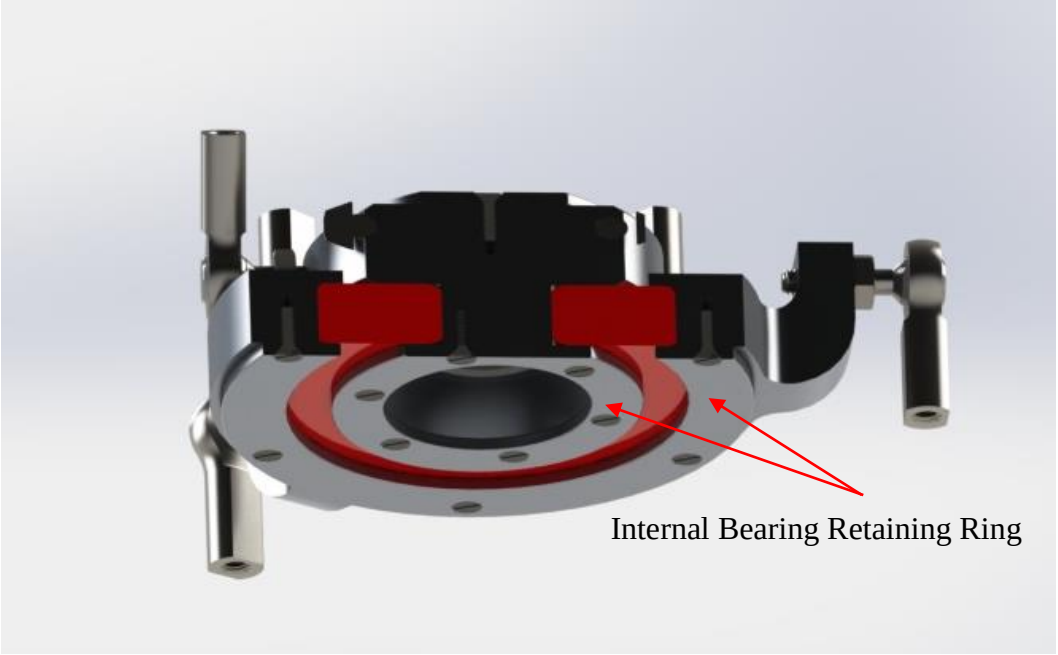

Figure 31: A Bottom view of the swashplate illustrating the two retaining rings.

In order to connect the swashplate with the rotor hub and the control servos we elected to use ball links. We choose ball links because transmit the vertical force of the control servo but allow the swashplate and control arms to pivot and tilt. The links in our preliminary designs consisted of a plastic M5 ball and socket type link from Igus®. After contacting Igus® we chose to use an alternative ball link from McMasterCarr® because they were available immediately. These links, shown in Figure 32, are all metal and have #10-32 thread.

In order to keep the control links all in the same plane the lower swashplate has control horns that raise 0.55 inches to the match the control plane of the upper swashplate. Each ball link's male thread is threaded into its respective half of the swashplate or rotor head. The female half of the ball links is attached to #10-32 threaded rod. Threaded rod is used to complete the control links by attaching the lower swashplate with the control servos and the upper swashplate with the rotor hub. The ball links are also used to attach each half of the swashplate to its

respective torque link. In total there are 13 ball links in our design, 4 of which are found on the rotor head, 5 on the upper swashplate, and the final 4 on the lower swashplate.

Figure 32: All metal #10-32 ball links from McMasterCarr®

3.1.10 Swashplate Torque Link Design

Torque Link Components

Since the upper half of the swashplate is located in the rotating frame and the lower half of the swashplate is located in the stationary frame, it is important to ensure that the upper half rotates at exactly the same speed as the rotor head while the lower half remains stationary. This is achieved by connecting the lower half of the swashplate to a fixed object and the upper half to the rotor head. The only caveat to this is that the swashplate must still be free to tilt and move in the vertical direction.

One option to limit the motion of the lower half and transmit the motion of the upper half is to just use the control linkages as torque links. The down fall of this is that the control linkages are comparatively fragile and are not designed to handle the torque and transmit control inputs. Therefore, two scissor links were designed.

The upper scissor link, shown in Figure 33 connects directly from a clamp on the driveshaft to the upper half of the swashplate. This transmits the torque from the driveshaft to the upper half of the swashplate forcing it to rotate at the same angular velocity. The clamp is a simple, two part, friction style clamp who internal radius matches the outside diameter of the upper driveshaft. It uses two 0.25 inch bolts to clamp down on the driveshaft. The clamp is connected to one side of an elbow. The other side of this elbow is connected to a ball link. The elbow in conjunction with the ball link allows the swashplate to travel vertically and tilt while still transmitting the rotational motion from the clamp to the upper half of the swashplate.

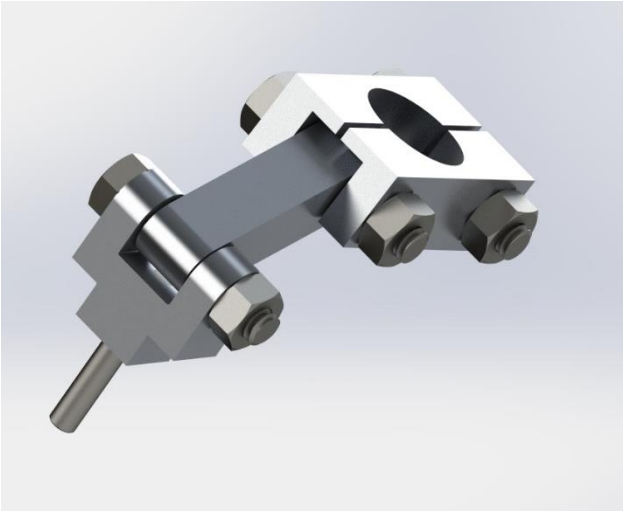

Figure 33: The upper torque link and driveshaft clamp

The lower scissor link operates in much the same way. The only difference is that instead of a clamp the elbow is connected directly to the servo mounting plate. This eliminates any rotation that is transmitted thought the internal bearing while still allowing the swashplate to tilt and travel up and down.

In both cases the friction at the elbow is small enough that we decided to forgo any sort of bearings. Although we have not incorporated them into our scissor links, we allotted space in

our design for nylon washers and inserts that could be used to negate any friction and allow for smooth vertical motion.

Follower Stress Analysis

The weakest point in the design of both scissor links is the #10-32 threaded rod. In the case of the upper scissor link the rod is placed in pure shear because it transmits the shaft torsion to the upper swashplate and must be mounted exactly vertical due to clearance issues with the control rods.

Using equation 26 the maximum shear stress can be calculated,

$$\tau_{Max=}\frac{F}{A} \qquad 26$$

where A is the cross sectional area which based on the #10 minor diameter of 0.1508 inches is 0.0178 square inches and an F of 200 lbf is the maximum estimated force the rod will be subjected to. This results in a shear stress of 11.19 ksi. When this is compared to 11,500 ksi which is the maximum allowable shear stress for A36 steel we can safely say that the threaded rod will not snap.

After ensuring that the control rods would not break, it was important to figure out if they would bend or deform. To do this the same equation, equation 26, was used to calculate the stress on the rod. Using the same parameters as shear stress calculation, this resulted in a stress of 11.19 ksi. To understand if the rod would bend this is compared to A36 steel's yield strength of 36 ksi. Based on this it is clear that the material will not bend, in fact based on the geometry of the control rods a force of 642 lbf would be need bend them.

In the case of the lower scissor link the forces will be much less due to the internal swashplate bearing and the rod can be angled so that it is placed in compression as well as shear. Base on this it is safe to say that the upper link will fail before the lower one.

3.1.11 Pitch Control System

The pitch control system is designed to move the lower nonrotating half of the swashplate via the lower control links. This causes the upper half of the swashplate to move and thru the upper control linkages forces the rotor head to adjust the pitch of each blade.

It does this by moving the 3 lower control linkages in the vertical direction. To achieve collective control all 3 linkages are moved at the same rate and time. To provide cyclic pitch control each control linkage would be moved on its own at its own rate.

Throughout our design process there has been three methods for pitch control. The first and simplest method is to use lead screws. This would require 1 lead screw per control rod for a total of 3. To change the pitch of the blades the lead screws would be adjusted as necessary. The down side to this system is that due to the fact the lead screws must be mounted on the servo mounting plate they could only be adjusted when the motor was off. The second option second option is to connect the lower control linkages to a mechanical system that through the use of pulleys and cables connected to joystick like control faces. This system would be very similar to that of an actual helicopter. It would require two separate control interfaces for collective and cyclic controls. The advantage that this system has over lead screws is that the pitch of the blade could be adjusted while the motor was running. The final option we considered is the use of digital control servos. This would require 3 servos, one for each of the lower control linkages. The servos would be controlled through a computer program such as LabView. Although this is the most complex and expensive option it has the advantage of being remotely controlled and it is the only option that can be fully integrated with the data acquisition system.

3.1.12 Rotor Head Design

The driving factor for the final diameter of the rotor head was spatial constraints. This was because the lab that the test stand is designed to operate in has very limited space. It was determined that the maximum allowable rotor diameter for the lab was around 1.5 meter. This required us to scale our rotor head and all its parameter to fit the lab. Scaling of the rotor head provided the necessary information on the rotational speed for the proper simulation of a full scale helicopter. This was done by matching the tip Mach number of the scaled rotor blades with the actual tip Mach number of a full scale helicopter. The result of the scaling led to a stand that is designed to operate with any rotor head system up to 1.5 meters in diameter.

Fully Articulating Rotor Head

In order to better simulate the conditions a full scale helicopter experiences we chose to design a fully articulated rotor head. This was because the fully articulated system provides considerable control and flexibility at the small scale sizes we are working with. By allowing the blade grip assemblies to rotate around all three primary axes via the feathering, drag, and flapping hinges, our fully articulated rotor head designed to minimize the stresses put on it in hovering conditions. Additionally, a fully articulated rotor head allows testing a greater variety of hovering conditions.

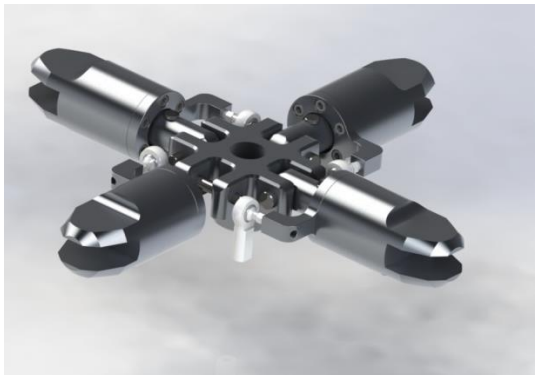

Figure 34: The fully articulated rotor head pictured without the driveshaft or blades

For this test stand we chose to go with a four blade rotor head, as shown in Figure 34. We chose a 4 bladed system because it provides the ability to test 4 or 2 blades. In our design there are 3 major hinges. They are the flapping hinge, the drag hinge, and the feathering hinge. The blade grip assemblies attach to the rotor hub via the flapping hinge, and the blades connect to the grip assemblies via the drag hinge. The feathering hinge is contained within the blade grip assembly.

Feathering Spindle and Blade Grip Assembly

The most important of the 3 hinges is the feathering hinge. Although it isn't a true hinge it is the joint that allows the pitch of the blades to be controlled. It does this by mounting a thrust bearing and a pair of roller bearings on a 0.375 inch spindle. The spindle is connected at one end to the flapping hinge while the bearings connect the other end to the blade grip. We chose to use two roller bearings because it eliminates the possibility of twist on the spindle while the single thrust bearing transmits any forces that act along the plane of rotation. This combination of bearings is important because it allows for smooth linear control inputs.

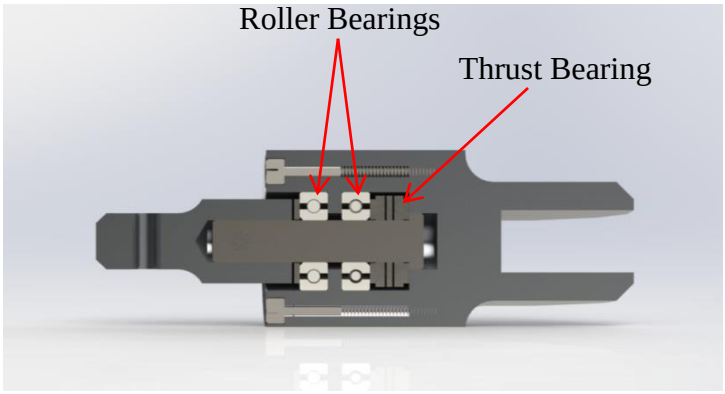

Figure 35: A cut away view of the control arm assembly

The bearings are contained within a 1.625 inch outside diameter housing that is connected to the control arms and the blade grip with 6 #8-32 socket head screws. The blade grip

contains a 14 mm wide by 30 mm deep slot that the rotor blade mounts into. The blade grip connects to the rotor blade with a single M5 screw.

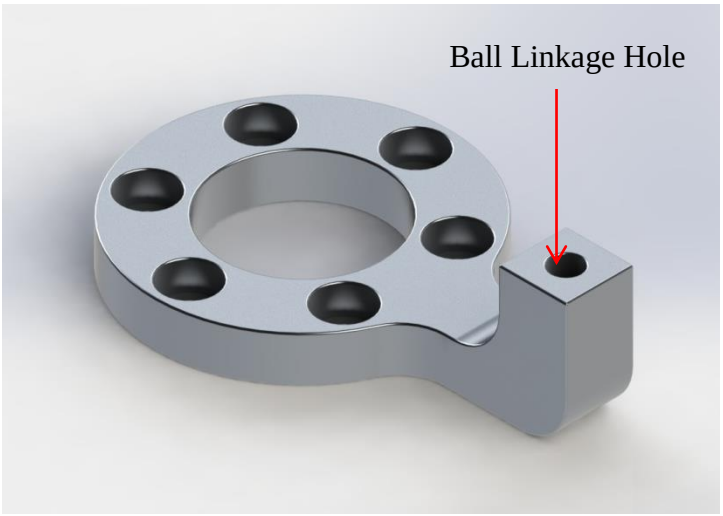

Figure 36: Control arm face plate viewed from the top down.

The control arm is bolted to the blade grip and bearing housing using the same 6 #8-32 socket head screws. The control arms control horn is connected to a ball link which connects it to the swashplate. The control horn is design so that at zero angle of attack on the blade the control linkages are perpendicular to the horizontal plane.

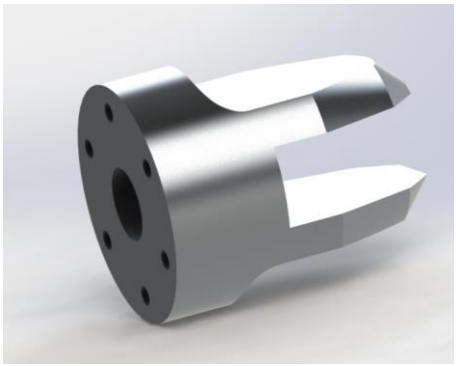

Figure 37: Side view of the blade grip

Flapping Hinge

The feathering spindle is connected to the flapping hinge by a 1 inch 0.1875 inch OD steel clevis pin. The pin passes through the end of the feathering spindle as well as the flapping

hinge and is held in place by a cotter pin. The flapping hinge, which allows each blade to flap up and down to reduce stress, is 1.8 inches long with a ¾ inch outside diameter. The innermost end is squared off so that it acts as a droop stop and prevents the blades from sagging below the horizontal plate of the rotor head when the motor isn't operating. The flapping hinge is connected to the rotor hub by a 1.625 inch ¼ inch OD clevis pin.

Figure 38: Side view of the flapping hinge.

Rotor Hub

Largest piece of the rotor head design is the rotor hub. It transfers the rotational motion and torque from the driveshaft to the blade grips which passes it on the rotor blades. Because of this the rotor hub is subject to the larges forces of our entire rotor head. With this in mind we decided to design our rotor hub out of a single piece of 6061T6 aluminum. We did this to eliminate joints and minimize the overall size of our rotor hub. The final overall dimensions of the rotor hub are 3.175 by 3.175 by 1.6 inches. The lower 0.8 inch half of the rotor hub is a 1.2 inch diameter cylinder that is expands into the upper 0.8" of rotor hub via a 0.1875" radius fillet.

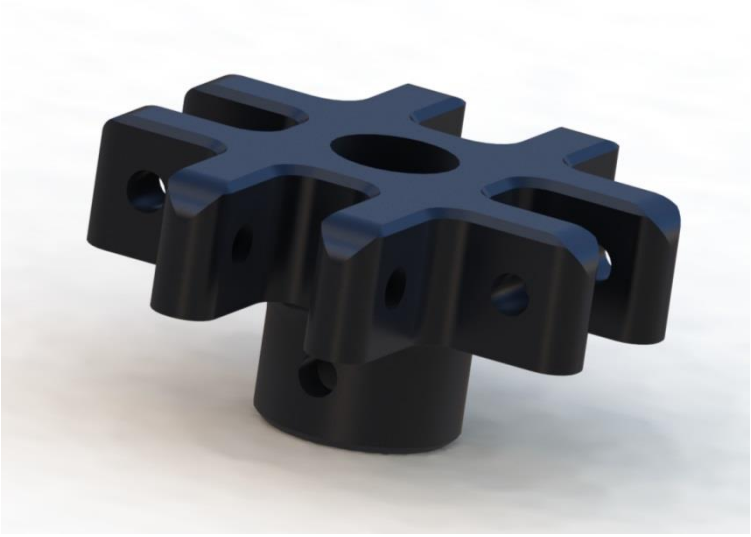

Figure 39: Side top view of the rotor hub

Since our design specification called for a rotor head that could accommodate up to 4 rotor blades our rotor hub was designed to this. It has 4 0.8875 by 0.6 inch slots that the flapping hinges are centered in. The pins that connect the flapping hinges to the rotor hub pass through the 0.4 inch thick arms of the slots via ¼ inch holes that are centered with respect to the arms. The top of each arm is 0.25" fillet on to allow the rotor blades to flap up unhindered. The rotor hub is connected concentrically the driveshaft via a combination of a 0.75 inch diameter through hole which the upper driveshaft passes through and 0.25 inch pin. The 0.25" diameter pin serves two purposes. It prevents the rotor head from sliding down the driveshaft and at the same time it forces rotor head to rotate at the same angular velocity as the driveshaft.

Stresses on the Rotor head

In order to determine if the rotor head design will withstand the forces it will be subjected to during normal operations, the maximum forces and moments were calculated. The forces were needed to calculate the stresses on individual components while the moments were used to

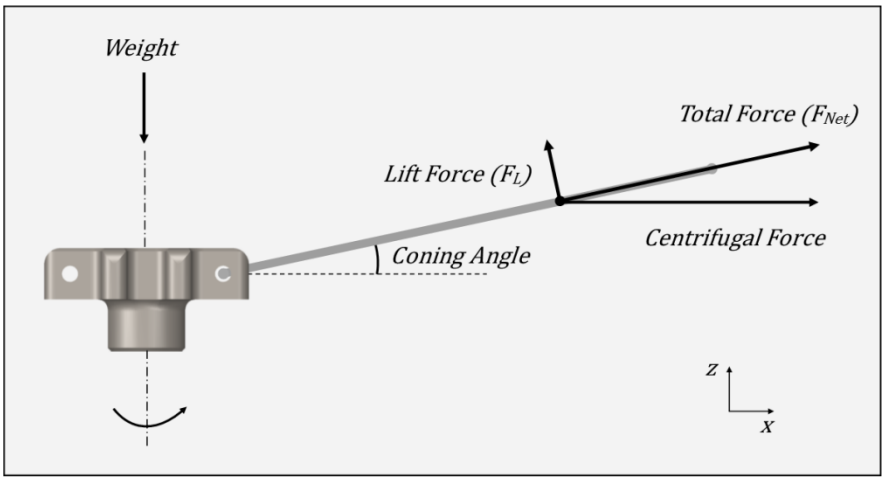

Figure 40: Principal Forces and Moments on the Rotor Hub

calculate the coning angle. By calculating the coning angle it was possible to evaluation of the various force components. The two most significant forces and moments on the components are those generated by the centrifugal force and the lift force as shown in Figure 40.

The rotor head is designed to operate between 1000 to 1350 rpms with a maximum radius of 0.6 meters based on this the forces and moments are calculated using 1500rpms. By using 1500rpm a margin of safety was built directly into the calculations.

When the moment generated by centrifugal force and moment generated by lift are equal the coning angle can be calculated. This is done by setting the equation 27

$$M_{cf} = \int_{er}^{r} m\Omega^2 y^2 \beta dy \tag{27}$$

equal to equation 28

$$M_{L_y} = -\int_{er}^{r} L_y dy \tag{28}$$

and solving for β. This yields formula, shown in equation 29

$$\beta = \frac{3\int_{er}^{r} L_y dy}{\int_{er}^{r} m\Omega^2 y^2 \beta dy} \tag{29}$$

after simplifications this leads to equation 30.

$$\beta = \frac{3\int_{er}^{r} L_y dy}{m\Omega^2 r^3(1-e^3)} \quad (30)$$

This results $\beta \approx 2°$ degrees when using an untwisted NACA 0012 airfoil spinning at 1500 RPMs and were r = 0.6m and er = .06m.

The component of force that acts horizontally outwards can be calculated using equation 31

$$F_{net} = \sqrt{F_x^2 + F_z^2} \quad (31)$$

Where

$$F_x = F_{cf} - F_{Lx}$$

and (32)

$$F_z = F_{Lz}$$

This can be further broken down using the coning angle to obtain equation 33

$$F_{Lx} = F_L \sin\beta$$

$$F_{Lz} = F_L \cos\beta \quad (33)$$

and equation 34.

$$F_{cf} = \int_{er}^{r} m\Omega^2 y dy = \frac{m\Omega^2(r^2 - er^2)}{2} \quad (34)$$

Then after substitution this leads to the equation 35

$$F_{net} = \sqrt{\left(\frac{m\Omega^2(r^2 - er^2)}{2} - F_L \sin\beta\right)^2 + (F_L \cos\beta)^2} \quad (35)$$

which using 1800 RPMs, m = 0.434 kg, a lift force of 12 N, r = 0.6m and er = 0.06m gives an F_{net} of 2751.9 N, or 618.65 lbf.

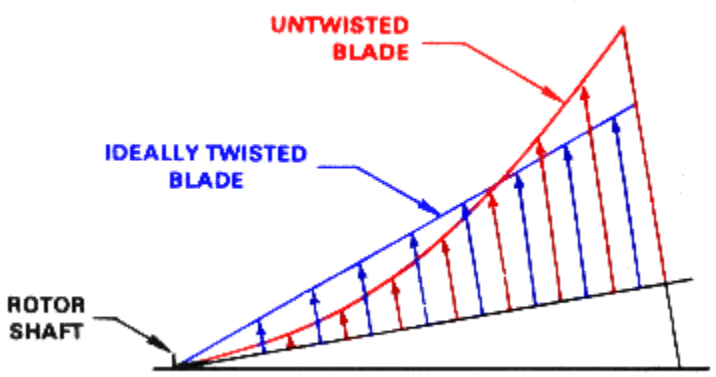

Figure 41: Lift Distribution on Twisted and Untwisted Blades (Cantrell)

The maximum allowable forces on each component are tabulated in Table 4. The maximum allowable forces were found using the equation 36

$$F = \sigma A \quad (36)$$

were σ a material property which changes depending on what type of stress the part is experiencing and A is the surface area under stress.

The maximum F_{net} is 618.56 lbf, which was compared to the maximum allowable force on each part to determine which parts will fail, if any. This comparison showed that the weakest part is HHTS-002-006, which will break if the force exerted on it exceeds 1374 lbf. This is more than 200% greater than the maximum possible force. Based on this information it is safe to say that the parts will not fail due to tensile or shear stresses.

Table 4: Maximum Forces on Each Component

Location of Force	N	lbf
Max force on HHTS-003-002	9424.8	2120.6
Max force on HHTS-003-001	32903	7403.2
Max force on HHTS-002-001	10282	2313.5
Max force on HHTS-002-006	6108.9	1374.5
Max Force on HHTS-002-003 at HHTS-002-006	9329.8	2099.2
Max Force on HHTS-002-001 at HHTS-002-006	9613.3	2163
Max Force on HHTS-002-002 at its head	17671	3976
Max Force on HHTS-001-006 at HHTS-002-002	24939	5606
Max Force on HHTS-002-002 at HHTS-001-006	72024	16205.4
Max Force on interior HHTS-001-001	9260.6	2083.6
Max Force on Blade Grip Hole	9139.2	2056.3

3.1.13 Design for Manufacturing

With a complex assembly such as our rotor head, manufacturing limitations were considered in the design. While performing conceptual and CAD design of the rotor internal radii, hole and tap sizes were selected to ease manufacturing. When milling, the internal radius is limited by the size of the tool used. For example, when using a .25 inch diameter tool, the minimum radius which can be machined is 0.125 inches. Internal radii were made as large as possible to allow the use of the largest tool possible for more robust machining. The internal radius design is especially important on the rotor hub, where a small radius is ideal for clearance around the flapping hinge. The internal radius of the rotor hub was optimized for the most compact clearance, and for use of a common sized end mill.

Hole and tap sizes were designed to be constant across the entire assembly when possible. For machining, common screw size and type reduces the variety of drills and taps required. This also simplifies hardware procurement and assembly.

3.1.14 Computer-Aided Design

Prior to manufacturing a Solidworks model was created to help dimension the sizes and clearances of each part and assembly. Each part was modeled to accurately represent the actual part on a 1:1 scale. All of the parts were assigned respective material properties, including density and yield strength, so that simulations, moments of inertia, and weights could be observed in Solidworks. Each part and assembly was given a part and assembly number designation and instructions on how to assemble them.

The rotor hub parts were subsequently combined into two subassemblies. The first contained the bearings for the feathering spindle and the control arm. The second contains the feathering spindle, blade grip, and flapping hinge. These two subassemblies were combined with the rotor hub and necessary fasteners to create the rotor head assembly.

The rotor head assembly was then combined with the driveshaft and control assemblies. The drive shaft assembly is made up of the upper and lower sections, the driveshaft drive pulley, the driveshaft bearings and all of the required fasteners. The control assembly contains the pitch control servos, the swashplate, the scissors link, and the control arms. These assemblies and the rotor blades are combined into a single rotor assembly.

The final two subassemblies are the stand assembly and the engine and engine mount assembly. The stand assembly comprises the frame and safety system on which the rotor head, drive shafts, control system, and engine are mounted. The engine and engine mount assembly contains the engine model, the engine drive pulley, the engine mounts and required fasteners.

Finally the stand, rotor assembly, and engine and engine mount assembly are combined into a single assembly that represents the entire design.

Each part was then represented in a drawing for manufacturing of the parts in-house. The drawings contained all of the necessary dimensions, tolerances, and other information required for manufacturing. Drawings were also created for all of the sub-assemblies and the final assembly. The subassembly drawings contain assembly instructions, fastener types, information on where thread-lock or thread-locking wire is recommended, and reference dimensions. The final assembly drawing contains the necessary information for assembling the subassemblies.

3.2 Budgeting

The funding provided to this MQP through the WPI Aerospace Engineering Department was $160.00 per student, or $480.00 total. After the initial research it was quickly determined that this budget would not be sufficient. Any data acquisition system or slip ring would cost thousands of dollars, and a low cost motor and VFD combination would cost several hundred. As a first attempt to secure more funding we attempted to contact helicopter and component supplier companies explaining our research and the need for additional funding. Of these cold contacted companies we had no responses. The only aid we were able to secure was from J&E Precision Tool Inc., a manufacturing company which also employed a member of our team. Through that existing relationship, J&E offered access to their excess raw material stock and scrap.

The first two-thirds of this project were advised by Professor Maria Chierichetti, who created the initial requirements and had a specific use intended for this device. With her research funding through the Structural Vibrations lab which she administered, she agreed to purchase a fiber-optic strain measuring system. After being required to change advisors to Professor Anthony Linn, the MQP lost access to the research funding provided by Professor Chierichetti.

The small budget has severely affected the design of the helicopter hover test stand. All efforts were taken in the design stage to stay within the budget. One of the most time and energy consuming compromises was being forced to design and manufacture a rotor hub and swashplate system. These systems are readily commercially available, but were too expensive for us to consider.

Our final itemized budget is included in

Appendix F.

3.3 Manufacturing

3.3.1 Process Documentation

Due to the large number of complex parts included in the rotor head assembly, a process documentation system was created. Manufacturing process sheets were developed to outline the steps involved in manufacturing each particular part and assembly. They feature part identification, a list of operations, and record quantities and dates of parts produced. The purpose of the process sheets is to ensure part quality and traceability, with the secondary purpose of allowing future collaborators to modify or remanufacture parts.

The operation lists outline the detailed steps taken to manufacture each part. These documents contain setup and tooling information, computer numeric controlled (CNC) programs, and a dimensioned drawing for inspection.

A sample of these manufacturing and operation sheets were included in Appendix B, as well as published in a binder to be kept with the testing apparatus should modifications be necessary. All CNC and CAD files were also published to a USB drive to be stored in the manufacturing binder.

3.3.2 Computer-Aided Machining

Computer-Aided Machining (CAM) was performed when CNC machining equipment was desired. The CAM software used was ESPRIT, which utilizes reference geometry to create tool paths which produce the desired part. The program outputs this tool path information as a G-code, which is a system of commands and coordinate points which control the CNC machines.

For a particular part, there may be multiple set-ups required in order to complete the part. These set-ups must be planned in conjunction with the CAM programming.

3.4 Safety Enclosure

A very important aspect of the design of the helicopter hover test stand is the safety enclosure. Without it, it is too dangerous to run the system. That being said, the safety enclosure must be able to successfully contain any and all parts that come off of the rotor hub. This means that, in the event of a failure during testing, the safety system must provide complete protection to the operator and any other occupants of the lab.

The preliminary conceptual design of the system used a wire mesh, such as chain link, to completely surround the test stand and contain any large parts that break off during testing. The problem with the preliminary design was the size of the wire mesh, which limited the size of piece that could be contained to the size of the chain link. Any object smaller than the gaps in the chain link would pass though the safety system without any loss of energy.

To eliminate the possibility of small pieces passing through a wire mesh barrier, the next conceptual design incorporated solid barriers. It used 4 solid sheets that, when connected to each other, form a box around the helicopter hover test stand. When the stand is not in use the box can be broken down into individual sheets to maximize lab space and easy storage. One possibility for the sheet material is plywood with a Lexan viewing window.

Another option for the solid barriers was steel sheets backed by steel ribs. They would form a barrier of approximately 60”x60” that would be mounted at the height of the rotor hub. In addition to the steel sheets the system would have a mesh that extended below the sheets to contain anything that fell below the main containment sheets. An advantage to this containment system that it is very strong for its weight, however it would require its own stand and is more difficult to breakdown for storage.

After debating the advantages and disadvantages to each type of system, we settled on the steel barrier containment system. This was because it provides the best strength to weight of all the options available and it provides more complete containment unlike wire mesh. Another large factor in the decision to use a steel sheet containment system was the price. It is important to note that old wind tunnel ducts were donated to our project and with some minor modifications were converted into the containment system.

3.5 Assembly

The following subsections are meant to supplement the assembly drawings contained in Appendix A. They describe the basic assembly process for each individual assembly.

3.5.1 Feathering Spindle Assembly

To assemble the feathering spindle assembly (HHTS-001), begin with the bearing housing (HHTS-001-001) itself. First, the two roller bearings (HHTS-001-003) were seated in the center hole, followed by a washer (HHTS-001-005). Next, a thrust bearing (HHTS-001-004) was placed on top of the washer (HHTS-001-005) on the deeper side of the bore. This was also followed by a washer (HHTS-001-005). The assembly was completed by adding the faceplate control arm (HHTS-001-002) opposite the thrust bearing. This process was repeated 4 times, once for each of the thrust bearing housings.

3.5.2 Pitch Control Arm Assembly

First, to begin assembling the pitch arms, the feathering spindle (HHTS-002-003) was added to feathering spindle assembly (HHTS-001) by threading it through the center bore of the bearing housing and faceplate control arm. The head of the feathering spindle was then inserted into the counter bore of the blade grip (HHTS-002-002). The blade grip was then fastened to the feathering spindle assembly, after the alignment was double checked, by 6 control arm screws (HHTS-001-006) that were installed using thread lock to ensure that they don’t back out while the rotor head is spinning.. Finally to complete the control arm the flapping hinge (HHTS-002-001) was attached by placing it over the end of the feathering spindle and locking the two together using the feathering spindle clevis pin (HHTS-002-004), which was secured using a cotter pin. This process was completed 4 times to make the pitch control arms (HHTS-002).

3.5.3 Rotor Head Assembly

To complete the rotor head (HHTS-003), the 4 control arms (HHTS-002) were attached to the rotor hub (HHTS-003-001) using a single flapping hinge clevis pin (HHTS-003-002) each. Each pin was secured using a single cotter pin. Finally, on each of the control arms a single ball link (HHTS-006-004) was attached to the faceplate control arm using thread lock to ensure it would not back out during operation. The complete rotor head was then set aside to allow for the completion of other assemblies.

3.5.4 Follower Assembly

The lower half of the follower was assembled prior to the final assembly. This was done by attaching the receiver link (HHTS-005-004) to the force link (HHTS-005-003) using a single upper link bolt (HHTS-005-006) and nut (HHTS-005-006). The rest of this assembly had to wait until the final assembly due to how it fit together with the driveshaft and attached to the swashplate.

3.5.5 Swashplate Assembly

To begin the swashplate assembly (HHTS-006), the spherical bearing (HHTS-006-006) was pressed into the bore of the upper swashplate (HHTS-006-001). The spherical bearing retaining ring (HHTS-006-007) was then attached to the upper swashplate to hold the spherical bearing in place using six retaining ring screws (HHTS-006-005) secured with thread lock.

Next, the swashplate roller bearing (HHTS-006-003) was pressed onto the bottom of the upper swashplate. The upper swashplate was then fitted into the bore in the lower swashplate (HHTS-006-002). A retaining ring (HHTS-006-008) was then attached to the inside of the lower swashplate, and secured with six retaining screws and thread lock. Another retaining ring, the outer retaining ring (HHTS-006-009) was also attached to the bottom of the lower swashplate

and secured using six retaining screws and thread lock to ensure that none of the screws backed our during operation.

Completing the swashplate required attaching nine ball links (HHTS-006-004) to the swashplate. Five ball links were attached to the upper swashplate: four for the control rods and one for the follower. Four ball links were attached to the lower swashplate: three for the servo control rods and one for the lower follower. All the ball links were secured in the swashplate using thread lock.

3.5.6 Final Assembly

Completing the assembly of the rotor head system required having each of the above assemblies completed and inspected to ensure all components were properly secured.

The first step in beginning the final assembly was to slide the completed swashplate assembly (HHTS-006-006) onto the driveshaft. Once the swashplate was mounted to the shaft, the articulation of the swashplate was checked to ensure there were no clearance issues before completing the final assembly.

The next step in the final assembly was to place the rotor head assembly (HHTS-003) onto the driveshaft. Once on the driveshaft, the head would be secured to the shaft using the rotor hub retaining pin (HHTS-003-003), which slides through the base of the rotor head and the driveshaft. This pin keeps the rotor head spinning with the shaft and is secured with a cotter pin. Next, the Jesus Nut (HHTS-004-004) was threaded onto the top of the driveshaft and secured a cotter pin. The cotter pin runs between the posts on the, castle style, Jesus Nut and through a hole in the upper driveshaft to keep the Jesus Nut from backing off during operation.

Next, the follower was attached to the driveshaft below the rotor head. The two pieces of the follower clamp (HHTS-005-001 and HHTS-005-002) were fitted around the driveshaft and

secured using the two ¼-20, 1. 5” bolts (HHTS-005-006) secured with ¼ nuts (HHTS-005-005). Thread lock was used to keep the bolts from backing out during operation. The follower post (HHTS-005-007) was then attached to the fifth ball on the upper swashplate, completing the follower assembly.

The final step in completing the final assembly was to attach the control rods (HHTS-010-004) to the swashplate and pitch control arms. The four rods were first threaded into the four ball links on the upper swashplate. Then, the four rods were aligned with the pitch control arms on the rotor hub and threaded into the ball links on the four pitch control arms.

3.6 Data Acquisition System

Due to budgetary constraints, a DAQ system could not be acquired, however research into DAQ options was performed to determine the most suitable option. In this section we discuss the types of applications the DAQ system would need to be capable of analyzing. This includes stresses and strains along the blades, as well as being compact enough to mount on the hover test stand without interfering with its operation.

The chosen DAQ system for this application was fiber optic Bragg gratings since they offer the most flexibility for measurements and mounting.

3.6.1 Data Acquisition Box

The main component of the data acquisition (DAQ) system is the data acquisition box. The DAQ box will enable all of the data that the various sensors gather to be organized and compiled into a signal that a computer program such as LabVIEW can understand. This is crucial for data analysis and allows the operator to gather accurate real time data for analysis at a later time. Using a DAQ box in conjunction with LabVIEW allows the operator to build virtual programs and measure numerous quantities of interest. A few of the quantities that could be measured are the stresses and strains on the rotor blades as well as blade rpms.

3.6.2 Stress Measurements and Data Transfer

Stresses and strains on the rotor blades are two important quantities which the DAQ system would be used to analyze. This would be accomplished through the use of fiber optic cables that use Bragg gratings to quantify stresses. To successfully operate fiber optic cables with Bragg gratings a number of components are required. These components include a light source such as a LED, a source of power for the light, a coupler and a detector.

The power source must be mounted somewhere in the rotational frame. The LED is used to illuminate the fiber optic cable, which can be mounted on the blades as desired. The Bragg gratings are also completely customizable, meaning that they can be placed at any number of points on the fiber optic cable. The coupler must be mounted on the rotor hub above the driveshaft so that it sends the light pulse down another fiber optic cable that passes through the center of the driveshaft. At the end of the driveshaft the fiber is output towards the receiver.

At the receiver, there will be a small gap between the end of the fiber and the receiver. This allows the fiber to rotate freely with the shaft while also allowing the receiver to remain stationary with respect to the DAQ box. The receiver will be wired to the DAQ box, and converts the light signals to electrical signals which can then be processed by the DAQ box and sent to a computer for analysis.

3.6.3 Angular Velocity Measurement

Another important quantity that must be measured is the rotational velocity. In order for the rotor blades and rotor heads to be successfully tested, the scaled rate of rotation must be successfully matched and maintained. The rate of rotation can be measured in a number of ways. One simple solution is establishing a relationship between the VFD output and the rotor head rotational velocity. However, since the load on the motor is dependent on the angle of attack of the blades, the rate of rotation changes for any given VFD output as the angle of attack of the blades change. Therefore, the VFD output method only gives a rough estimate of the blade velocity.

Another method of measuring rotor head rpms is fitting a tachometer to the driveshaft. This would measure the rate of rotation of the driveshaft which is fixed to the rotor head, meaning that the rotor head speed must equal the driveshaft speed. An important advantage to

this system is that the tachometer can be mounted in the stationary frame and still successfully measure the rate of rotation of the rotor head. This means that the tachometer could be connected to the DAQ box and its data collected and outputted directly to a computer analysis program. This method would also give real time rpm measurements that would be crucial to running the rotor head at the correct speed.

3.7 Test Plan

In order to judge the success of this project, the design and its components must be tested. The first component that would be tested is the motor in conjunction with the VFD to ensure proper functionality and to gain a better understanding of how the two components interact. After completing the preliminary engine and engine control testing, the safety system would be tested.

The safety system would be tested to ensure that it can contain any failures in subsequent operational tests. Once the safety system is tested to satisfaction the motor would be combined with the rotor head to test the drive shafts, the stand, and the rotor hub functionality.

The most critical component of the rotor head system is the swashplate since it provides pitch control. Due to the size of the rotor head, a custom swashplate was designed and manufactured. The first test would be to analyze the articulation of the swashplate on the driveshaft to ensure it can provide the necessary angles of attack. This test would be performed with the swashplate mounted on the driveshaft with the scissor link attached.

The second test performed would be on the rotor head itself to analyze the range of articulation. In order to operate as designed, the rotor head must be able to fully articulate to simulate collective and cyclic control inputs, changing simultaneously the pitch blades. To conduct this test, the rotor head would be mounted on the driveshaft and left static. This would ensure that the droop stops incorporated into the design keep the arms from articulating vertically downward. Next, the flapping motion of the arms would be tested to ensure they move freely and without interference. Finally, the pitch arms would be used to check that the angle of attack of the blades can be changed.

For the final test, the rotor hub would be attached to the drive shaft, and the control rods would be connected to both the swashplate and the rotor head. Testing the articulation of the swashplate and the corresponding collective and pitch change in the blades will be conducted. This test will ensure that the swashplate functions properly and results in pitch change of the blades. Alignment of the swashplate with the pitch arms on the rotor head will also be checked to ensure the control rods are positioned vertically upward at zero lift, rather than at an angle to the mast.

The final test prior to attaching the rotor blades would be the testing and verification of the pitch control system. This test is designed to verify the functionality of the pitch control servos, their corresponding linkages and the feathering spindle.

After successfully completing tests on the safety system, the motor, the stand, and the pitch control, the blades would be attached to the rotor head. The tests would then be run again to verify that our design could withstand day to day operation. Some of the data that would be collected from this test is the relationship between engine speed and rotor hub speed. The test would also verify that the control system can successfully vary the pitch of the blades under any condition. Finally, this test would confirm that the whole system can operate safely as a helicopter hover test stand and preform all of the experiments for which it is designed.

Chapter 4: Conclusions and Recommendations

The following section documents the changes that were made in the design specifications throughout the course of the entire project. It also details compromises that we were forced to make to complete the project on time and on budget. Finally this section contains the conclusions and recommendations that we have for future design changes and addition to the test stand.

4.1 Changes in the Project Scope

Initially the design specifications for this project were to design, build and test a helicopter hover test stand. The preliminary purpose of the test stand was to run structural and vibrational analyses on rotor blades in order to achieve a better understanding of various blade designs. The project requirements called for a rotor head, a control system, a motor, a stand, a safety system, and data collection equipment. Other parameters included meeting a 480 dollar budget requirement and a completion deadline of March 6, 2015.

The first major change in this project came early on when the requirements for physical data collection and analysis equipment was dropped. Due to the cost of data collection systems, such as slip rings and the proposed fiber optic sensors, it was decided that it would be better to use the limited budget designing and building the rotor head and associated components. The limited budget would not allow for the purchase of both the data collection equipment and the components needed to build the test stand.

The next and most significant design change came as a result of a change in project advisors, which readjusted the focus of the project from building a test stand that would be used for structural and vibrational testing in hover situations to a test stand that could be used under a variety of conditions and for a variety of tests in a wind tunnel. The new conditions included forward flight as well as hover.

The addition of forward flight to the test stand allows for the testing of dynamic stalls as well as other flight characteristics. To successfully control the rotor head when it was under forward flight conditions a fully functional swashplate was needed. The swashplate had to be able to accept and relay inputs from a minimum of at least 3 servos or lead screws.

The final change in the design specifications was a reduction in what was required to be physically manufactured and built. Build requirements were reduced to just the upper section of the driveshaft, the rotor head, and the swashplate, which decreased the time needed to manufacture and assemble the components. The elimination of the power source reduced the budget stress significantly due to the cost associated with the electric motor and its corresponding VFD.

4.2 Design Compromises

As the project progressed it became clear that we would have to make some compromises in order to complete the project with in the budget and before the deadline. The first compromise that was made was a manufacturing compromise. Early on in the design of the test stand, we had to decide which components to manufacture and which to purchase. Initially, we chose to purchase as many commercially available components as possible due to their ready availability and generally proven designs. Due to budgetary constraints this was not feasible.

Designing a Rotor Head

The rotor head designed for this project is the most prominent example of components needing to be manufactured on campus in order to remain within budget. Purchasing a rotor head would have allowed the project focus to shift to designing a stand and data acquisition system. However, due to the costs associated with rotor heads large enough to accommodate 0.5m blades, it became clear that designing and manufacturing our own rotor head was more cost effective. By designing our own rotor head, the only associated costs were those of raw materials and hardware. The raw material cost was further minimized by material donations from several sources.

Designing a Swashplate

Initially, as with the rotor head, we looked into buying a commercially available swashplate, such as a replacement swashplate for a 700 series model helicopter. Again this proved to be too expensive, and like with the rotor head, we were able to design and manufacture a swashplate for less than the cost of those that were commercially available. This proved beneficial for a number of other reasons. The first of which was that by designing our own swashplate, we were able to expand the size of the driveshaft, making it much less difficult to

manufacture and leaving room for sensors and electronics run through the shaft. Another benefit that the custom swashplate has over a stock model is the location of the ball links which connect to the control rods. It is important that the control rods be as close to vertical as possible when all of the blades are at zero degrees of pitch. Commercially available swashplates were too small in diameter, meaning that the diameter of the pitch arms on the rotor head would not line up with the ball links on the swashplate.

Designing a Driveshaft

Although the increased size of the swashplate allowed for an increase in the outside diameter of the driveshaft, the overall length still created problems. First, we were unable to find a commercial driveshaft with the desired combination of inside and outside diameters as well as the required length. Therefore, we were required to manufacture our own. Since the driveshaft had to be hollow to leave room for sensors and other electronics, we needed to drill out the center of a tube. Due to the extreme depth that would have had to be drilled, we elected to compromise and cut the driveshaft in half. Although this made manufacturing less difficult, it created its own set of challenges. Namely, the two driveshafts would have to be connected concentrically. To achieve this we designed a 0.984” diameter extrusion into the upper driveshaft and a matching hole into the lower driveshaft. The extrusion has a 60 degree chamfer on it to ensure the two parts seeds concentrically. This combined with the fasteners forces the driveshafts to rotate eventually and concentrically.

4.3 Recommendations

After the design, manufacture, and build of the hover test stand a number of recommendations for future versions of this project were established. They include a larger budget, well established project parameter, readily available internal components such as bearings, the use of commercially available rotor head components, building a prototype early on in the design and access to a fully stocked and functional machine shop.

The first recommendation, and perhaps the most important, is an increase in the 480 dollar budget. By increasing the budget the project would have become much more feasible. It would have allowed for the purchase of raw materials for manufacturing instead of having to rely on donations. It would have allowed for the purchase of an engine and required controls with excess power. This would have left room for expanded testing regimes and larger rotor heads. It would have made high quality bearings available, leading to reduction in size of all the swashplate and rotor head. More significantly an increase in budget would have allowed for the purchase of commercially available rotor heads and swashplates, or along the lines of our preliminary objectives it would have allowed for the purchase of data analysis equipment.

Based on the cost of raw materials, an engine, its associated controls, commercially available rotor heads and swashplates, and data analysis equipment a minimum of 10,000 dollars is recommended. This number would increase exponentially with the number and quality the data analysis equipment. If data analysis is taken out of the equation, the budget could be reduced to around 5,000 dollars. This would cover the cost of an engine, a VFD, material for the stand and safety system, controls for the rotor head, material for the rotor head, and possibly the use of commercially available rotor head components from large model helicopters.

One solution to the budget shortages is to obtain outside sponsors. By soliciting and gaining sponsorship from a commercial company or a person the budget would have been drastically increased. This would have allowed for better designs and less compromises. Additionally outside sponsorship could have provided raw materials, parts, and expertise such as industry knowledge that could have been used to further the design of the test stand.

The second recommendation is the establishment of project parameter at the beginning of the project. By establishing realistic and focused goals early on, the project would have been more achievable. This could have narrowed the focus of the project from building an entire rotor system, power system, stand, safety system and data analysis system on 480 dollars to just building the rotor head or just the stand. This would have allowed for a much more though design and a reduction in the number and size of the compromises that were made.

After having to make significant design changes in the later stages of the design, and even during some of the machining stages, it would have been beneficial to have the bearings and internal components on hand prior to manufacturing. This is because after struggling to find a bearing that fit the restrictive dimensions of the swashplate and budget of the project and beginning the process of manufacturing, it was discovered that the bearings have 8 plus week shipment times due to back orders. This called for a complete redesign of the swashplate in order to house a much larger and readily available internal bearing. This dilemma would have been avoided if the design and been established earlier on allowing for the internal components to be ordered prior to machining.

Another option that would have minimized the total machining would have been the use of commercially available helicopter parts, such as those used on large scale model helicopters. This would have been easier than manufacturing and it would have allowed more in-depth study

and the possible use of data analysis equipment, given a larger budget. By buying a commercially available rotor hub and swashplate the overall size of the rotor head would have been reduced since the need for readily available bearings would have been eliminated. Commercial parts would have the advantage of having replacements readily available, they would not have to be costume manufactured. The reason why commercial model helicopter parts where not used in this project came down to budget. With 480 dollars it was impossible to buy model parts and still have enough money for other required components.

For the production of high quality parts, good machine tools and equipment is essential. While it is understood that the vast majority of WPI students are not professional machinists, the tooling and inspection tools are of poor quality and insufficient for the production of a component as complicated and critical as a helicopter rotor hub and swashplate.

The one manual lathe on campus is inadequately tooled. Several holders for turning inserts have stripped screw heads, making it nearly impossible to change out a worn or cracked insert. There are several insert types without a replacement in stock. The poor quality of these turning tools leads to slower roughing and finishing and decreases surface finish quality. In one case, the inability to change an insert prompted the group to make a custom turning tool from tool steel. The group also believes that the manual lathe may have a timing issue which prevents the cutting of accurate threads.

Inspection tools at the WPI shops were also substandard. Anything more accurate than a digital caliper was in poor condition and prompted the group to borrow personal inspection tools. Also, with the complex parts inspection becomes more difficult. Simple inspection equipment such as a granite surface plate and gage blocks were unavailable. As a result, several critical dimensions went uninspected.

Accountability in the machine shops is very low, especially due to unauthorized, unsupervised, or unexperienced after-hours users. Upon several instances machine tools were found in a state of disrepair or neglect. For the manual machines, important handles and knobs have been found broken or missing. This forces the team to repair these parts before using the machine, costing time and patience.

The team was lucky to have connections with an outside machine shop with superior equipment and tooling. We traveled to this company several times to use their equipment and borrow cutting and inspection tools. The WPI machine shops should be properly tooled and stocked with quality equipment such as that we should not have had to find another shop to work in.

4.4 Conclusion

Our group successfully designed and manufactured a fully articulated four blade helicopter rotor head system for use on a helicopter hover test stand. These components included the rotor head, rotor mast, and swashplate to control the rotor. The design of the rotor allows for simulating both hover and forward flight conditions utilizing blades up to one half meter in length. In designing the rotor head system, the group also performed stress analyses on critical components of the rotor head system to ensure the components would not fail during testing.

Additionally, designs and analyses were completed for other stand components necessary for a functioning hover test stand. These include a driveshaft, power transmission system, motor mount, servo mount, motor, and motor drive specifications. Each of these components was thoroughly designed and evaluated throughout the project, and computer aided design models were created for each required component. The components were also analyzed analytically to ensure the proposed design would function properly without failure.

The final assembly of the manufactured components was the culmination of our design process. Although the fully functioning stand was not realized, the design and assembly of the rotor head system proposed a significant challenge. Our group was able to meet the requirements of that challenge and successfully design and build a functioning fully articulated rotor head system.

Works Cited

(n.d.). Retrieved from National Instruments Corporation: http://sine.ni.com/ds/app/doc/p/id/ds-371/lang/en

(n.d.). Retrieved from Rotary Systems Inc.: http://img.directindustry.com/images_di/photo-g/hollow-shaft-slip-rings-17337-3804803.jpg

Helicopter Flight Training Manual. (2010, May 21). Retrieved from Transport Canada: https://www.tc.gc.ca/eng/civilaviation/publications/tp9982-exercise3-4910.htm

Sikorsky. (2012, February 14). Retrieved from Press Releases: http://www.sikorsky.com/About+Sikorsky/News/Press+Details?pressvcmid=54d69880ddd75310VgnVCM1000004f62529fRCRD

Fiber Bragg Grating Principle. (2014). Retrieved from FBGS Technologies: http://www.fbgs.com/technology/fbg-principle/

Fiber Bragg Grating Sensors. (2014). Retrieved from Epsilon Optics: http://www.epsilonoptics.com/technology.html

AutomationDirect.com Inc. (2014, February 06). IronHorse GSD4 Series DC Drives User Manual.

Cansdale, R. (1974). *An Aeroelastic Model Helicopter Rotor*. London: Her Majesty's Stationery Office.

Cantrell, P. (n.d.). *Rotational Velocities.* Retrieved from Copters.com: http://www.copters.com/aero/rotational_vel.html

Commercial - Industrial Slip Rings. (n.d.). Retrieved from Moog: http://www.moog.com/products/slip-rings/commercial-industrial-slip-rings/high-speed-slip-ring-capsules/ac3757/

Fulton, M. P., Gold, N. P., Nielsen, G. E., Mansur, M. H., & Tischler, M. B. (2012). *Development and Hover Testing of the Active Elevon Rotor.* Moffett Field, California: US Army Research, Development, and Engineering Command.

Lecklider, T. (2008, January). *Wireless Sensor Networks are Taking Over.* Retrieved from Evaltuation Engineering: http://www.evaluationengineering.com/articles/200801/wireless-sensor-networks-are-taking-over.php

Lee, B.-E., Byun, Y.-S., Kim, J., & Kang, B.-S. (2011, March 15). Experimental hover performance evaluation on a small-scale rotor using a rotor test stand. *Journal of Mechanical Science and Technology*, pp. 1449-1456.

Leishman, J. G. (2006). *Principles of Helicopter Aerodynamics.* Cambridge, New York: Cambridge University Press.

Lewis, C., & Darbo, J. H. (2006, May `02). Helicopter Ground Resonance. *Flight Safety Information Journal*, p. 1.

Lienhard, J. H. (n.d.). *WHEN METALS GROW TIRED*. Retrieved from Engines of our Ingenuity: http://www.uh.edu/engines/epi2260.htm

Palacios, J. (n.d.). *Adverse Environment Rotor Test Stand*. Retrieved from Pennsylvanis State University Aerospace: http://www.aero.psu.edu/facilities/aerts/

Salt, J. (2014). *The Basics of Flybarless Rc Helicopters*. Retrieved from RCHelicopterFun.com: http://www.rchelicopterfun.com/images/Flybar_Head250pics.gif

Sicard, J., & Sirohi, J. (2013, May 14). Measurement of the deformation of an extremely flexible rotor blade using digital image correlation. *Measurement Science and Technology*.

Sirohi, J., & Lawson, M. S. (2012, April 6). Measurement of helicopter rotor blade deformation using digital image correlation. *Optical Engineering, 51*(4). doi:doi:10.1117/1.OE.51.4.043603

Timken. (2015, March 2). *Timken Online Catalog* . Retrieved from Timken.com : http://www.timken.com/en-us/products/Documents/Timken-Ball-Bearings-Catalog.pdf

UM Aerospace Engineering. (2014). *Active Aeroelasticity and Structrues Research Laboratory*. Retrieved from UMICH/MIT: http://a2srl.engin.umich.edu/facilities/helicopter_test_stand.html

University of Dayton Research Institute. (2014, December 8). *Fatigue Life Testing & Analysis* . Retrieved from University of Dayton Research Institute, shaping the technology of tomorrow : http://www.udri.udayton.edu/Capabilities/Aeropropulsion/Pages/FatigueLifeTestingAnalysis.aspx

Variable Frequency Drives. (n.d.). Retrieved from Dealers Industrial Equipment, LLC: http://dealerselectric.com/33HP115VoltInputBrookMotorVFDPackage.asp

Appendix A

Included in this appendix are SolidWorks drawings for the parts and assemblies described in Section 3.5, which provides explanations for the assemblies which were manufactured.

Additionally, this appendix contains SolidWorks drawings for parts and assemblies which were designed as part of the project requirements, but not manufactured.

ASSEMBLY NUMBERS AND COMPONENTS FOR HELICOPTER HOVER TEST STAND (HHTS)

ASSEMBLY	**COMPONENT**	**NAME**	**QTY**	**SPECIFICATIONS**
HHTS-001	**HHTS-001**	**FEATHERING SPINDLE HOUSING**	**4**	
	HHTS-001-001	BEARING HOUSING	4	
	HHTS-001-002	FACEPLATE CONTROL ARM	4	
	HHTS-001-003	ROLLER BEARING	8	
	HHTS-001-004	THRUST BEARING	4	
	HHTS-001-005	WASHER	12	
HHTS-002	**HHTS-002**	**CONTROL ARMS**	**4**	
	HHTS-002-001	FLAPPING HINGE	4	
	HHTS-002-002	BLADE GRIP	4	
	HHTS-002-003	FEATHERING SPINDLE	4	
	HHTS-002-004	FEATHERING SPINDLE CLEVIS PIN	4	13/16", Φ3/16"
	HHTS-002-005	CONTROL ARM SCREW	40	#8-32, 1.5"
HHTS-003	**HHTS-003**	**ROTOR HEAD**	**1**	
	HHTS-003-001	ROTOR HUB	1	
	HHTS-003-002	FLAPPING HINGE CLEVIS PIN	4	1 7/16", Φ1/4"
	HHTS-003-003	ROTOR HEAD RETAINING PIN	1	1 5/16", Φ1/4"
HHTS-004	**HHTS-004**	**DRIVESHAFT**	**1**	
	HHTS-004-001	UPPER DRIVESHAFT SECTION	1	
	HHTS-004-002	LOWER DRIVESHAFT SECTION	1	
	HHTS-004-003	DRIVESHAFT FASTENER	8	#10-32 x 0.75"
	HHTS-004-004	JESUS NUT	1	
HHTS-005	**HHTS-005**	**UPPER FOLLOWER**	**1**	
	HHTS-005-001	LEFT CLAMP COLLAR	1	
	HHTS-005-002	RIGHT CLAMP COLLAR	1	
	HHTS-005-003	FORCE LINK	1	
	HHTS-005-004	LINK RECEIVER	1	
	HHTS-005-005	UPPER LINK NUT	3	1/4-20 nut
	HHTS-005-006	UPPER LINK BOLT	3	1/4-20 x 1.5"
	HHTS-005-007	THREADED CONTROL ROD	1	#10-32
HHTS-006	**HHTS-006**	**SWASHPLATE**	**1**	

	HHTS-006-001	UPPER SWASHPLATE	1	
	HHTS-006-002	LOWER SWASHPLATE	1	
	HHTS-006-003	SWASHPLATE ROLLER BEARING	1	80 x 50 x 16 mm
	HHTS-006-004	BALL LINK	13	#10-32 thread
	HHTS-006-005	RETAINING RING SCREW		#4-40 x .375 c'sink
	HHTS-006-006	SWASHPLATE SPHERICAL BEARING	1	3/4" Bore
	HHTS-006-007	SPHERICAL BEARING RETAINING RING	1	
	HHTS-006-008	INNER RETAINING RING	1	
	HHTS-006-009	OUTER RETAINING RING	1	
HHTS-007	**HHTS-007**	**DRIVESHAFT BEARING HOUSING**		
	HHTS-007-001	SHAFT BEARING HOUSING	1	
	HHTS-007-002	BEARING SPACER	1	
	HHTS-007-003	SERVO MOUNTING PLATE	1	
	HHTS-007-004	LOWER MOUNTING PLATE	1	
	HHTS-007-005	SHAFT LOCK NUT	1	M30 x 2
	HHTS-007-006	SHAFT ROLLER BEARING	2	
	HHTS-007-007	SERVO PLATE BOLT	4	x 1"
	HHTS-007-008	SWASHPLATE RETAINER	1	
HHTS-008	**HHTS-008**	**POWER TRANSMISSION**		
	HHTS-008-001	TIMING PULLEY	2	
	HHTS-008-002	DRIVESHAFT PULLEY BUSHING	1	
	HHTS-008-003	MOTOR PULLEY BUSHING	1	
	HHTS-008-004	TIMING BELT	1	
	HHTS-008-005	BUSHING FASTNERS	6	
HHTS-009	**HHTS-009**	**MOTOR MOUNT**		
	HHTS-009-001	A/C ELECTRIC MOTOR	1	1Hp, 230VAC
	HHTS-009-002	MOTOR MOUNTING PLATE	1	
	HHTS-009-003	MOTOR MOUNT STANDOFF	4	
	HHTS-009-004	MOTOR MOUNT WASHER	4	
	HHTS-009-005	MOTOR MOUNT BOLT	4	3/8"-16
HHTS-010	**HHTS-010**	**CONTROLS**		
	HHTS-010-001	CONTROL SERVOS	3	
	HHTS-010-002	SERVO FASTNERS		
	HHTS-010-003	CONTROL ROD ATTACHMENT	3	

	HHTS-010-004	CONTROL RODS	7	
HHTS-012		**FINAL ASSEMBLY**		

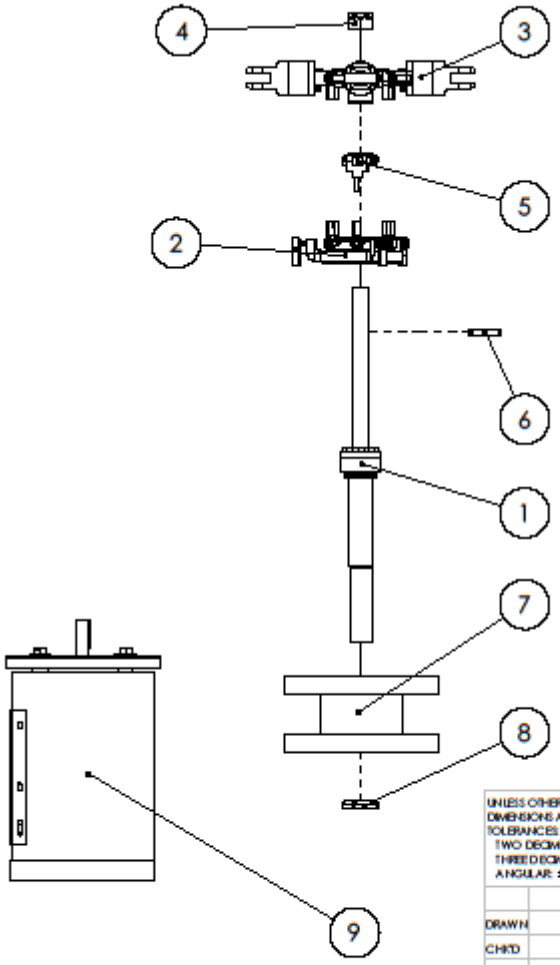

ITEM NO.	PartNo	DESCRIPTION	QTY.
1	HHTS-004	DRIVESHAFT ASSEMBLY	1
2	HHTS-006	SWASHPLATE ASSEMBLY	1
3	HHTS-003	ROTOR HUB ASSEMBLY	1
4	HHTS-004-004	JESUS NUT	1
5	HHTS-005	FOLLOWER ASSEMBLY	1
6	HHTS-003-003	ROTOR HEAD RETAINING PIN	1
7	HHTS-007	DRIVESHAFT BEARING HOUSING ASSEMBLY	1
8	HHTS-007-005	SHAFT LOCK NUT	1
9	HHTS-009	MOTOR MOUNT ASSEMBLY	1

UNLESS OTHERWISE SPECIFIED:
DIMENSIONS ARE IN INCHES
TOLERANCES:
TWO DECIMAL ± .01
THREE DECIMAL ± .005
ANGULAR: ±1°

FINISH:

DEBUR AND BREAK SHARP EDGES

DO NOT SCALE DRAWING

REVISION

	NAME	SIGNATURE	DATE
DRAWN	BEA		
CHK'D	JPJ		
APP'VD	ABL		
MFG	JPJ		
Q.A	JCF		

MATERIAL:

WEIGHT:

Helicopter Hover Test Stand

TITLE:

FINAL ASSEMBLY (DESIGNED)

DWG NO.

A4

SCALE:1:7

SHEET 1 OF 2

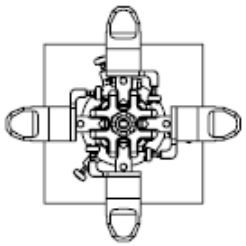

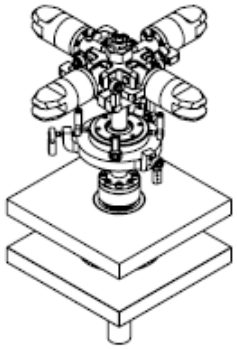

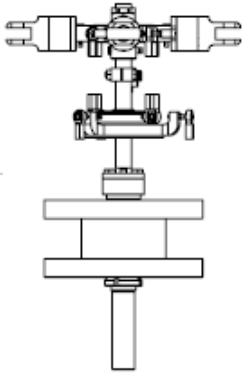

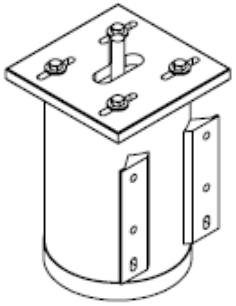

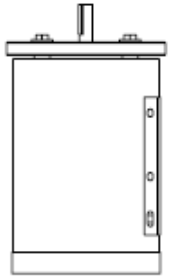

UNLESS OTHERWISE SPECIFIED: DIMENSIONS ARE IN MILLIMETERS SURFACE FINISH: TOLERANCES: LINEAR: ANGULAR:	FINISH:				DEBUR AND BREAK SHARP EDGES	DO NOT SCALE DRAWING	REVISION
	NAME	SIGNATURE	DATE			Helicopter Hover Test Stand	
DRAWN	JPLJ					TITLE: FINAL ASSEMBLY (DESIGNED)	
CHK'D	JCF						
APP'V'D	ABL						
MFG	JCF						
Q.A	BEA			MATERIAL:		DWG NO.	A4
				WEIGHT:		SCALE:1:7	SHEET 2 OF 2

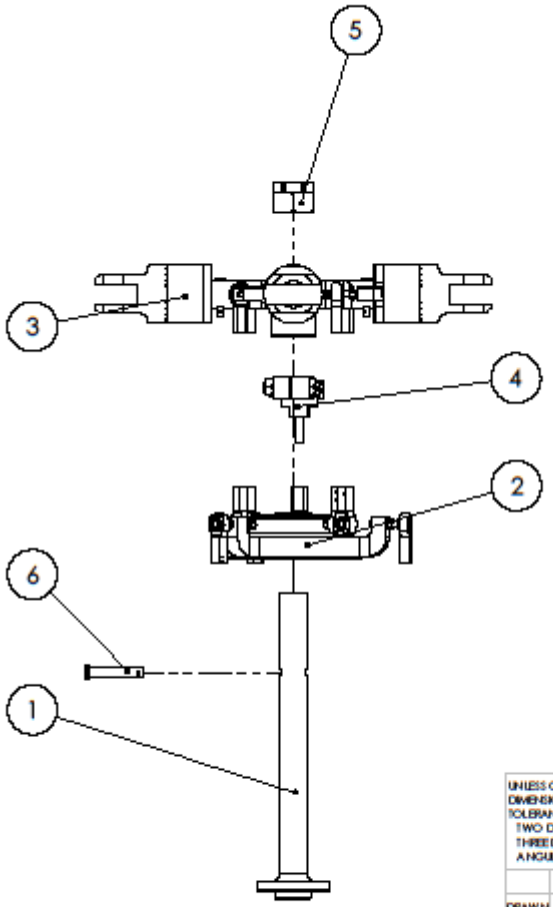

ITEM NO.	PartNo	DESCRIPTION	QTY.
1	HHTS-004-001	UPPER DRIVESHAFT	1
2	HHTS-006	SWASHPLATE ASSEMBLY	1
3	HHTS-003	ROTOR HUB ASSEMBLY	1
4	HHTS-005	FOLLOWER ASSEMBLY	1
5	HHTS-004-004	JESUS NUT	1
6	HHTS-003-003	ROTOR HEAD RETAINING PIN	1

UNLESS OTHERWISE SPECIFIED:
DIMENSIONS ARE IN INCHES
TOLERANCES
TWO DECIMAL ± .01
THREE DECIMAL ± .005
ANGULAR: ±1°

FINISH:

DEBUR AND BREAK SHARP EDGES

DO NOT SCALE DRAWING

REVISION

	NAME	SIGNATURE	DATE
DRAWN	BEA		
CHK'D	JPJ		
APP'VD	ABL		
MFG	JPJ		
Q.A	JCF		

MATERIAL:

WEIGHT:

Helicopter Hover Test Stand

TITLE:

FINAL ASSEMBLY (MANUFACTURED)

DWG NO.

A4

SCALE:1:4

SHEET 1 OF 1

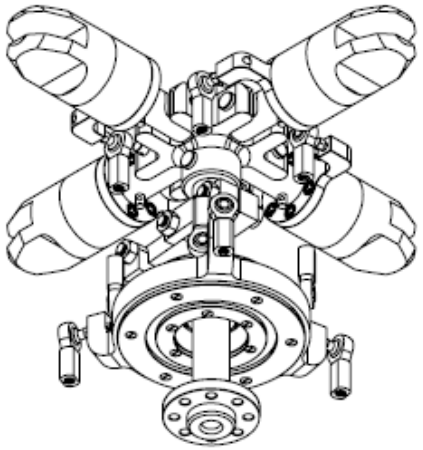

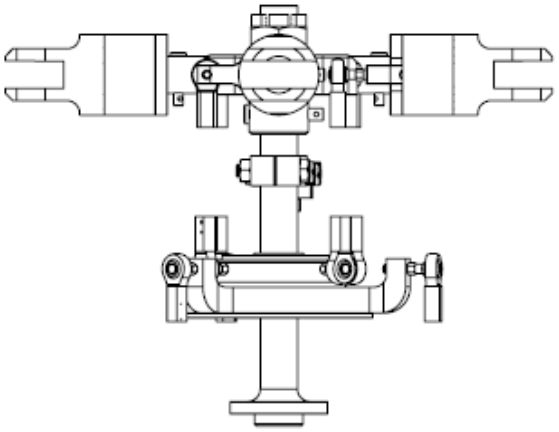

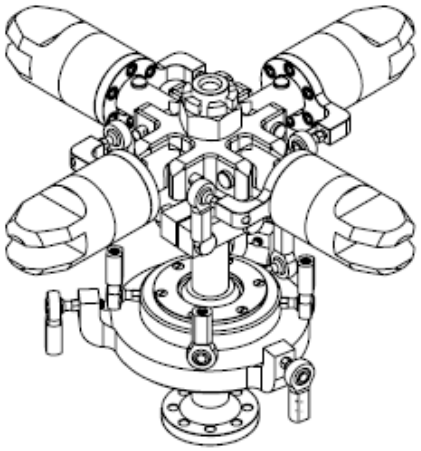

UNLESS OTHERWISE SPECIFIED: DIMENSIONS ARE IN MILLIMETERS SURFACE FINISH: TOLERANCES: LINEAR: ANGULAR:		FINISH:		DEBUR AND BREAK SHARP EDGES	DO NOT SCALE DRAWING	REVISION
	NAME	SIGNATURE	DATE		Helicopter Hover Test Stand	
DRAWN	JPLJ				TITLE: FINAL ASSEMBLY (MANUFACTURED)	
CHK'D	JCF					
APPV'D	ABL					
MFG	JCF					
Q.A	BEA			MATERIAL:	DWG NO.	A4
				WEIGHT:	SCALE:1:3	SHEET 2 OF 2

ITEM NO.	PartNo	Description	QTY.
1	HHTS-001-003	ROLLER BEARINGS	2
2	HHTS-001-004	THRUST BEARINGS	1
3	HHTS-001-005	WASHER	3
4	HHTS-001-001	BEARING HOUSING	1
5	HHTS-001-002	FACEPLATE CONTROL ARM	1

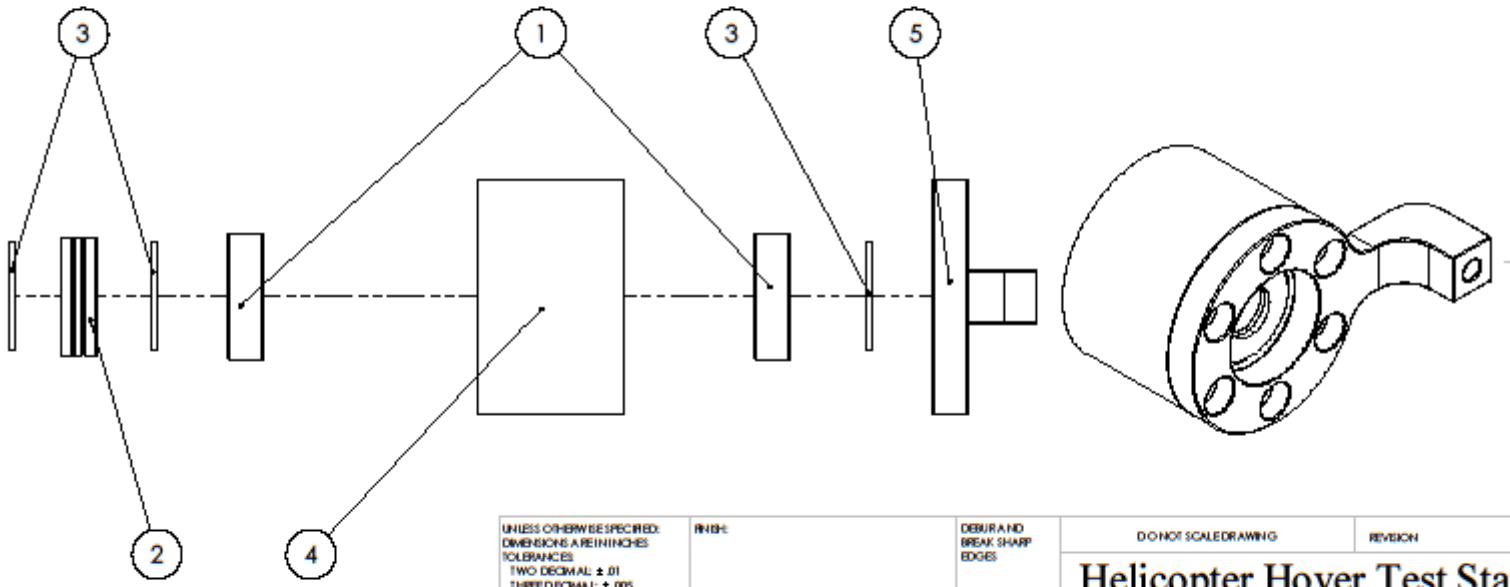

UNLESS OTHERWISE SPECIFIED:
DIMENSIONS ARE IN INCHES
TOLERANCES:
TWO DECIMAL ± .01
THREE DECIMAL ± .005
ANGULAR: ±1°

FINISH:

DEBUR AND BREAK SHARP EDGES

DO NOT SCALE DRAWING

REVISION

	NAME	SIGNATURE	DATE
DRAWN	JCF		
CHK'D	JPJ		
APP'VD	ABL		
MFG	JPJ		
Q.A	BEA		

MATERIAL:

WEIGHT: 0.27

Helicopter Hover Test Stand

TITLE:

BEARING HOUSING ASSEMBLY

DWG NO. HHTS-001

A4

SCALE:1:1

SHEET 1 OF 1

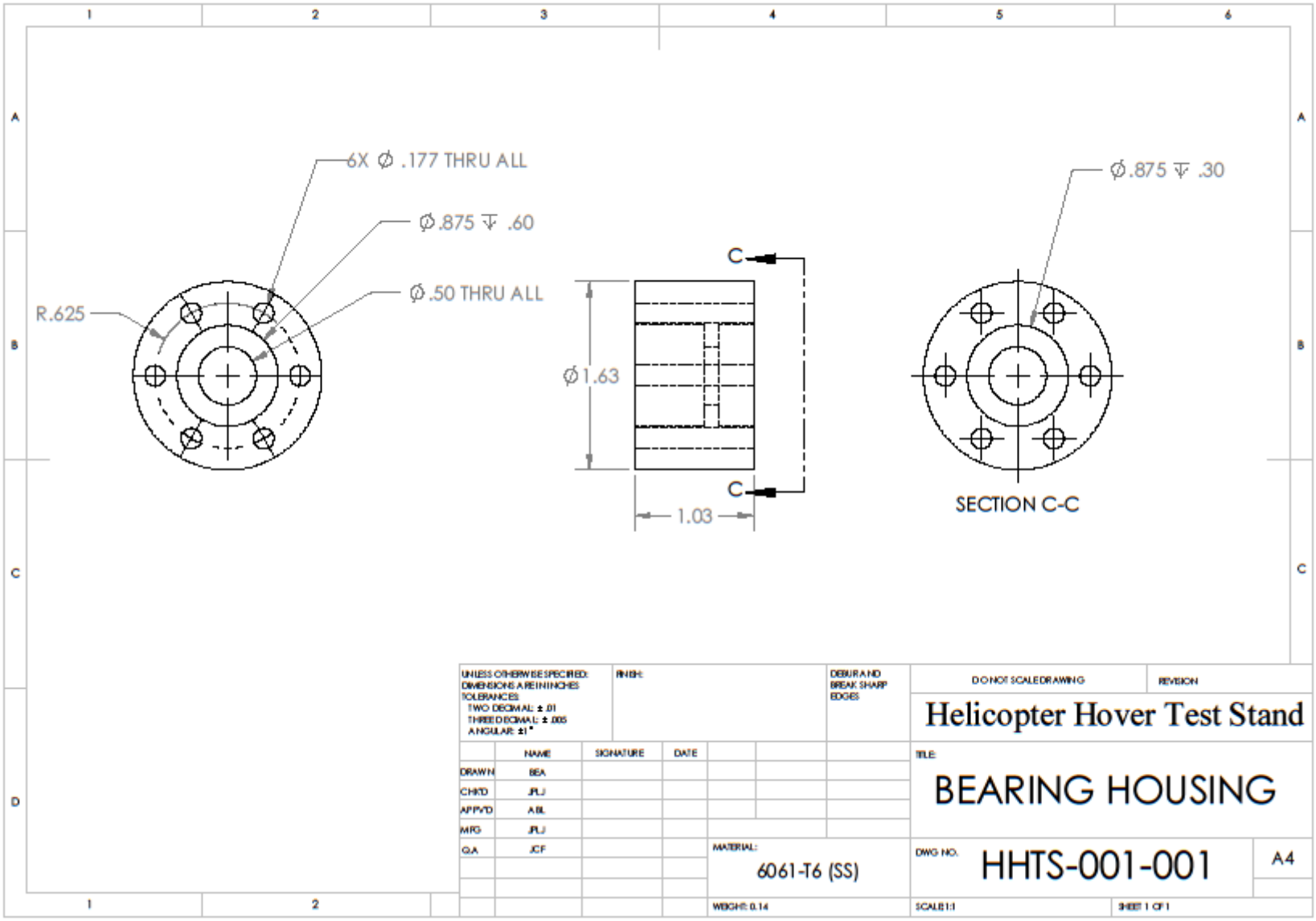
6X Ø .177 THRU ALL
Ø.875 ↧ .60
Ø.50 THRU ALL
R.625
C
C
Ø1.63
1.03
Ø.875 ↧ .30
SECTION C-C
UNLESS OTHERWISE SPECIFIED:
DIMENSIONS ARE IN INCHES
TOLERANCES:
TWO DECIMAL ± .01
THREE DECIMAL ± .005
ANGULAR: ±1°
FINISH:
DEBUR AND BREAK SHARP EDGES
DO NOT SCALE DRAWING
REVISION
Helicopter Hover Test Stand
NAME
SIGNATURE
DATE
DRAWN BEA
CHKD JPJ
APPVD ABL
MFG JPJ
Q.A JCF
MATERIAL:
6061-T6 (SS)
TITLE:
BEARING HOUSING
DWG NO.
HHTS-001-001
A4
WEIGHT: 0.14
SCALE:1:1
SHEET 1 OF 1

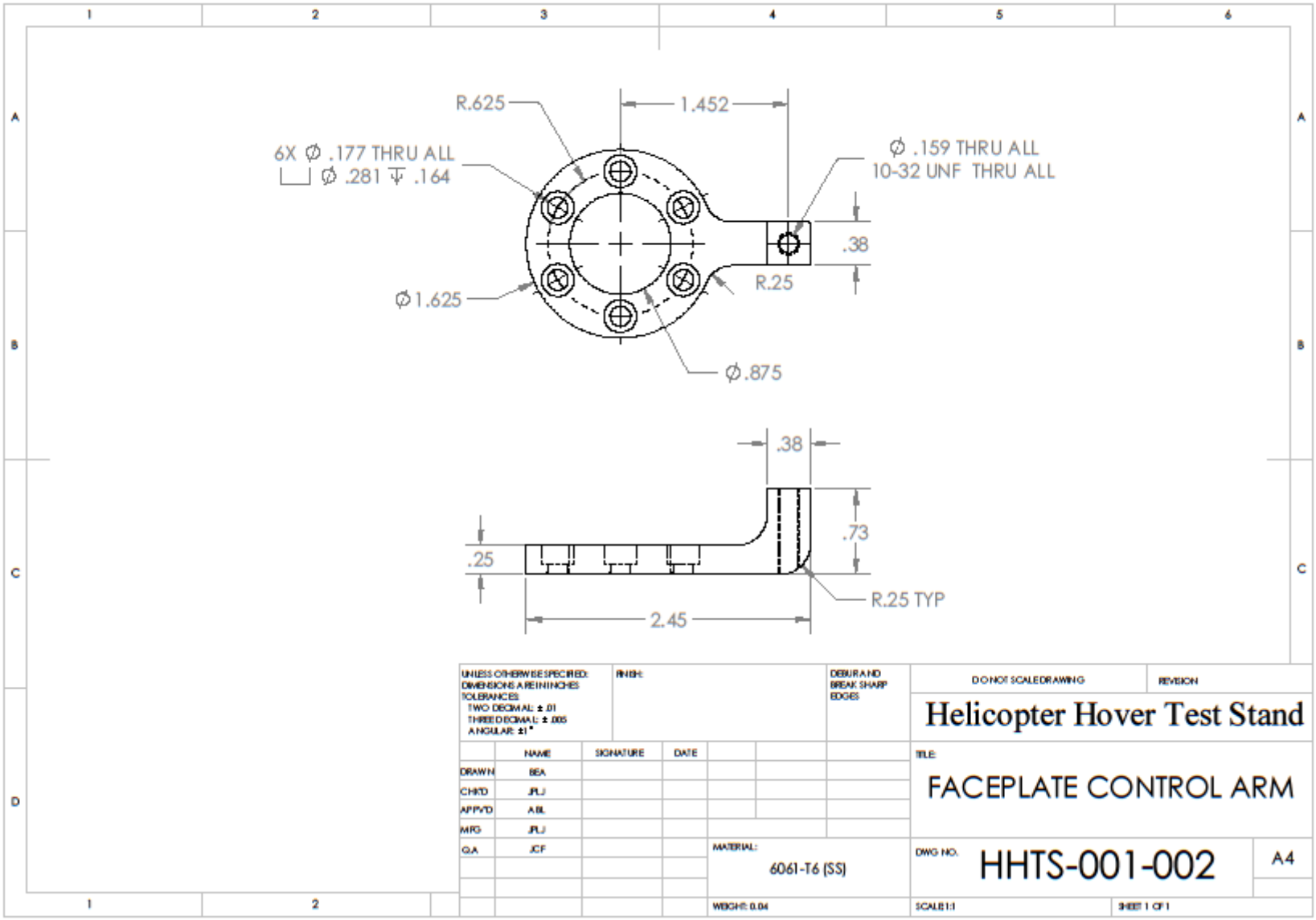
R.625
1.452
6X Ø .177 THRU ALL
⌴ Ø .281 ↧ .164
Ø .159 THRU ALL
10-32 UNF THRU ALL
.38
R.25
Ø1.625
Ø.875
.38
.73
.25
R.25 TYP
2.45
UNLESS OTHERWISE SPECIFIED:
DIMENSIONS ARE IN INCHES
TOLERANCES
TWO DECIMAL ± .01
THREE DECIMAL ± .005
ANGULAR: ±1°
FINISH:
DEBUR AND BREAK SHARP EDGES
DO NOT SCALE DRAWING
REVISION
Helicopter Hover Test Stand
NAME
SIGNATURE
DATE
DRAWN BEA
CHKD JLJ
APPVD ABL
MFG JLJ
Q.A JCF
TITLE:
FACEPLATE CONTROL ARM
MATERIAL:
6061-T6 (SS)
DWG NO.
HHTS-001-002
A4
WEIGHT: 0.04
SCALE:1:1
SHEET 1 OF 1

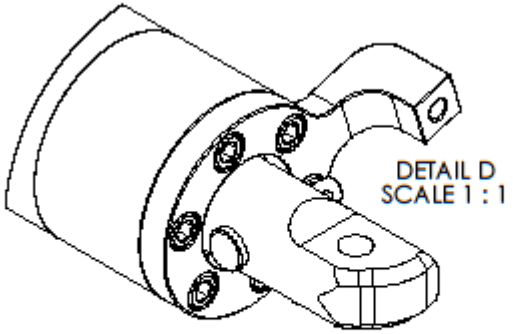

ITEM NO.	PartNo	Description	QTY.
1	HHTS-001	BEARING HOUSING ASSEMBLY	1
2	HHTS-002-003	FEATHERING SPINDLE	1
3	HHTS-002-004	FEATHERING SPINDLE CLEVIS PIN	1
4	HHTS-002-001	FLAPPING HINGE	1
5	HHTS-002-002	BLADE GRIP	1
6	HHTS-002-005	CONTROL ARM SCREW	6

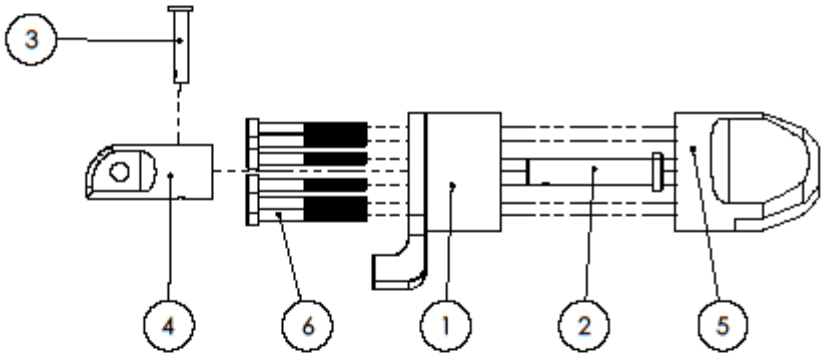

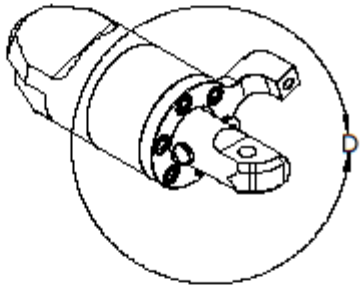

UNLESS OTHERWISE SPECIFIED:
DIMENSIONS ARE IN INCHES
TOLERANCES
TWO DECIMAL ± .01
THREE DECIMAL ± .005
ANGULAR: ±1°

FINISH:

DEBUR AND BREAK SHARP EDGES

DO NOT SCALE DRAWING

REVISION

	NAME	SIGNATURE	DATE
DRAWN	JCF		
CHK'D	JPJ		
APP'VD	ABL		
MFG	JPJ		
Q.A	BEA		

MATERIAL:

WEIGHT: 0.66

Helicopter Hover Test Stand

TITLE:

CONTROL ARM ASSEMBLY

DWG NO. HHTS-002

A4

SCALE:1:2

SHEET 1 OF 1

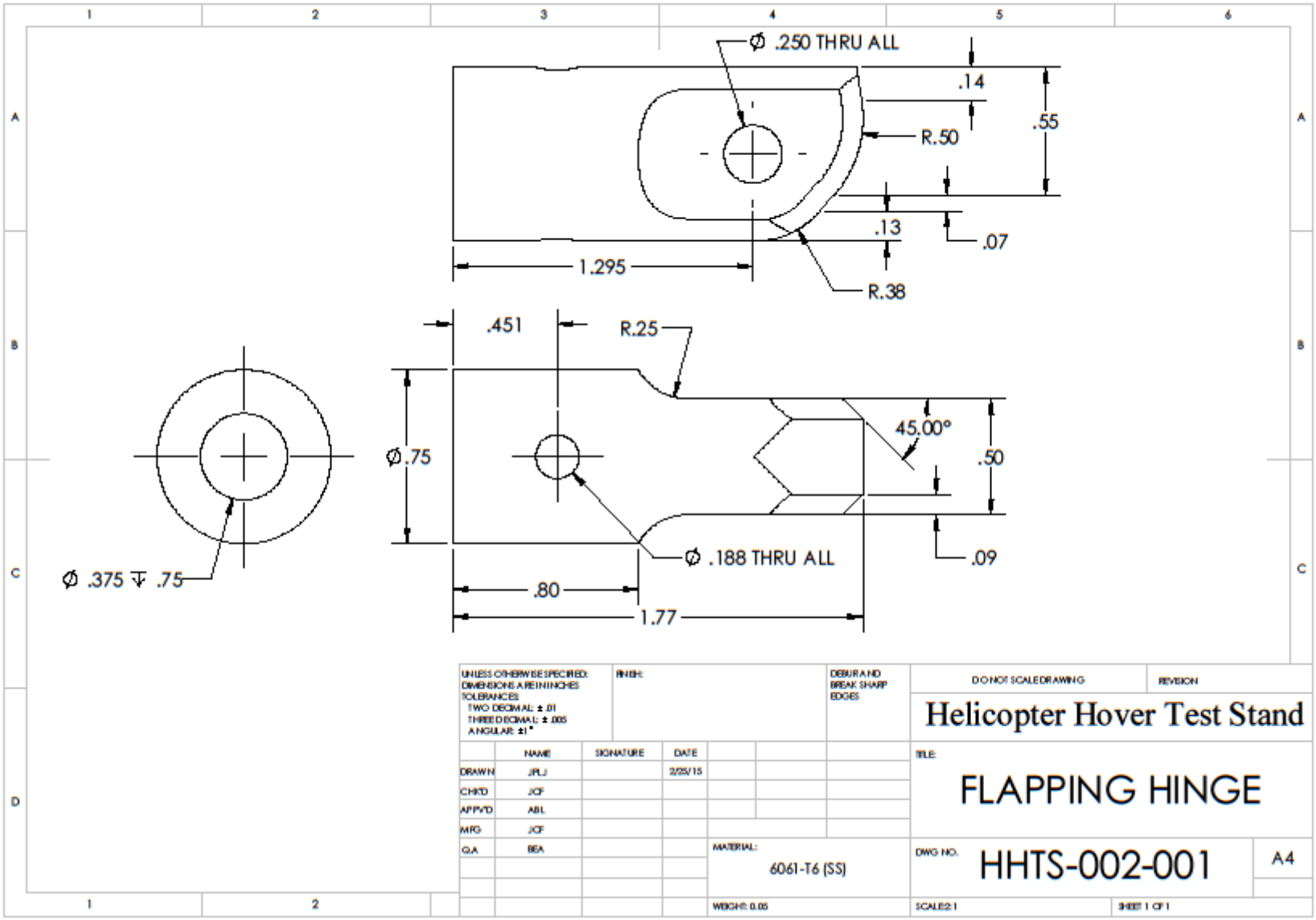
Ø .250 THRU ALL
.14
.55
R.50
.13
.07
1.295
R.38
.451
R.25
Ø.75
45.00°
.50
Ø .188 THRU ALL
.09
.80
1.77
Ø .375 ↧ .75
UNLESS OTHERWISE SPECIFIED:
DIMENSIONS ARE IN INCHES
TOLERANCES:
TWO DECIMAL ± .01
THREE DECIMAL ± .005
ANGULAR: ±1°
FINISH:
DEBUR AND BREAK SHARP EDGES
DO NOT SCALE DRAWING
REVISION
Helicopter Hover Test Stand
NAME
SIGNATURE
DATE
DRAWN
JPLJ
2/25/15
CHK'D
JCF
APP'VD
ABL
MFG
JCF
Q.A
BEA
MATERIAL:
6061-T6 (SS)
TITLE:
FLAPPING HINGE
DWG NO.
HHTS-002-001
A4
WEIGHT: 0.05
SCALE:2:1
SHEET 1 OF 1

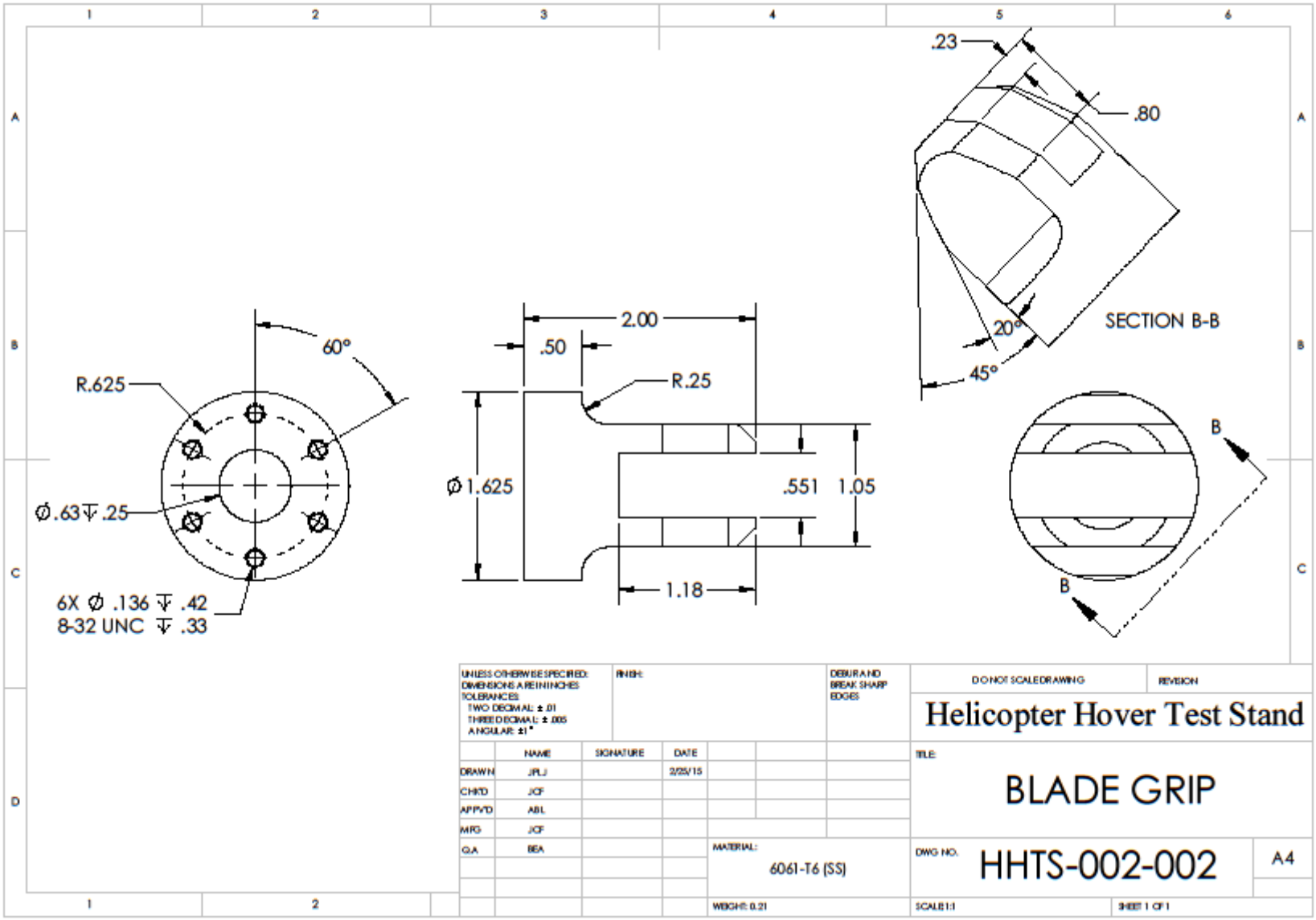
.23
.80
SECTION B-B
20°
45°
60°
R.625
Ø.63↧.25
6X Ø .136 ↧ .42
8-32 UNC ↧ .33
2.00
.50
R.25
Ø1.625
.551
1.05
1.18
B
B
UNLESS OTHERWISE SPECIFIED:
DIMENSIONS ARE IN INCHES
TOLERANCES
TWO DECIMAL ± .01
THREE DECIMAL ± .005
ANGULAR: ±1°
FINISH:
DEBUR AND BREAK SHARP EDGES
DO NOT SCALE DRAWING
REVISION
Helicopter Hover Test Stand
NAME
SIGNATURE
DATE
DRAWN JPLJ 2/25/15
CHK'D JCF
APP'D ABL
MFG JCF
Q.A BEA
TITLE:
BLADE GRIP
MATERIAL:
6061-T6 (SS)
DWG NO. HHTS-002-002
A4
WEIGHT: 0.21
SCALE:1:1
SHEET 1 OF 1

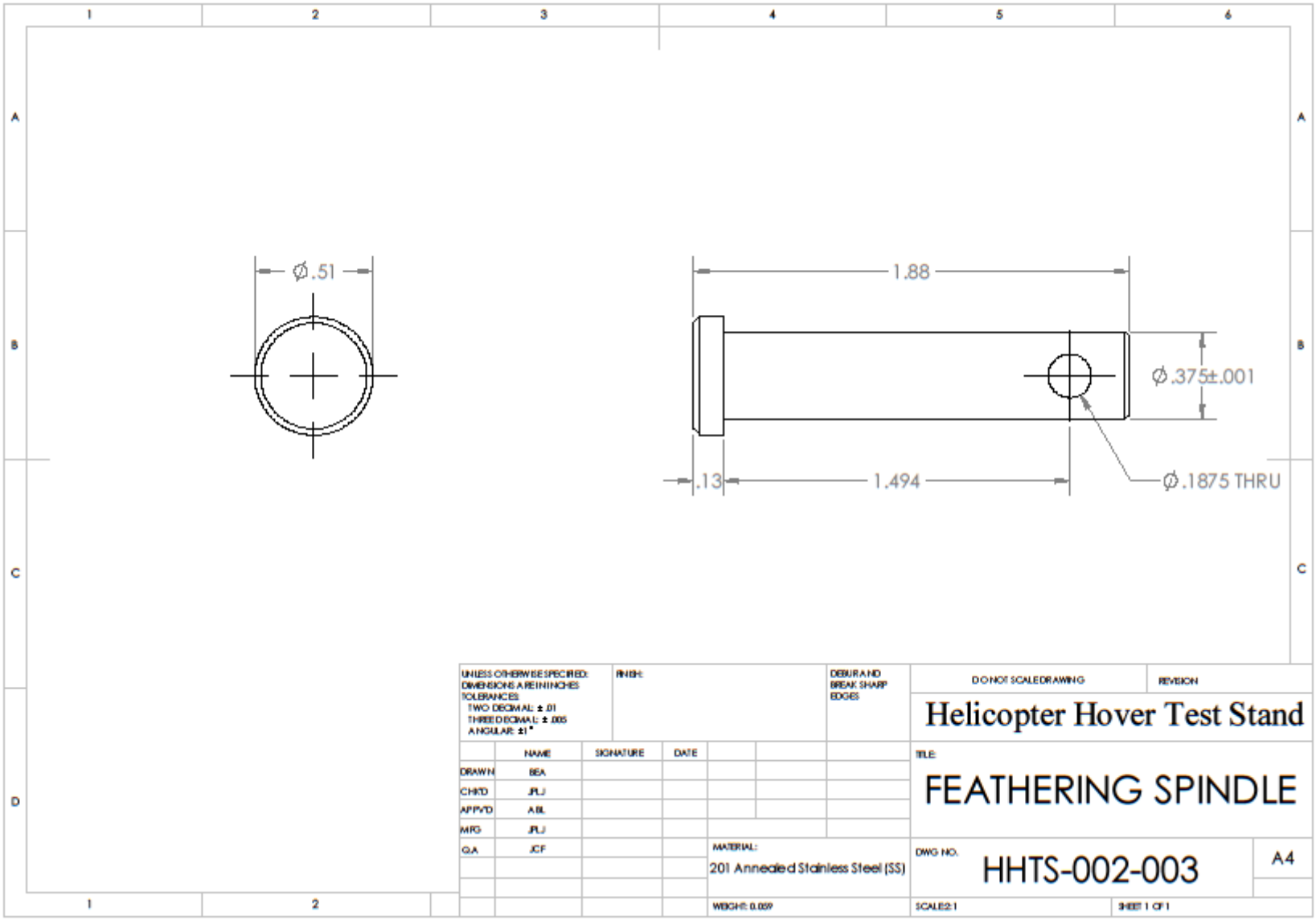
Ø.51
1.88
Ø.375±.001
.13
1.494
Ø.1875 THRU
UNLESS OTHERWISE SPECIFIED:
DIMENSIONS ARE IN INCHES
TOLERANCES
TWO DECIMAL ± .01
THREE DECIMAL ± .005
ANGULAR: ±1°
FINISH:
DEBUR AND BREAK SHARP EDGES
DO NOT SCALE DRAWING
REVISION
Helicopter Hover Test Stand
NAME
SIGNATURE
DATE
DRAWN BEA
CHKD JPJ
APPVD ABL
MFG JPJ
Q.A JCF
TITLE:
FEATHERING SPINDLE
MATERIAL:
201 Annealed Stainless Steel (SS)
DWG NO.
HHTS-002-003
A4
WEIGHT: 0.059
SCALE:2:1
SHEET 1 OF 1

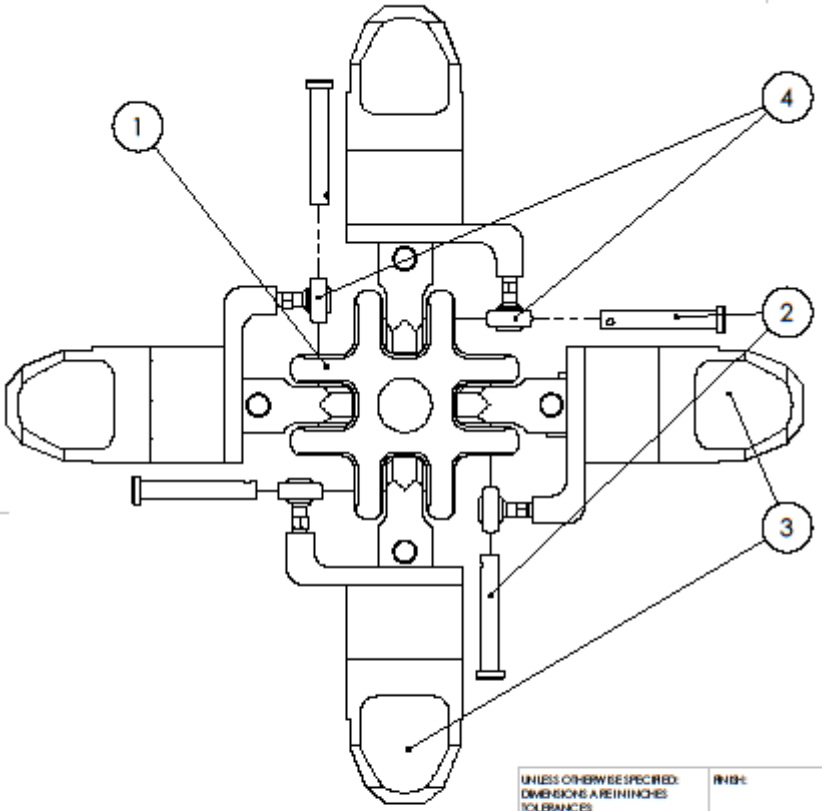

ITEM NO.	PartNo	Description	QTY.
1	HHTS-003-001	ROTOR HUB	1
2	HHTS-003-002	FLAPING HINGE CLEVIS PIN	4
3	HHTS-002	CONTROL ARM ASSEMBLY	4
4	HHTS-006-004	BALL LINKS	4

UNLESS OTHERWISE SPECIFIED:
DIMENSIONS ARE IN INCHES
TOLERANCES:
TWO DECIMAL ± .01
THREE DECIMAL ± .005
ANGULAR: ±1°

FINISH:

DEBUR AND BREAK SHARP EDGES

DO NOT SCALE DRAWING

REVISION

	NAME	SIGNATURE	DATE
DRAWN	JCF		
CHK'D	JPLJ		
APP'VD	ABL		
MFG	JPLJ		
Q.A	BEA		

MATERIAL:

WEIGHT: 3.29

Helicopter Hover Test Stand

TITLE:

ROTOR HEAD ASSEMBLY

DWG NO. HHTS-003

A4

SCALE:1:2

SHEET 1 OF 1

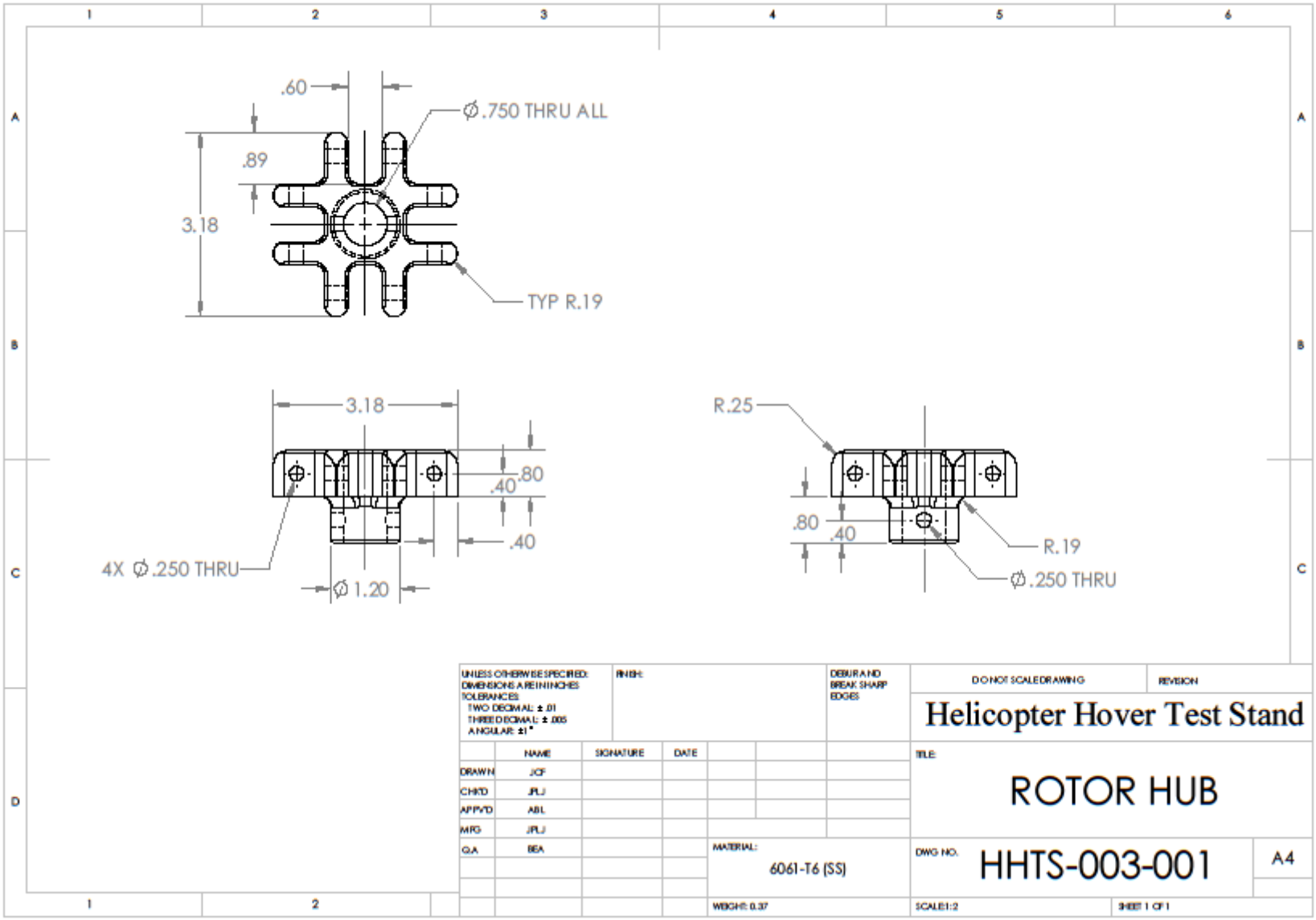
.60
Ø.750 THRU ALL
.89
3.18
TYP R.19
3.18
.80
.40
.40
4X Ø.250 THRU
Ø1.20
R.25
.80
.40
R.19
Ø.250 THRU
UNLESS OTHERWISE SPECIFIED:
DIMENSIONS ARE IN INCHES
TOLERANCES
TWO DECIMAL ± .01
THREE DECIMAL ± .005
ANGULAR: ±1°
FINISH:
DEBUR AND BREAK SHARP EDGES
DO NOT SCALE DRAWING
REVISION
Helicopter Hover Test Stand
NAME
SIGNATURE
DATE
DRAWN JCF
CHKD JPJ
APPVD ABL
MFG JPJ
Q.A BEA
MATERIAL:
6061-T6 (SS)
TITLE:
ROTOR HUB
DWG NO.
HHTS-003-001
A4
WEIGHT: 0.37
SCALE:1:2
SHEET 1 OF 1

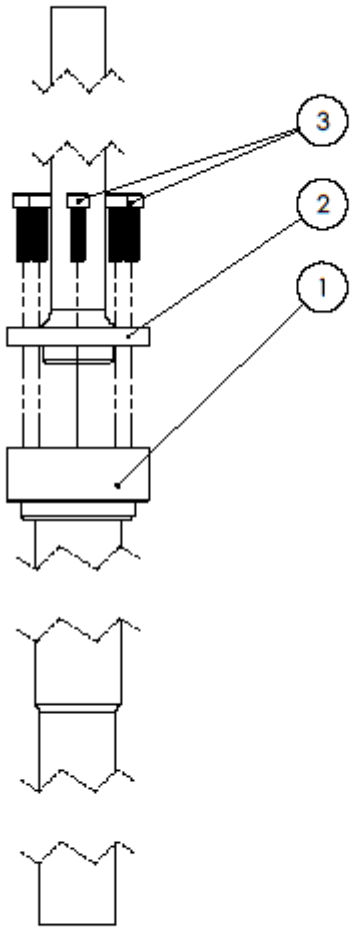

ITEM NO.	PartNo	DESCRIPTION	QTY.
1	HHTS-004-002	LOWER DRIVESHAFT	1
2	HHTS-004-001	UPPER DRIVESHAFT	1
3	HHTS-004-003	DRIVESHAFT FASTENER	8

UNLESS OTHERWISE SPECIFIED:
DIMENSIONS ARE IN INCHES
TOLERANCES:
TWO DECIMAL ± .01
THREE DECIMAL ± .005
ANGULAR: ±1°

FINISH:

DEBUR AND BREAK SHARP EDGES

DO NOT SCALE DRAWING

REVISION

	NAME	SIGNATURE	DATE
DRAWN	JCF		
CHK'D	JPLJ		
APP'VD	ABL		
MFG	JPLJ		
Q.A	BEA		

MATERIAL:

WEIGHT: 2.71

Helicopter Hover Test Stand

TITLE:

DRIVESHAFT ASSEMBLY

DWG NO. HHTS-004

A4

SCALE: 1:2

SHEET 1 OF 1

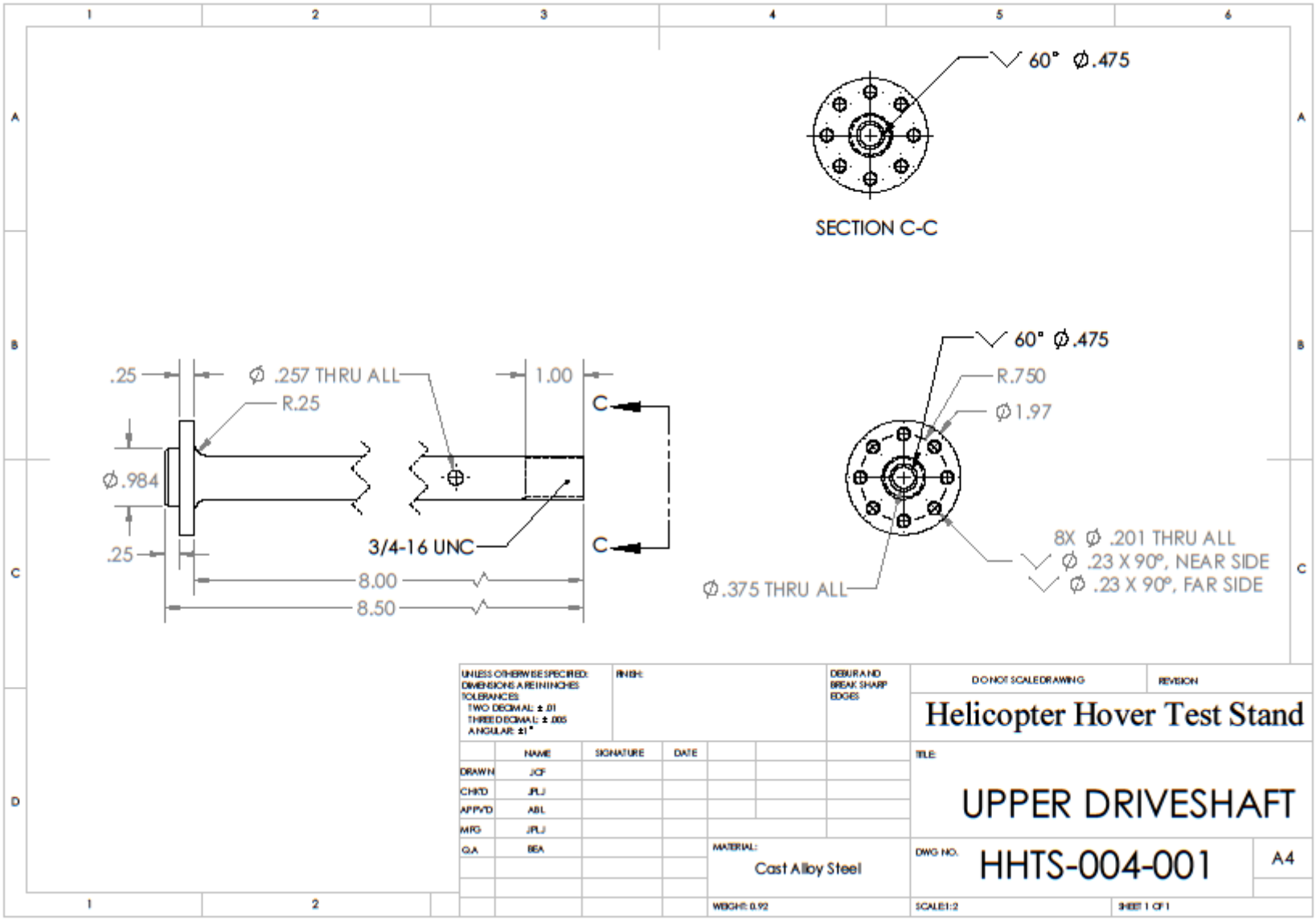
60° Ø.475
SECTION C-C
.25
Ø .257 THRU ALL
1.00
R.25
Ø.984
C
C
.25
3/4-16 UNC
8.00
8.50
60° Ø.475
R.750
Ø1.97
8X Ø .201 THRU ALL
Ø .23 X 90°, NEAR SIDE
Ø .23 X 90°, FAR SIDE
Ø.375 THRU ALL
UNLESS OTHERWISE SPECIFIED:
DIMENSIONS ARE IN INCHES
TOLERANCES
TWO DECIMAL ± .01
THREE DECIMAL ± .005
ANGULAR: ±1°
FINISH:
DEBUR AND BREAK SHARP EDGES
DO NOT SCALE DRAWING
REVISION
Helicopter Hover Test Stand
NAME
SIGNATURE
DATE
DRAWN JCF
CHKD JPJ
APPVD ABL
MFG JPJ
Q.A BEA
TITLE:
UPPER DRIVESHAFT
MATERIAL:
Cast Alloy Steel
DWG NO.
HHTS-004-001
A4
WEIGHT: 0.92
SCALE:1:2
SHEET 1 OF 1

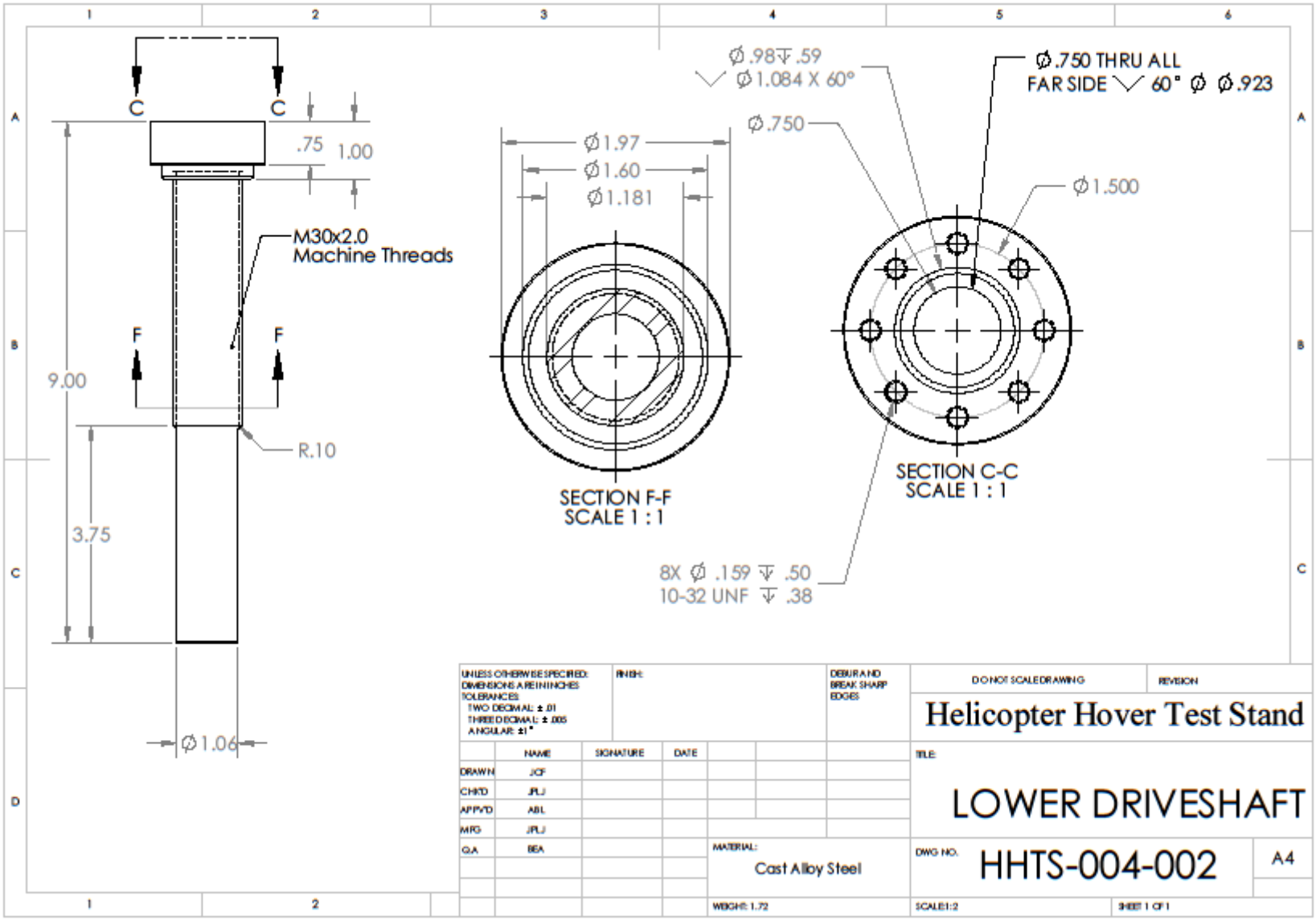
C
C
.75
1.00
M30x2.0
Machine Threads
F
F
9.00
R.10
3.75
Ø1.06
Ø1.97
Ø1.60
Ø1.181
SECTION F-F
SCALE 1 : 1
Ø.98↧.59
Ø1.084 X 60°
Ø.750
Ø.750 THRU ALL
FAR SIDE 60° Ø Ø.923
Ø1.500
SECTION C-C
SCALE 1 : 1
8X Ø .159 ↧ .50
10-32 UNF ↧ .38
UNLESS OTHERWISE SPECIFIED:
DIMENSIONS ARE IN INCHES
TOLERANCES:
TWO DECIMAL ± .01
THREE DECIMAL ± .005
ANGULAR: ±1°
FINISH:
DEBUR AND BREAK SHARP EDGES
DO NOT SCALE DRAWING
REVISION
Helicopter Hover Test Stand
NAME
SIGNATURE
DATE
DRAWN JCF
CHKD JPJ
APPVD ABL
MFG JPJ
Q.A BEA
MATERIAL:
Cast Alloy Steel
WEIGHT: 1.72
TITLE:
LOWER DRIVESHAFT
DWG NO.
HHTS-004-002
A4
SCALE:1:2
SHEET 1 OF 1

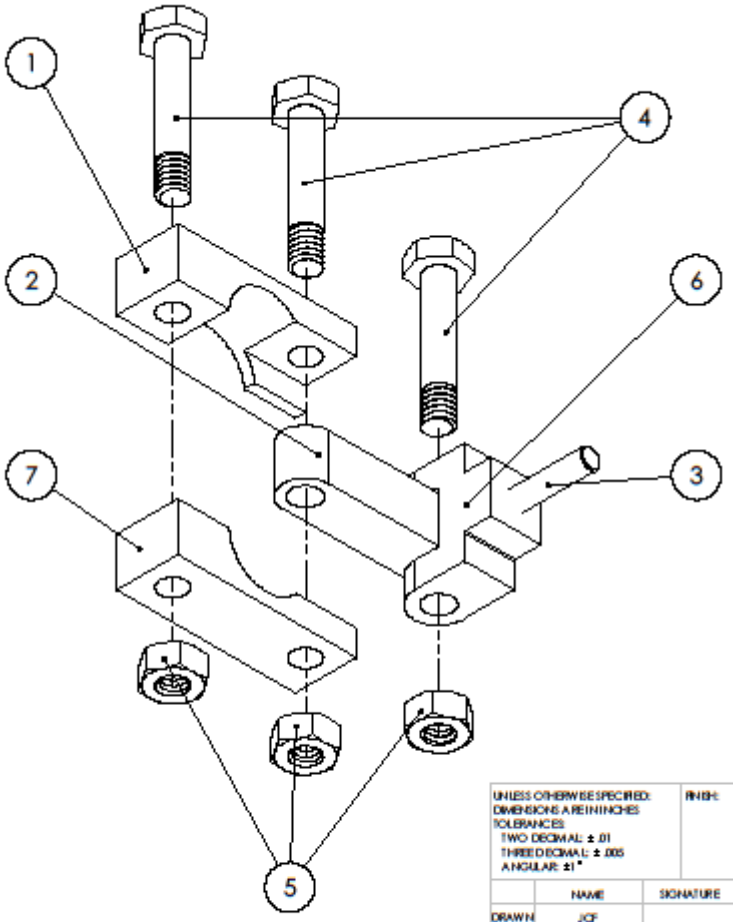

ITEM NO.	PartNo	Description	QTY.
1	HHTS-005-001	LEFT CLAMP COLLAR	1
2	HHTS-005-003	FORCE LINK	1
3	HHTS-005-007	THREADED CONTROL ROD	1
4	HHTS-005-006	UPPER LINK BOLT	3
5	HHTA-005-005	UPPER LINK NUT	3
6	HHTS-005-004	LINK RECIEVER	1
7	HHTS-005-002	RIGHT CLAMP COLLAR	1

UNLESS OTHERWISE SPECIFIED:
DIMENSIONS ARE IN INCHES
TOLERANCES:
TWO DECIMAL ± .01
THREE DECIMAL ± .005
ANGULAR: ±1°

FINISH:

DEBUR AND BREAK SHARP EDGES

DO NOT SCALE DRAWING

REVISION

	NAME	SIGNATURE	DATE
DRAWN	JCF		
CHK'D	JPJ		
APP'VD	ABL		
MFG	JPJ		
Q.A	BEA		

MATERIAL:

WEIGHT: 0.22

Helicopter Hover Test Stand

TITLE:

UPPER FOLLOWER ASSEMBLY

DWG NO. HHTS-005

A4

SCALE:1:1

SHEET 1 OF 1

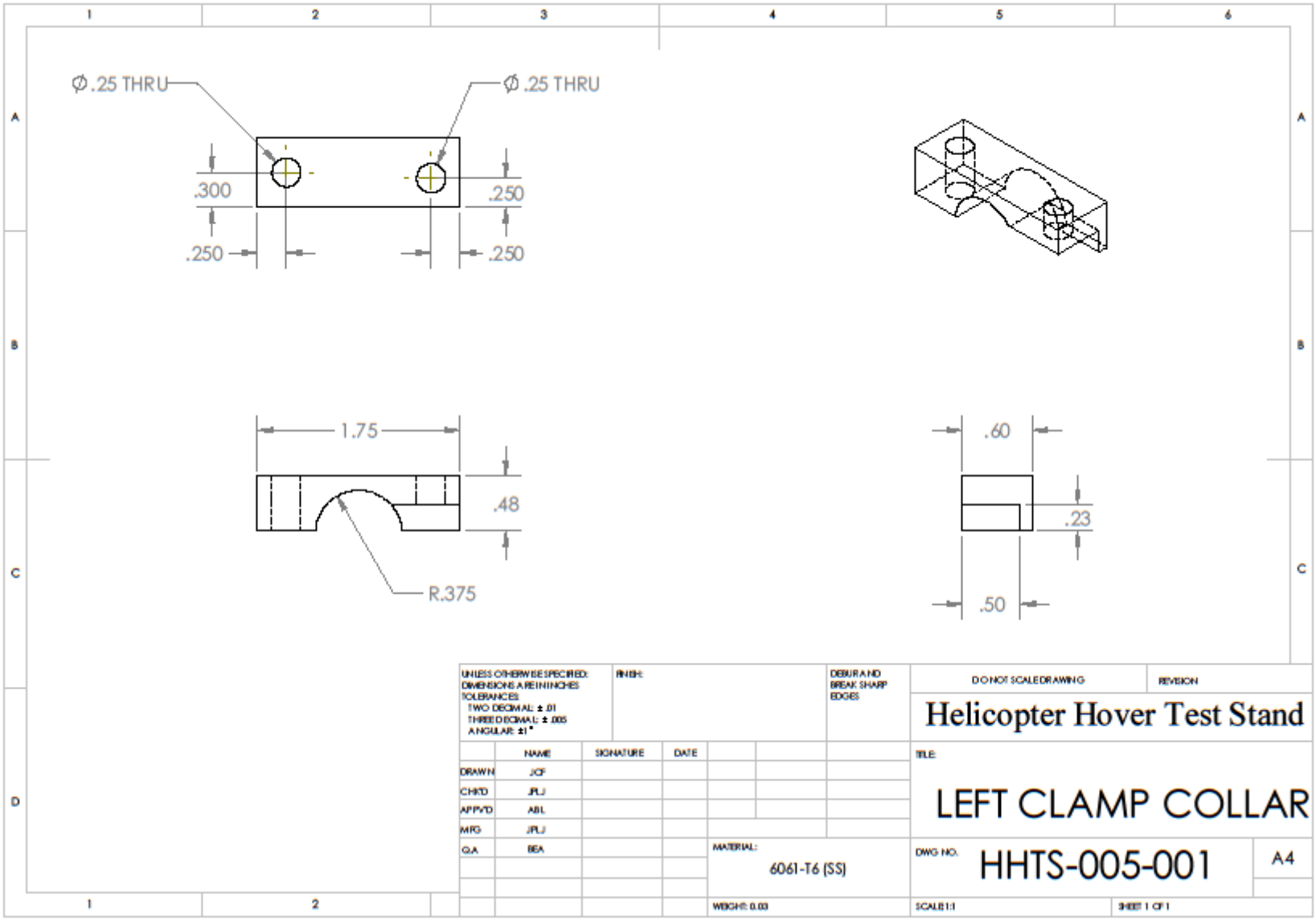
Ø .25 THRU
Ø .25 THRU
.300
.250
.250
.250
1.75
.48
R.375
.60
.23
.50
UNLESS OTHERWISE SPECIFIED:
DIMENSIONS ARE IN INCHES
TOLERANCES
TWO DECIMAL ± .01
THREE DECIMAL ± .005
ANGULAR: ±1°
FINISH:
DEBUR AND BREAK SHARP EDGES
DO NOT SCALE DRAWING
REVISION
Helicopter Hover Test Stand
NAME
SIGNATURE
DATE
DRAWN JCF
CHKD JPJ
APPVD ABL
MFG JPJ
Q.A BEA
TITLE:
LEFT CLAMP COLLAR
MATERIAL:
6061-T6 (SS)
DWG NO.
HHTS-005-001
A4
WEIGHT: 0.03
SCALE:1:1
SHEET 1 OF 1

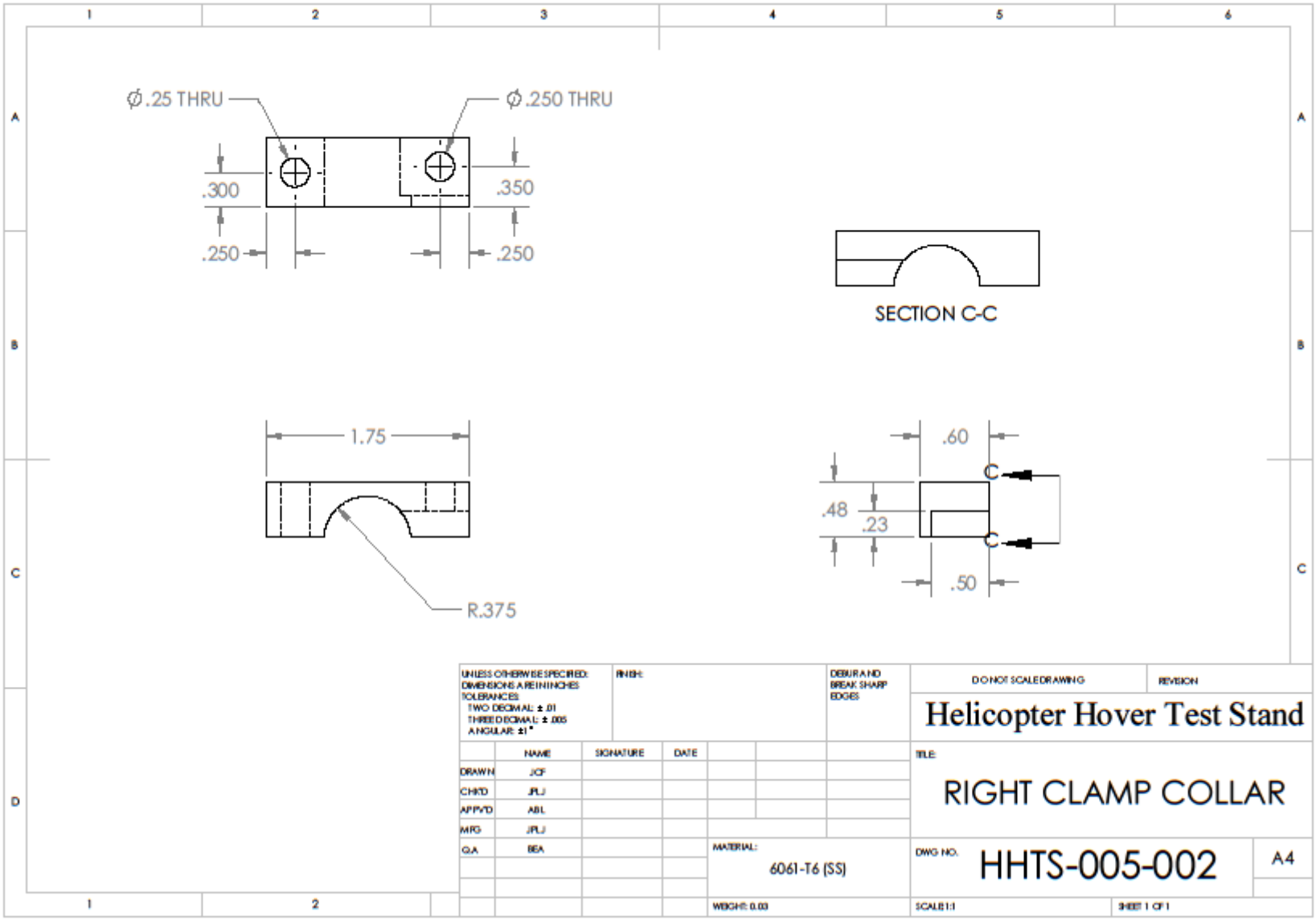
Ø.25 THRU
Ø.250 THRU
.300
.350
.250
.250
SECTION C-C
1.75
R.375
.60
.48
.23
.50
C
C
UNLESS OTHERWISE SPECIFIED:
DIMENSIONS ARE IN INCHES
TOLERANCES:
TWO DECIMAL ± .01
THREE DECIMAL ± .005
ANGULAR: ±1°
FINISH:
DEBUR AND BREAK SHARP EDGES
DO NOT SCALE DRAWING
REVISION
Helicopter Hover Test Stand
NAME
SIGNATURE
DATE
DRAWN JCF
CHKD JPLJ
APPVD ABL
MFG JPLJ
Q.A BEA
TITLE:
RIGHT CLAMP COLLAR
MATERIAL:
6061-T6 (SS)
DWG NO.
HHTS-005-002
A4
WEIGHT: 0.03
SCALE:1:1
SHEET 1 OF 1

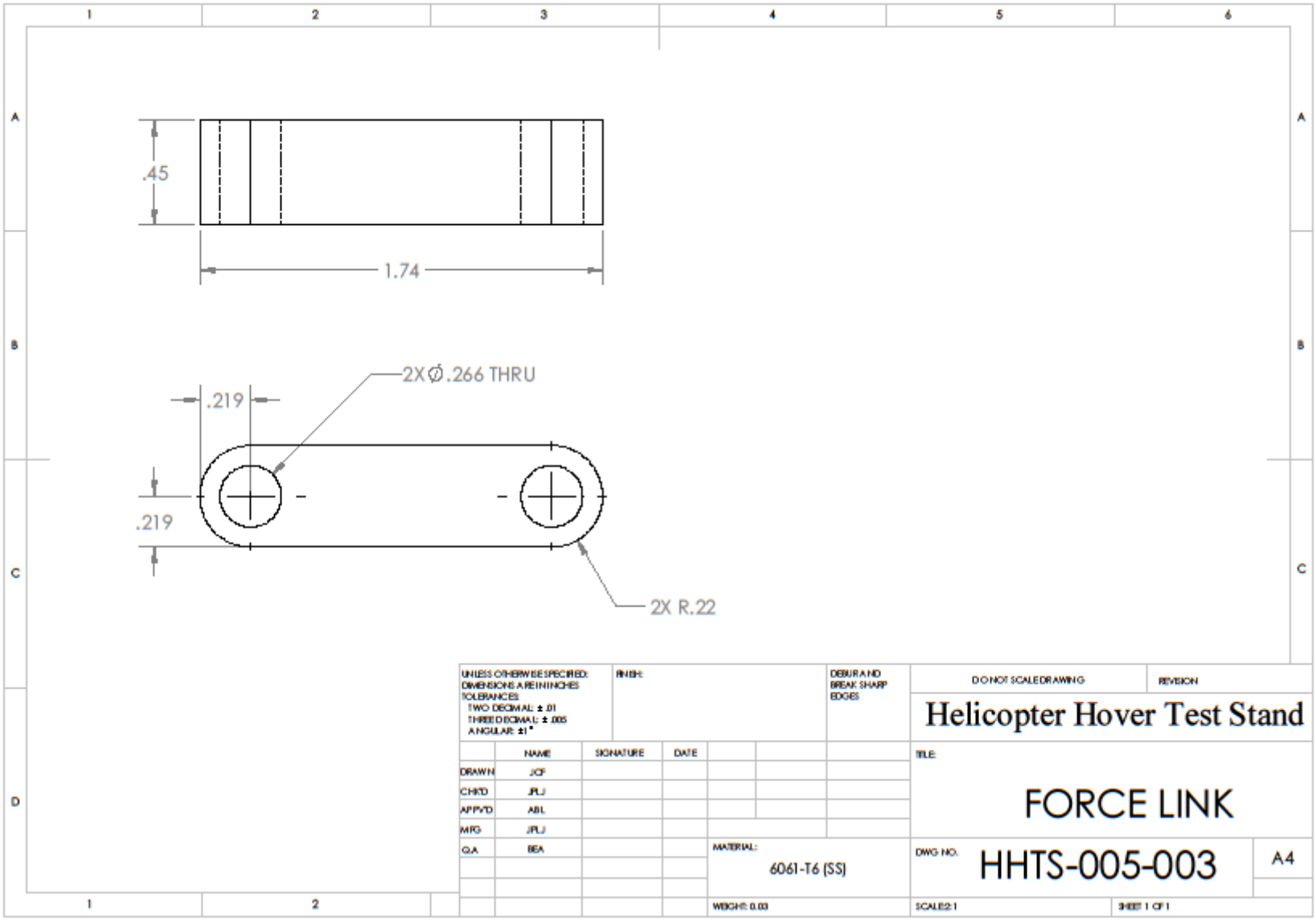
1
2
3
4
5
6
A
B
C
D
.45
1.74
2X Ø.266 THRU
.219
.219
2X R.22
UNLESS OTHERWISE SPECIFIED:
DIMENSIONS ARE IN INCHES
TOLERANCES:
TWO DECIMAL ± .01
THREE DECIMAL ± .005
ANGULAR: ±1°
FINISH:
DEBUR AND BREAK SHARP EDGES
DO NOT SCALE DRAWING
REVISION
Helicopter Hover Test Stand
NAME
SIGNATURE
DATE
DRAWN JCF
CHKD JPLJ
APPVD ABL
MFG JPLJ
Q.A BEA
MATERIAL:
6061-T6 (SS)
TITLE:
FORCE LINK
DWG NO.
HHTS-005-003
A4
WEIGHT: 0.03
SCALE: 2:1
SHEET 1 OF 1

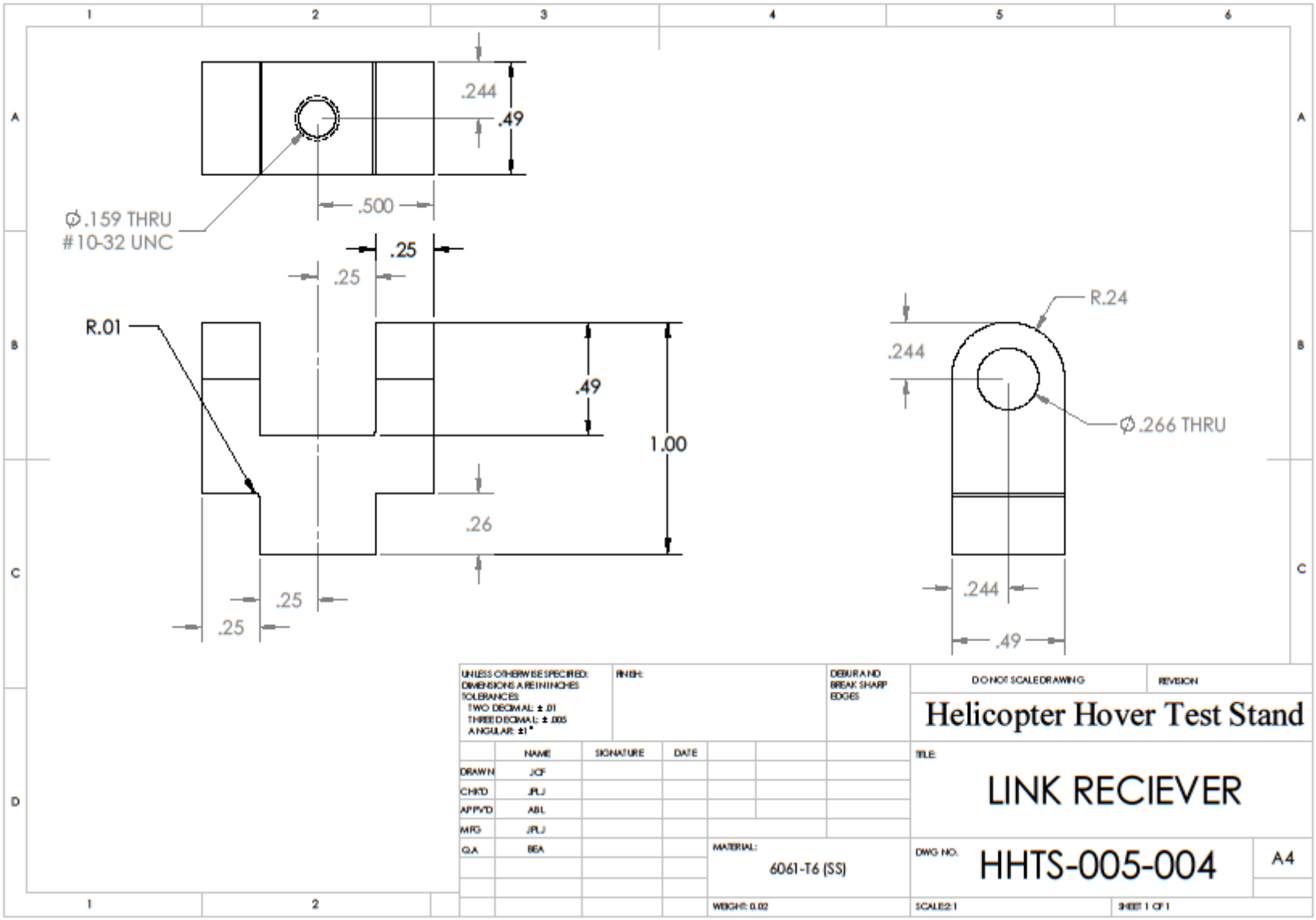
.244
.49
.500
Ø.159 THRU
#10-32 UNC
.25
.25
R.01
.49
1.00
.26
.25
.25
R.24
.244
Ø.266 THRU
.244
.49
UNLESS OTHERWISE SPECIFIED:
DIMENSIONS ARE IN INCHES
TOLERANCES
TWO DECIMAL ± .01
THREE DECIMAL ± .005
ANGULAR: ±1°
FINISH:
DEBUR AND BREAK SHARP EDGES
DO NOT SCALE DRAWING
REVISION
Helicopter Hover Test Stand
NAME
SIGNATURE
DATE
DRAWN JCF
CHKD JPJ
APPVD ABL
MFG JPJ
Q.A BEA
MATERIAL:
6061-T6 (SS)
TITLE:
LINK RECIEVER
DWG NO.
HHTS-005-004
A4
WEIGHT: 0.02
SCALE:2:1
SHEET 1 OF 1

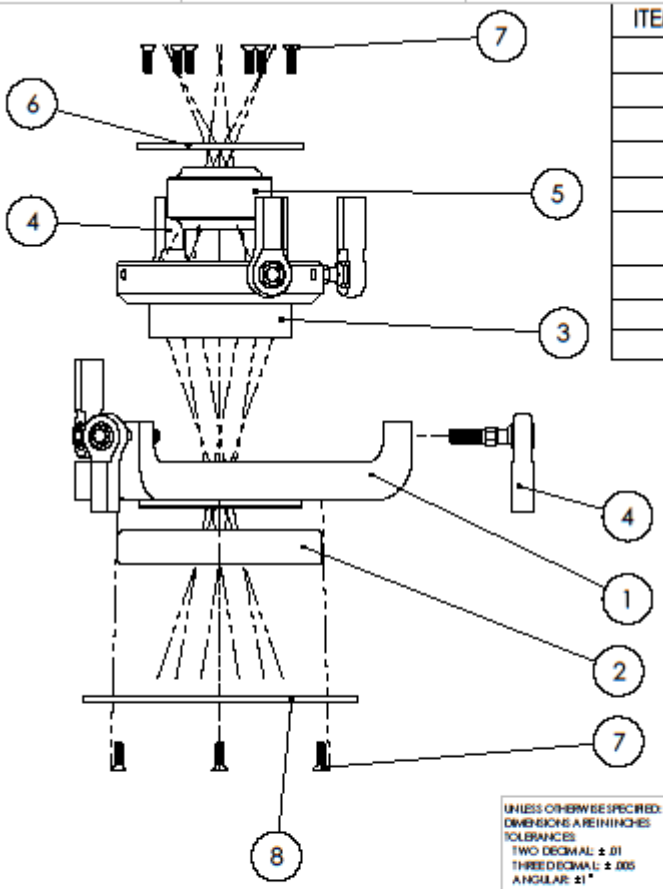

ITEM NO.	PartNo	Description	QTY.
1	HHTS-006-002	LOWER SWASHPLATE	1
2	HHTS-006-003	SWASHPLATE ROLLER BEARING	1
3	HHTS-006-001	UPPER SWASHPLATE	1
4	HHTS-006-004	BALL LINKS	8
5	HHTS-006-006	SPHERICAL BEARING	1
6	HHTS-006-007	SPHERICAL BEARING RETAINING RING	1
7	HHTS-006-005	RETAINING RING SCREW	18
8	HHTS-006-009	OUTER RETAINING RING	1
9	HHTS-006-008	INNER RETAINING RING	1

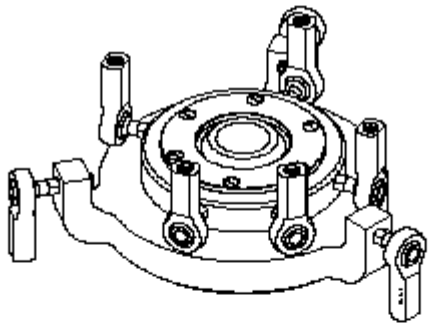

UNLESS OTHERWISE SPECIFIED:
DIMENSIONS ARE IN INCHES
TOLERANCES
TWO DECIMAL ± .01
THREE DECIMAL ± .005
ANGULAR: ±1°

FINISH:

DEBUR AND BREAK SHARP EDGES

DO NOT SCALE DRAWING

REVISION

	NAME	SIGNATURE	DATE
DRAWN	JCF		
CHK'D	JPJ		
APP'VD	ABL		
MFG	JPJ		
Q.A	BEA		

MATERIAL:

WEIGHT: 761.6707

Helicopter Hover Test Stand

TITLE:

SWASHPLATE ASSEMBLY

DWG NO. HHTS-006

A4

SCALE:1:2

SHEET 1 OF 1

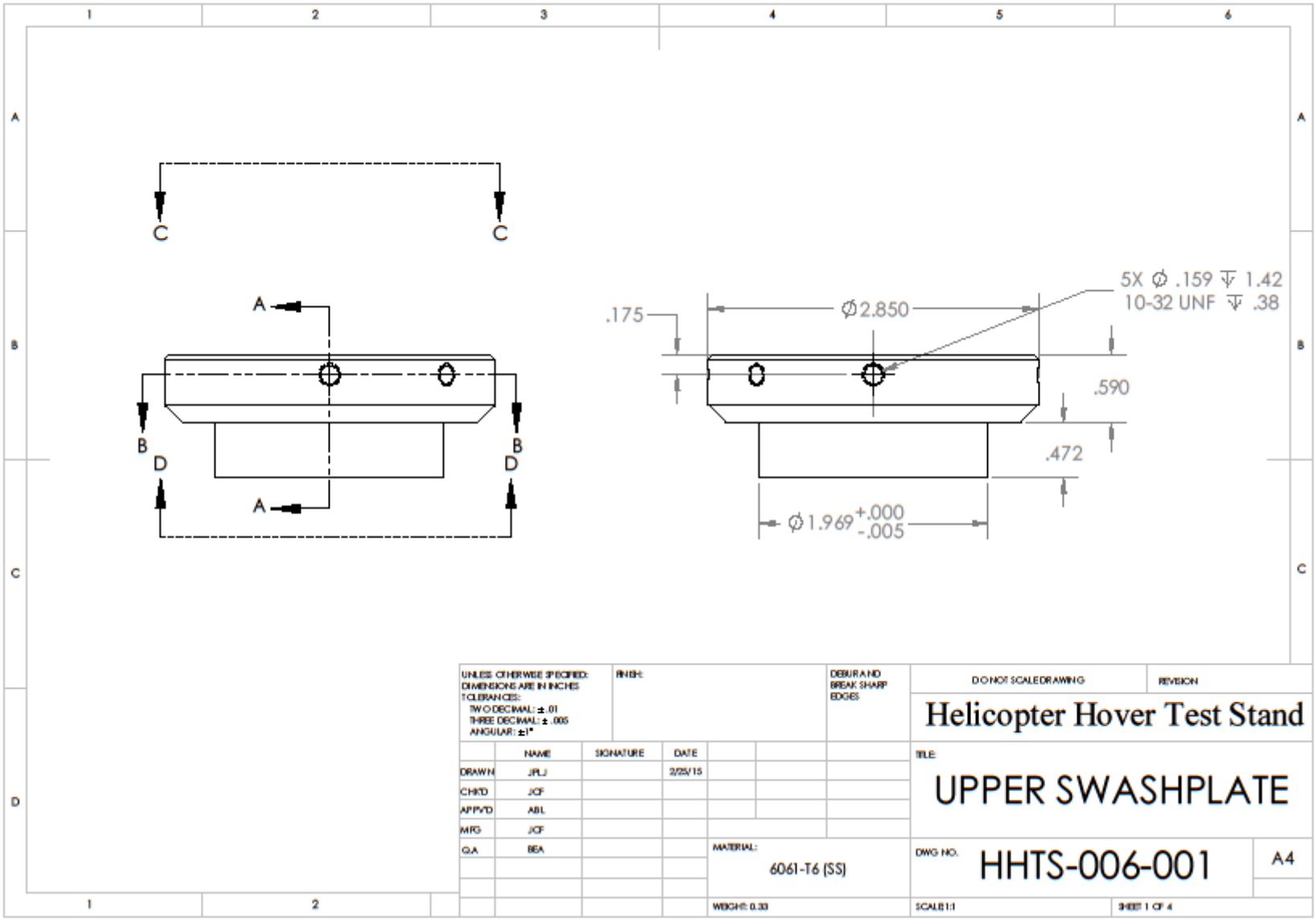
C
C
A
B
D
B
D
A
.175
Ø2.850
5X Ø .159 ↧ 1.42
10-32 UNF ↧ .38
.590
.472
Ø1.969 +.000 -.005
UNLESS OTHERWISE SPECIFIED:
DIMENSIONS ARE IN INCHES
TOLERANCES:
TWO DECIMAL: ± .01
THREE DECIMAL: ± .005
ANGULAR: ±1°
FINISH:
DEBUR AND BREAK SHARP EDGES
DO NOT SCALE DRAWING
REVISION
Helicopter Hover Test Stand
NAME
SIGNATURE
DATE
DRAWN
JPLJ
2/25/15
CHK'D
JCF
APP'VD
ABL
MFG
JCF
Q.A
BEA
MATERIAL:
6061-T6 (SS)
TITLE:
UPPER SWASHPLATE
DWG NO.
HHTS-006-001
A4
WEIGHT: 0.33
SCALE:1:1
SHEET 1 OF 4

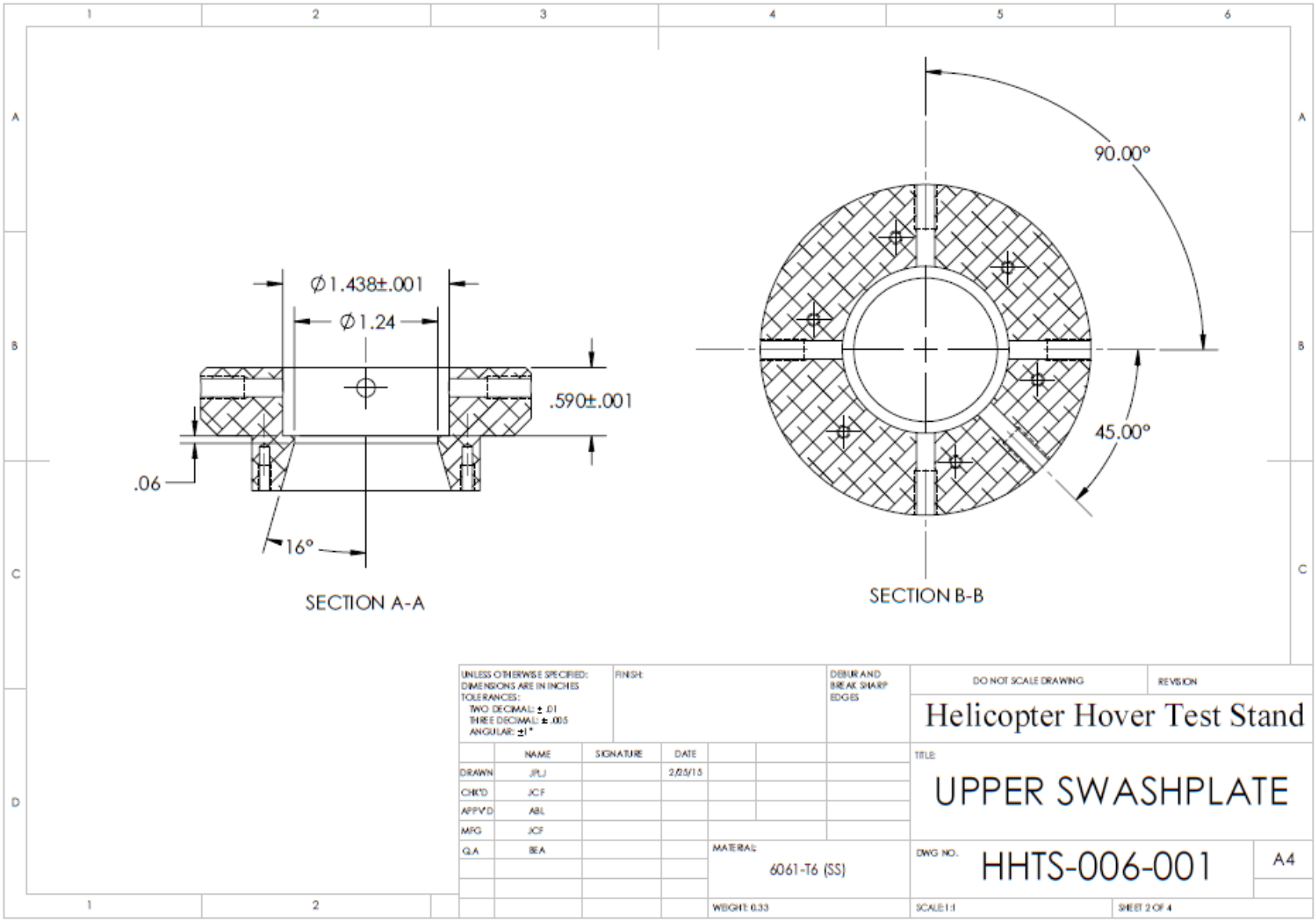
Ø1.438±.001
Ø1.24
.590±.001
.06
16°
SECTION A-A
90.00°
45.00°
SECTION B-B
UNLESS OTHERWISE SPECIFIED:
DIMENSIONS ARE IN INCHES
TOLERANCES:
TWO DECIMAL: ± .01
THREE DECIMAL: ± .005
ANGULAR: ±1°
FINISH:
DEBUR AND BREAK SHARP EDGES
DO NOT SCALE DRAWING
REVISION
Helicopter Hover Test Stand
NAME
SIGNATURE
DATE
DRAWN
JPLJ
2/25/15
CHK'D
JCF
APPV'D
ABL
MFG
JCF
Q.A
BEA
TITLE:
UPPER SWASHPLATE
MATERIAL:
6061-T6 (SS)
DWG NO.
HHTS-006-001
A4
WEIGHT: 0.33
SCALE:1:1
SHEET 2 OF 4

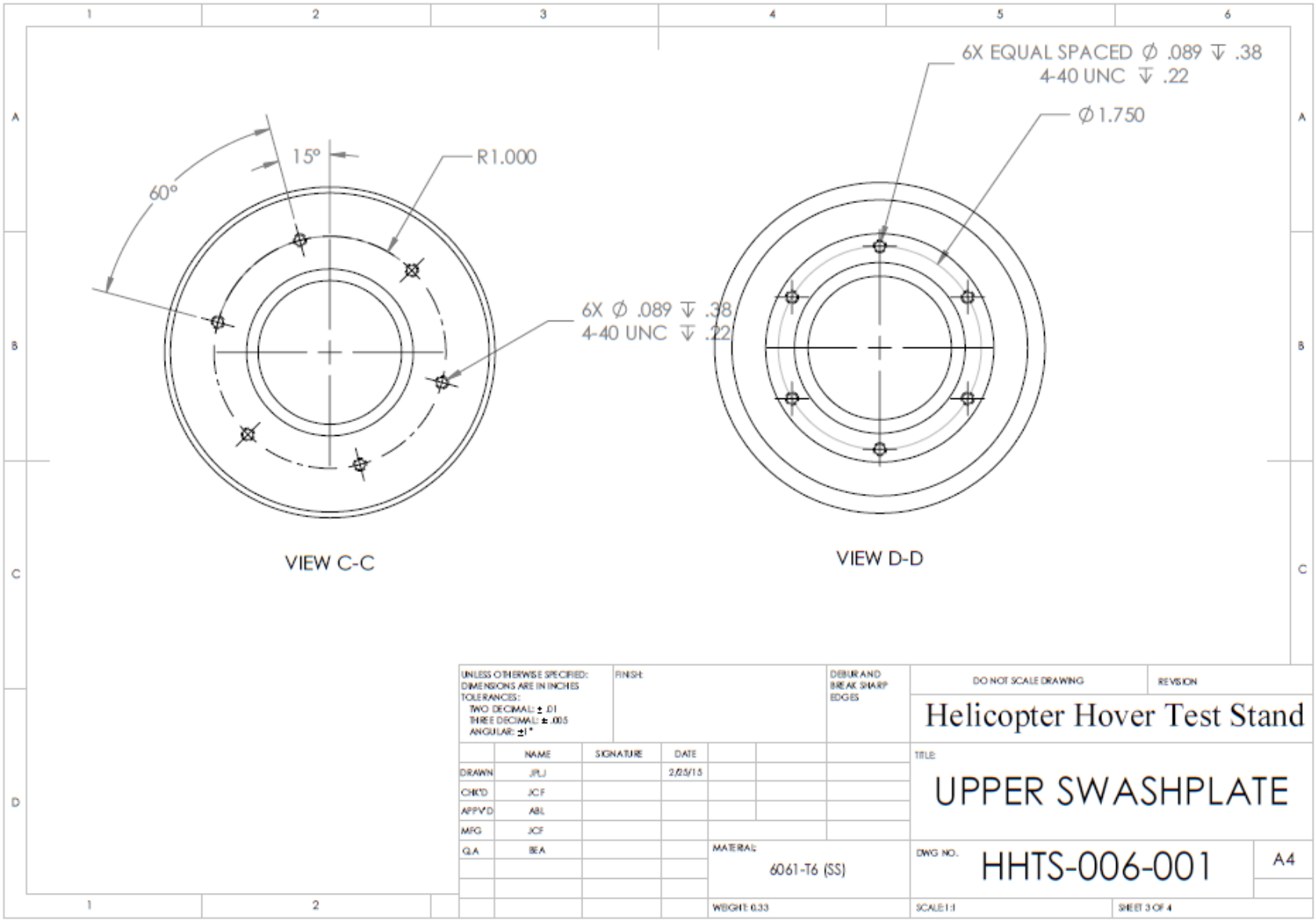
6X EQUAL SPACED ∅ .089 ↧ .38
4-40 UNC ↧ .22
∅1.750
15°
60°
R1.000
6X ∅ .089 ↧ .38
4-40 UNC ↧ .22
VIEW C-C
VIEW D-D
UNLESS OTHERWISE SPECIFIED:
DIMENSIONS ARE IN INCHES
TOLERANCES:
TWO DECIMAL: ± .01
THREE DECIMAL: ± .005
ANGULAR: ±1°
FINISH:
DEBUR AND BREAK SHARP EDGES
DO NOT SCALE DRAWING
REVISION
Helicopter Hover Test Stand
NAME
SIGNATURE
DATE
DRAWN
JPLJ
2/25/15
CHK'D
JCF
APP'V'D
ABL
MFG
JCF
Q.A
BEA
MATERIAL:
6061-T6 (SS)
TITLE:
UPPER SWASHPLATE
DWG NO.
HHTS-006-001
A4
WEIGHT: 0.33
SCALE: 1:1
SHEET 3 OF 4

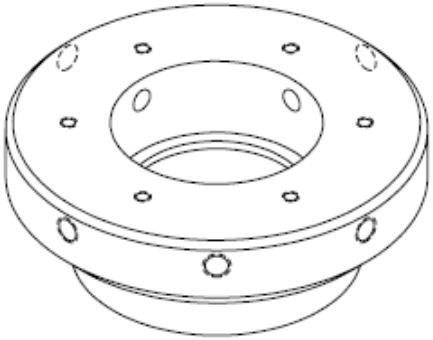

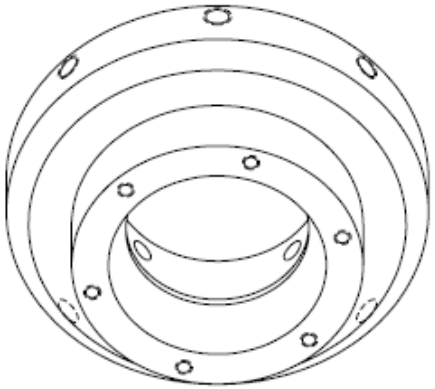

UNLESS OTHERWISE SPECIFIED: DIMENSIONS ARE IN INCHES TOLERANCES: TWO DECIMAL: ± .01 THREE DECIMAL: ± .005 ANGULAR: ±1°	FINISH:				DEBUR AND BREAK SHARP EDGES	DO NOT SCALE DRAWING	REVISION
	NAME	SIGNATURE	DATE			Helicopter Hover Test Stand	
DRAWN	JPLJ		2/23/15			TITLE: UPPER SWASHPLATE	
CHK'D	JCF						
APP'V'D	ABL						
MFG	JCF						
Q.A	BEA			MATERIAL: 6061-T6 (SS)		DWG NO. HHTS-006-001	A4
				WEIGHT: 0.33		SCALE:1:1	SHEET 4 OF 4

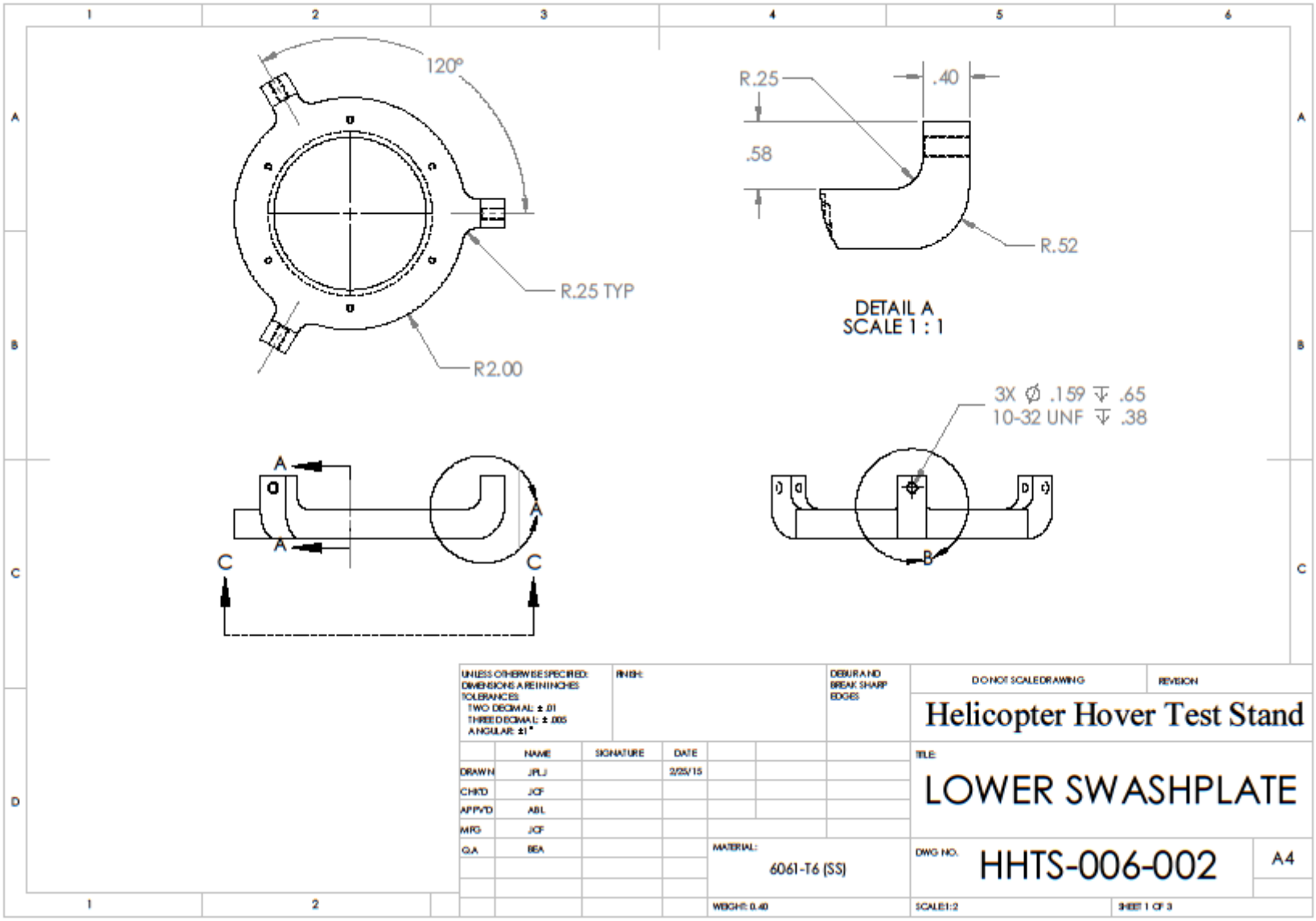
120°
R.25 TYP
R2.00
R.25
.40
.58
R.52
DETAIL A
SCALE 1 : 1
3X Ø .159 ↧ .65
10-32 UNF ↧ .38
A
A
A
C
C
B
UNLESS OTHERWISE SPECIFIED:
DIMENSIONS ARE IN INCHES
TOLERANCES
TWO DECIMAL ± .01
THREE DECIMAL: ± .005
ANGULAR: ±1°
FINISH:
DEBUR AND BREAK SHARP EDGES
DO NOT SCALE DRAWING
REVISION
NAME
SIGNATURE
DATE
DRAWN
JPLJ
2/25/15
CHK'D
JCF
APP'VD
ABL
MFG
JCF
Q.A
BEA
MATERIAL:
6061-T6 (SS)
WEIGHT: 0.40
Helicopter Hover Test Stand
TITLE:
LOWER SWASHPLATE
DWG NO.
HHTS-006-002
A4
SCALE:1:2
SHEET 1 OF 3

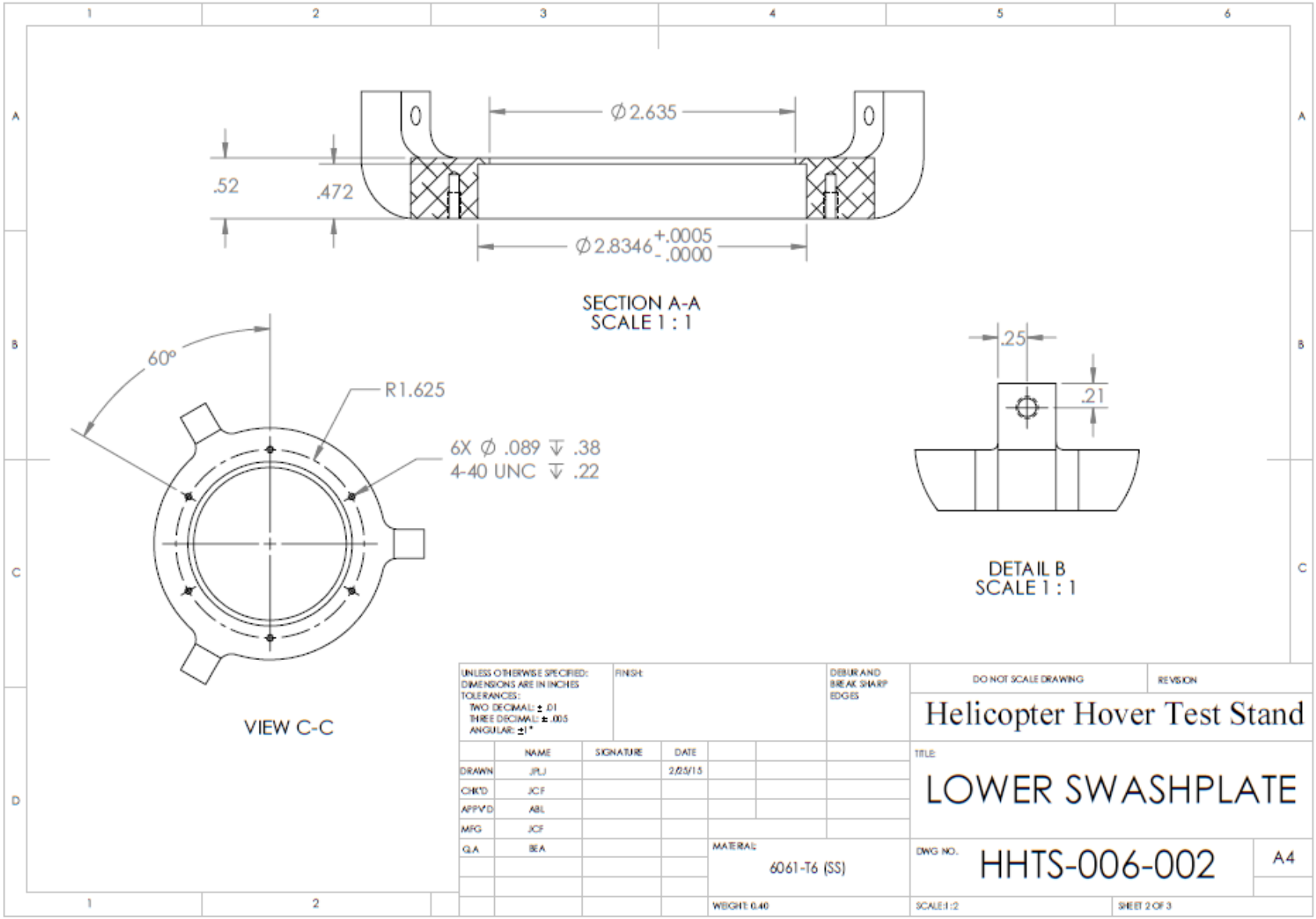
Ø2.635
.52
.472
Ø2.8346 +.0005 -.0000
SECTION A-A
SCALE 1 : 1
60°
R1.625
6X Ø .089 ↧ .38
4-40 UNC ↧ .22
VIEW C-C
.25
.21
DETAIL B
SCALE 1 : 1
UNLESS OTHERWISE SPECIFIED:
DIMENSIONS ARE IN INCHES
TOLERANCES:
TWO DECIMAL: ± .01
THREE DECIMAL: ± .005
ANGULAR: ±1°
FINISH:
DEBUR AND BREAK SHARP EDGES
DO NOT SCALE DRAWING
REVISION
Helicopter Hover Test Stand
NAME
SIGNATURE
DATE
DRAWN
JPLJ
2/23/15
CHK'D
JCF
APPV'D
ABL
MFG
JCF
Q.A
BEA
MATERIAL:
6061-T6 (SS)
TITLE:
LOWER SWASHPLATE
DWG NO.
HHTS-006-002
A4
WEIGHT: 0.40
SCALE:1:2
SHEET 2 OF 3

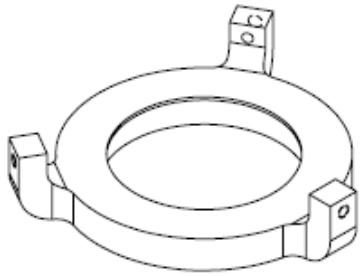

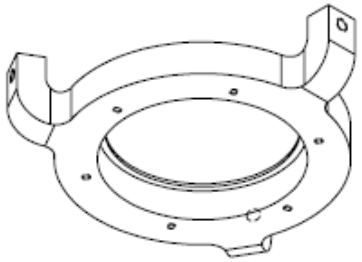

UNLESS OTHERWISE SPECIFIED: DIMENSIONS ARE IN INCHES TOLERANCES: TWO DECIMAL: ± .01 THREE DECIMAL: ± .005 ANGULAR: ±1°	FINISH:		DEBUR AND BREAK SHARP EDGES	DO NOT SCALE DRAWING	REVISION	
				Helicopter Hover Test Stand		
	NAME	SIGNATURE	DATE	TITLE:		
DRAWN	JPLJ		2/25/15	LOWER SWASHPLATE		
CHK'D	JCF					
APP'V'D	ABL					
MFG	JCF					
Q.A	BEA					
				MATERIAL: 6061-T6 (SS)	DWG NO. HHTS-006-002	A4
				WEIGHT: 0.40	SCALE:1:2	SHEET 3 OF 3

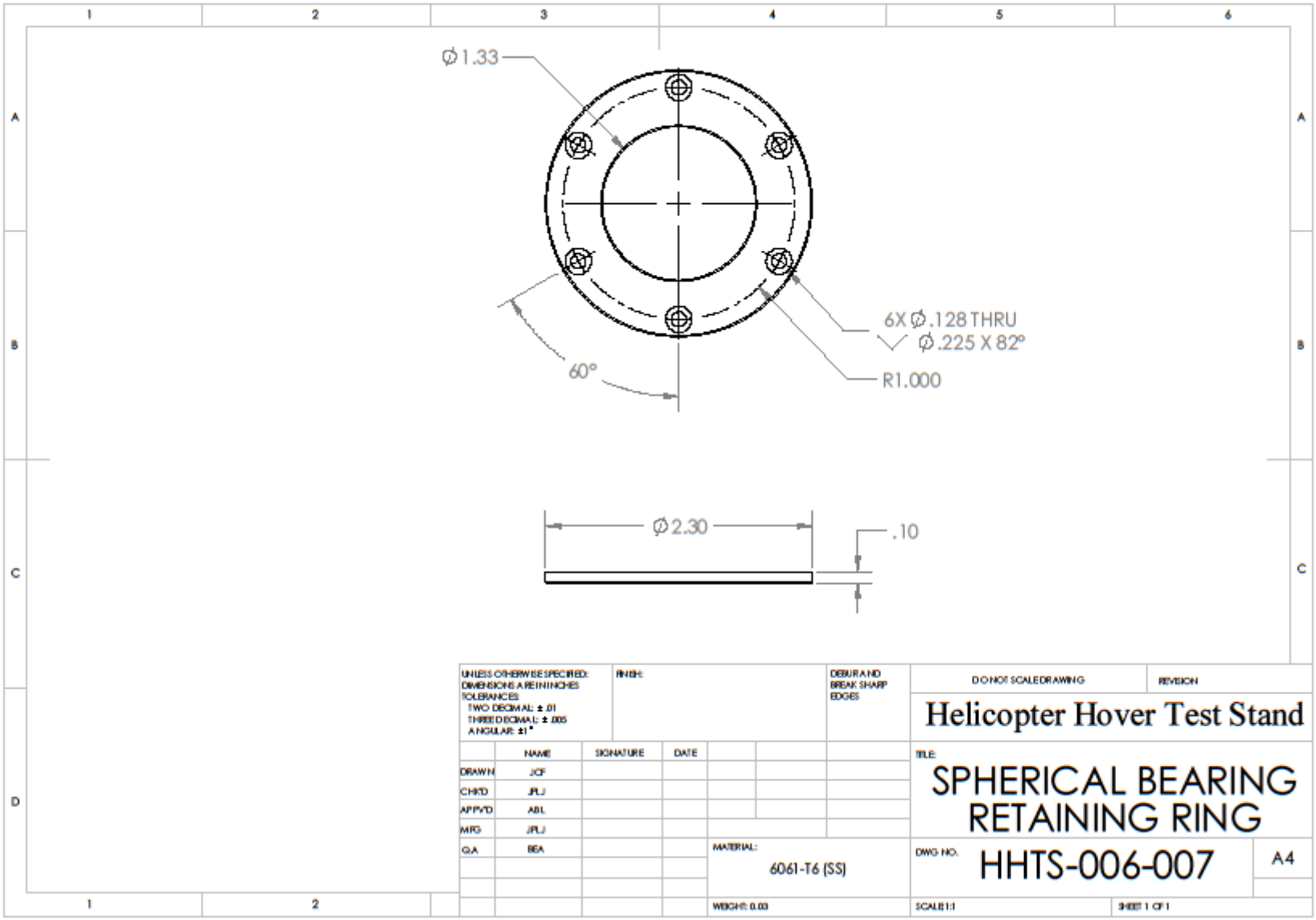
Ø1.33
6X Ø.128 THRU
Ø.225 X 82°
60°
R1.000
Ø2.30
.10
UNLESS OTHERWISE SPECIFIED:
DIMENSIONS ARE IN INCHES
TOLERANCES
TWO DECIMAL ± .01
THREE DECIMAL ± .005
ANGULAR: ±1°
FINISH:
DEBUR AND BREAK SHARP EDGES
DO NOT SCALE DRAWING
REVISION
Helicopter Hover Test Stand
NAME
SIGNATURE
DATE
DRAWN JCF
CHK'D JPJ
APP'VD ABL
MFG JPJ
Q.A BEA
MATERIAL:
6061-T6 (SS)
WEIGHT: 0.03
TITLE:
SPHERICAL BEARING RETAINING RING
DWG NO.
HHTS-006-007
A4
SCALE:1:1
SHEET 1 OF 1

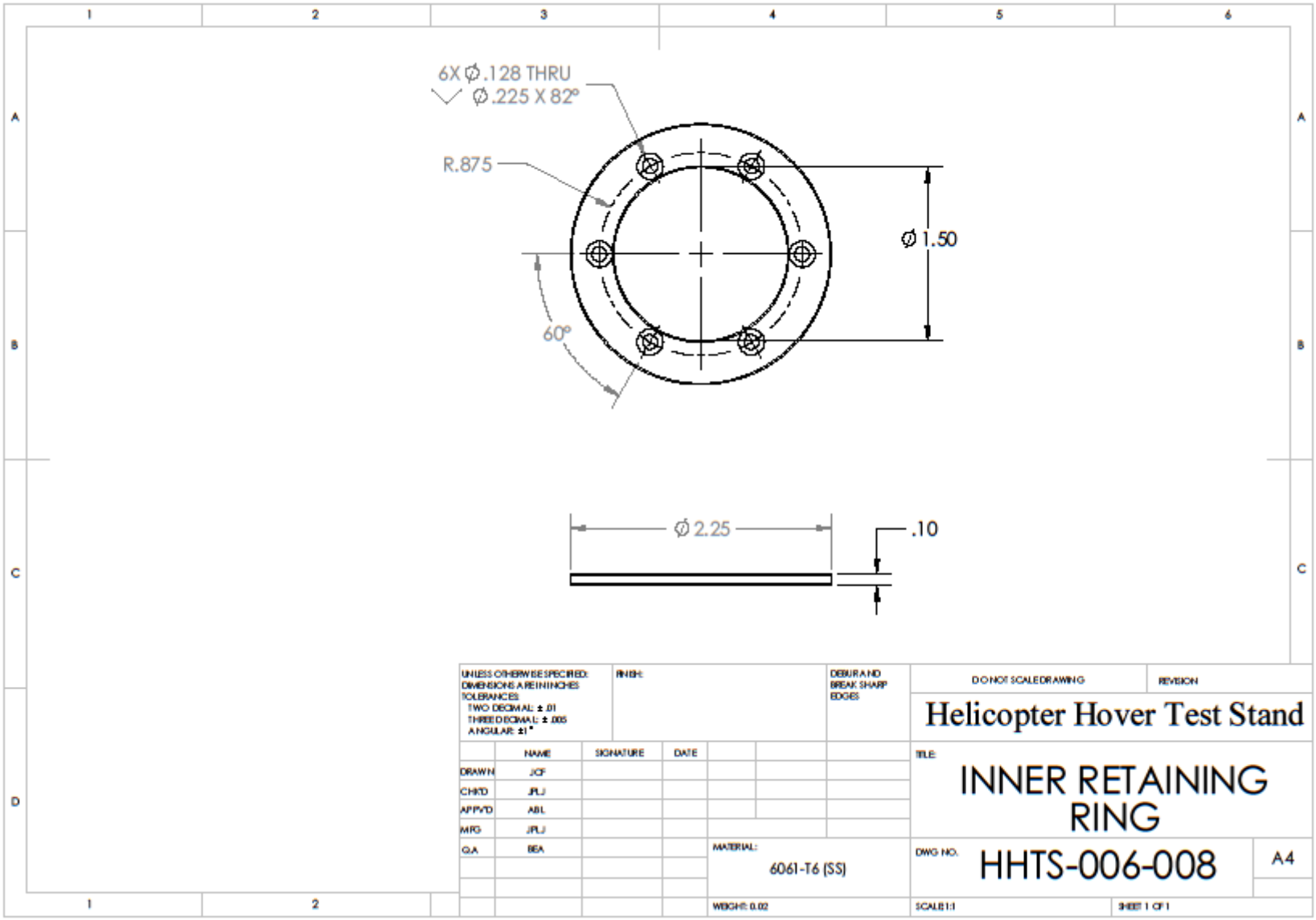
6X Ø.128 THRU
Ø.225 X 82°
R.875
Ø1.50
60°
Ø2.25
.10
UNLESS OTHERWISE SPECIFIED:
DIMENSIONS ARE IN INCHES
TOLERANCES:
TWO DECIMAL ± .01
THREE DECIMAL: ± .005
ANGULAR: ±1°
FINISH:
DEBUR AND BREAK SHARP EDGES
DO NOT SCALE DRAWING
REVISION
Helicopter Hover Test Stand
NAME
SIGNATURE
DATE
DRAWN JCF
CHK'D JPLJ
APP'VD ABL
MFG JPLJ
Q.A BEA
TITLE:
INNER RETAINING RING
MATERIAL:
6061-T6 (SS)
DWG NO.
HHTS-006-008
A4
WEIGHT: 0.02
SCALE:1:1
SHEET 1 OF 1

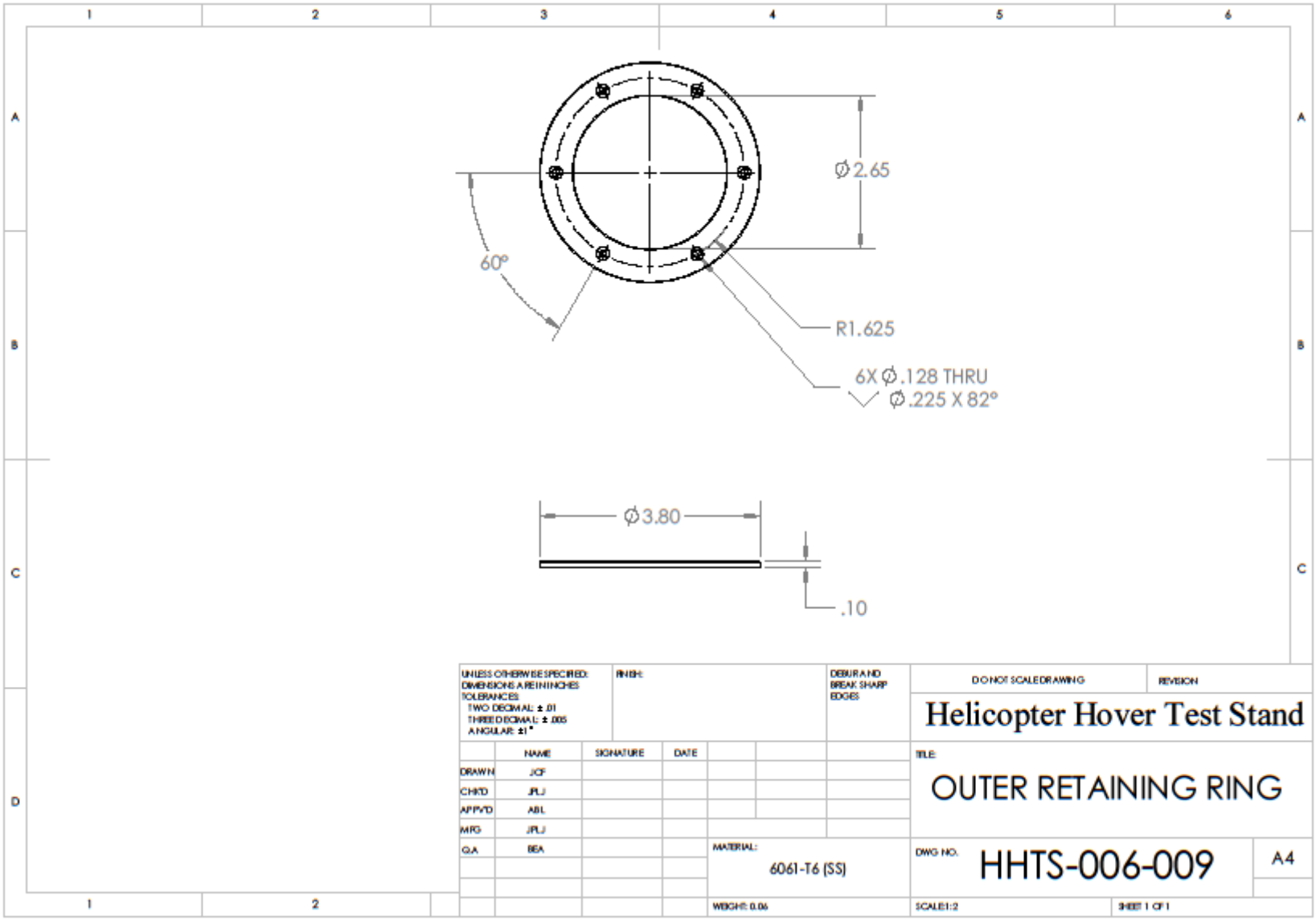

UNLESS OTHERWISE SPECIFIED:
DIMENSIONS ARE IN INCHES
TOLERANCES:
TWO DECIMAL ± .01
THREE DECIMAL ± .005
ANGULAR: ±1°

FINISH:

DEBUR AND BREAK SHARP EDGES

DO NOT SCALE DRAWING | REVISION

	NAME	SIGNATURE	DATE
DRAWN	JCF		
CHK'D	JPLJ		
APP'VD	ABL		
MFG	JPLJ		
Q.A	BEA		

MATERIAL: 6061-T6 (SS)

WEIGHT: 0.06

Helicopter Hover Test Stand

TITLE:

OUTER RETAINING RING

DWG NO. HHTS-006-009

A4

SCALE: 1:2

SHEET 1 OF 1

ITEM NO.	Description	PartNo	QTY.
1	LOWER MOUNTING PLATE	HHTS-007-004	1
2	SERVO MOUNTING PLATE	HHTS-007-003	1
3	BEARING SPACER	HHTS-007-002	1
4	SHAFT BEARING	HHTS-007-006	2
5	SHAFT BEARING HOUSING	HHTS-007-001	1

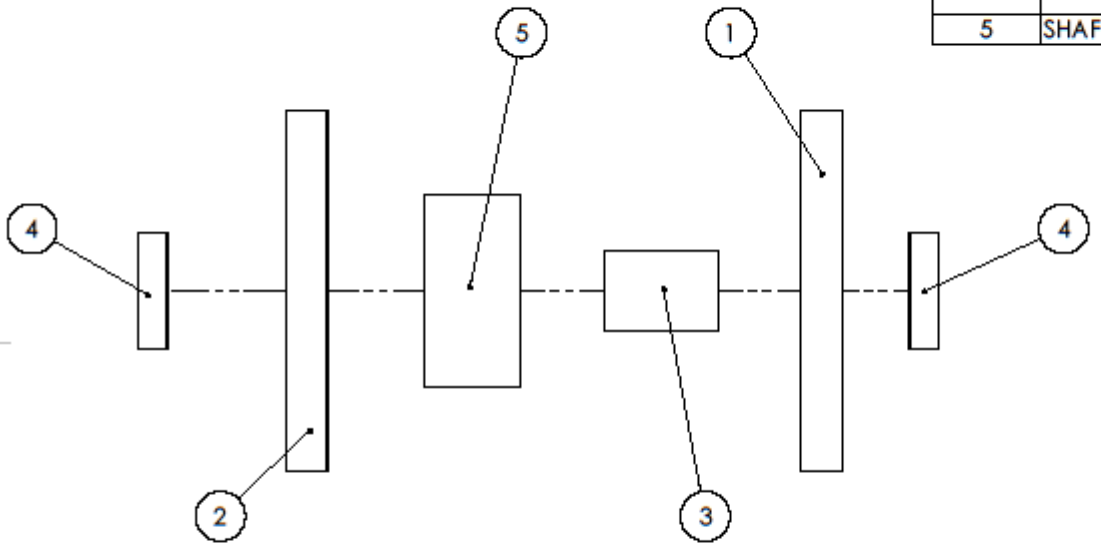

UNLESS OTHERWISE SPECIFIED:
DIMENSIONS ARE IN INCHES
TOLERANCES:
TWO DECIMAL ± .01
THREE DECIMAL ± .005
ANGULAR: ±1°

FINISH:

DEBUR AND BREAK SHARP EDGES

DO NOT SCALE DRAWING

REVISION

	NAME	SIGNATURE	DATE
DRAWN	BEA		
CHK'D	JPJ		
APP'VD	ABL		
MFG	JPJ		
Q.A	JCF		

MATERIAL:

WEIGHT:

Helicopter Hover Test Stand

TITLE:

DRIVESHAFT BEARING HOUSING

DWG NO. HHTS-007

A4

SCALE:1:3

SHEET 1 OF 1

ITEM NO.	Description	PartNo	QTY.
1	LOWER MOUNTING PLATE	HHTS-007-004	1
2	SERVO MOUNTING PLATE	HHTS-007-003	1
3	BEARING SPACER	HHTS-007-002	1
4	SHAFT BEARING	HHTS-007-006	2
5	SHAFT BEARING HOUSING	HHTS-007-001	1

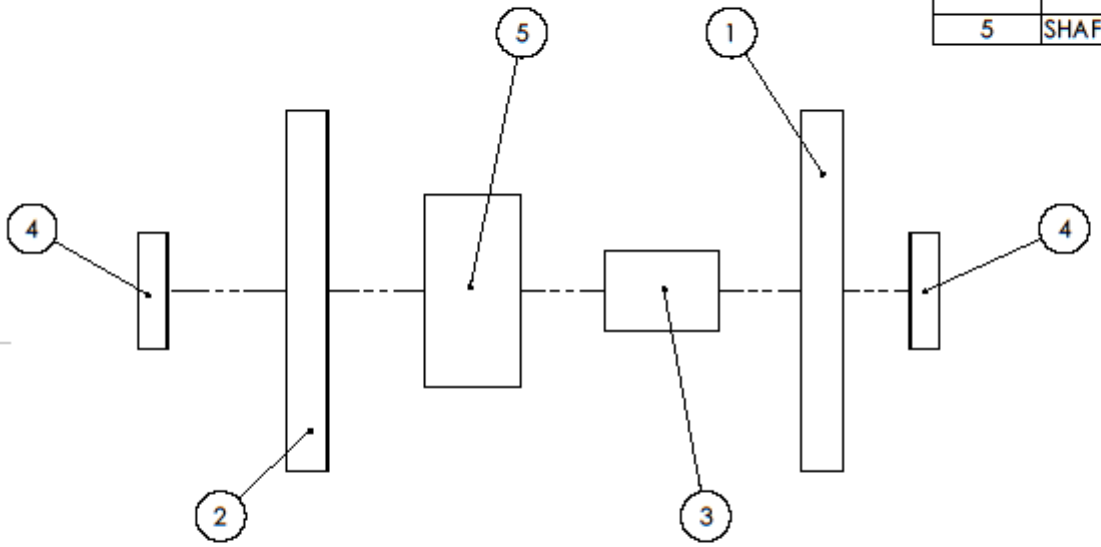

UNLESS OTHERWISE SPECIFIED:
DIMENSIONS ARE IN INCHES
TOLERANCES
TWO DECIMAL ± .01
THREE DECIMAL ± .005
ANGULAR: ±1°

FINISH:

DEBUR AND BREAK SHARP EDGES

DO NOT SCALE DRAWING

REVISION

	NAME	SIGNATURE	DATE
DRAWN	BEA		
CHK'D	JPJ		
APP'VD	ABL		
MFG	JPJ		
Q.A	JCF		

MATERIAL:

WEIGHT:

Helicopter Hover Test Stand

TITLE:

DRIVESHAFT BEARING HOUSING

DWG NO. HHTS-007

A4

SCALE:1:3

SHEET 1 OF 1

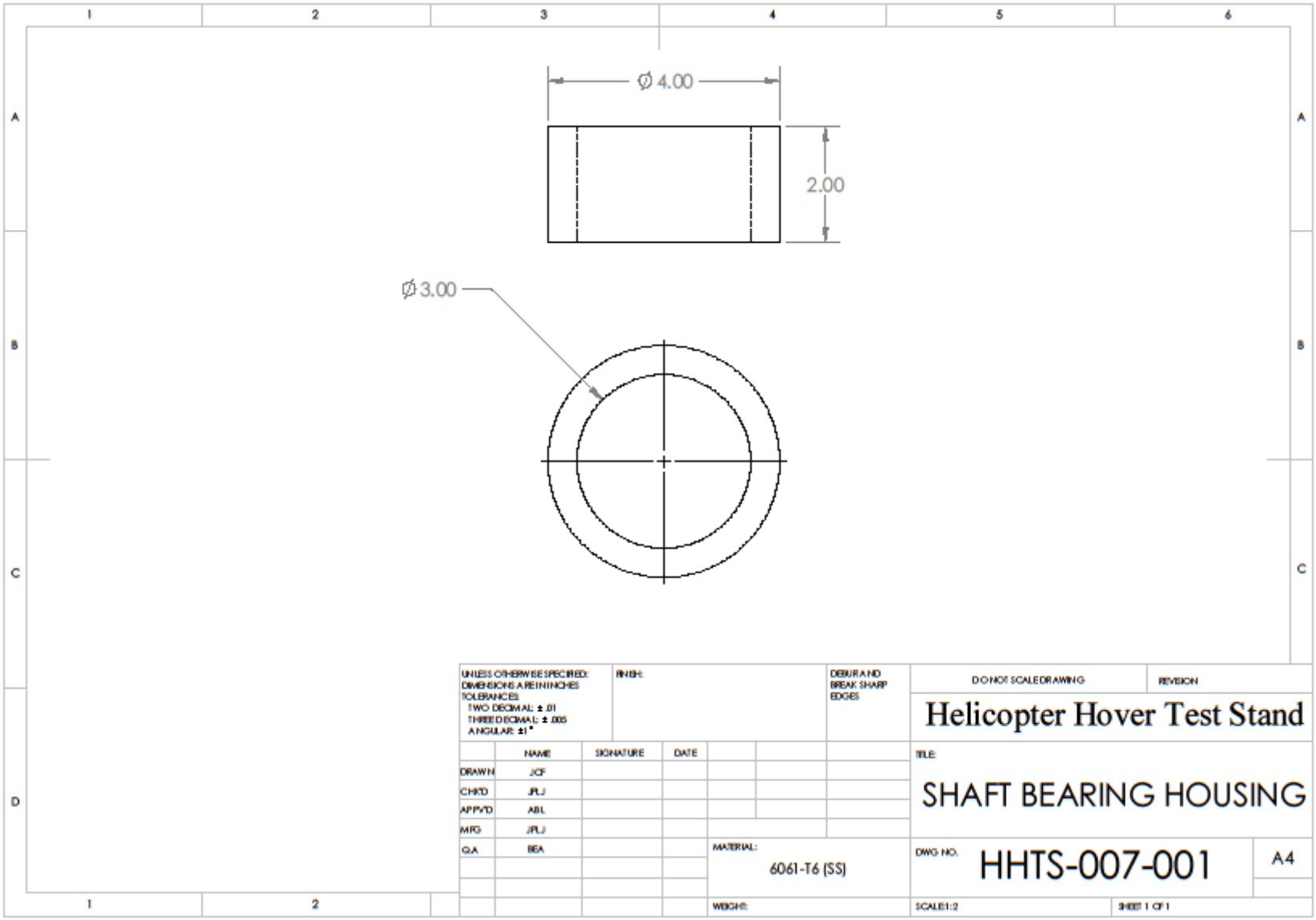
Ø 4.00
2.00
Ø 3.00
UNLESS OTHERWISE SPECIFIED:
DIMENSIONS ARE IN INCHES
TOLERANCES:
TWO DECIMAL ± .01
THREE DECIMAL ± .005
ANGULAR: ±1°
FINISH:
DEBUR AND BREAK SHARP EDGES
DO NOT SCALE DRAWING
REVISION
Helicopter Hover Test Stand
NAME
SIGNATURE
DATE
DRAWN JCF
CHK'D JPLJ
APP'VD ABL
MFG JPLJ
Q.A BEA
MATERIAL:
6061-T6 (SS)
TITLE:
SHAFT BEARING HOUSING
DWG NO.
HHTS-007-001
A4
WEIGHT:
SCALE:1:2
SHEET 1 OF 1

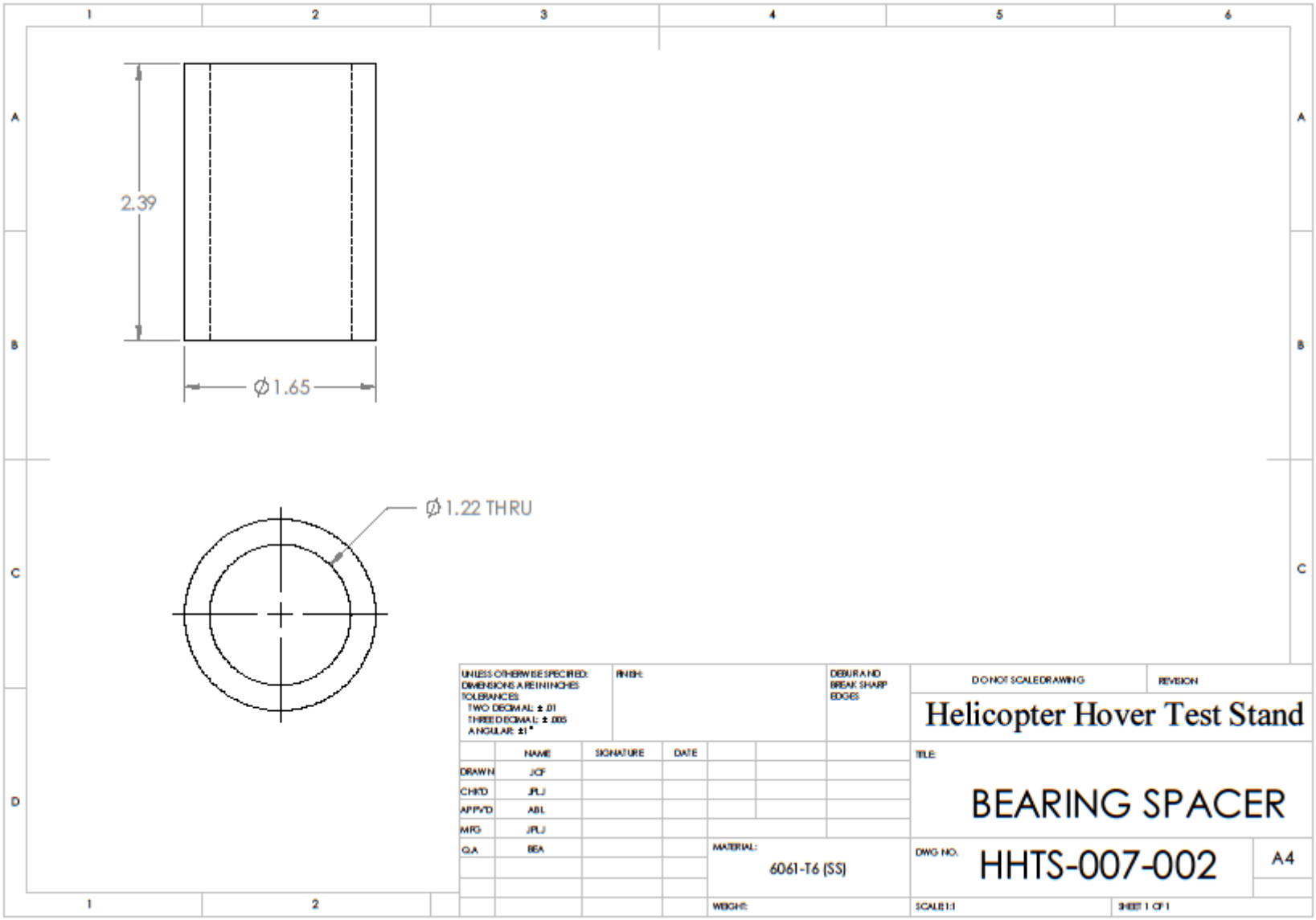
2.39
Ø1.65
Ø1.22 THRU
UNLESS OTHERWISE SPECIFIED:
DIMENSIONS ARE IN INCHES
TOLERANCES:
TWO DECIMAL: ± .01
THREE DECIMAL: ± .005
ANGULAR: ±1°
FINISH:
DEBUR AND BREAK SHARP EDGES
DO NOT SCALE DRAWING
REVISION
Helicopter Hover Test Stand
NAME
SIGNATURE
DATE
DRAWN JCF
CHKD JPLJ
APPVD ABL
MFG JPLJ
Q.A BEA
MATERIAL:
6061-T6 (SS)
TITLE:
BEARING SPACER
DWG NO.
HHTS-007-002
A4
WEIGHT:
SCALE:1:1
SHEET 1 OF 1

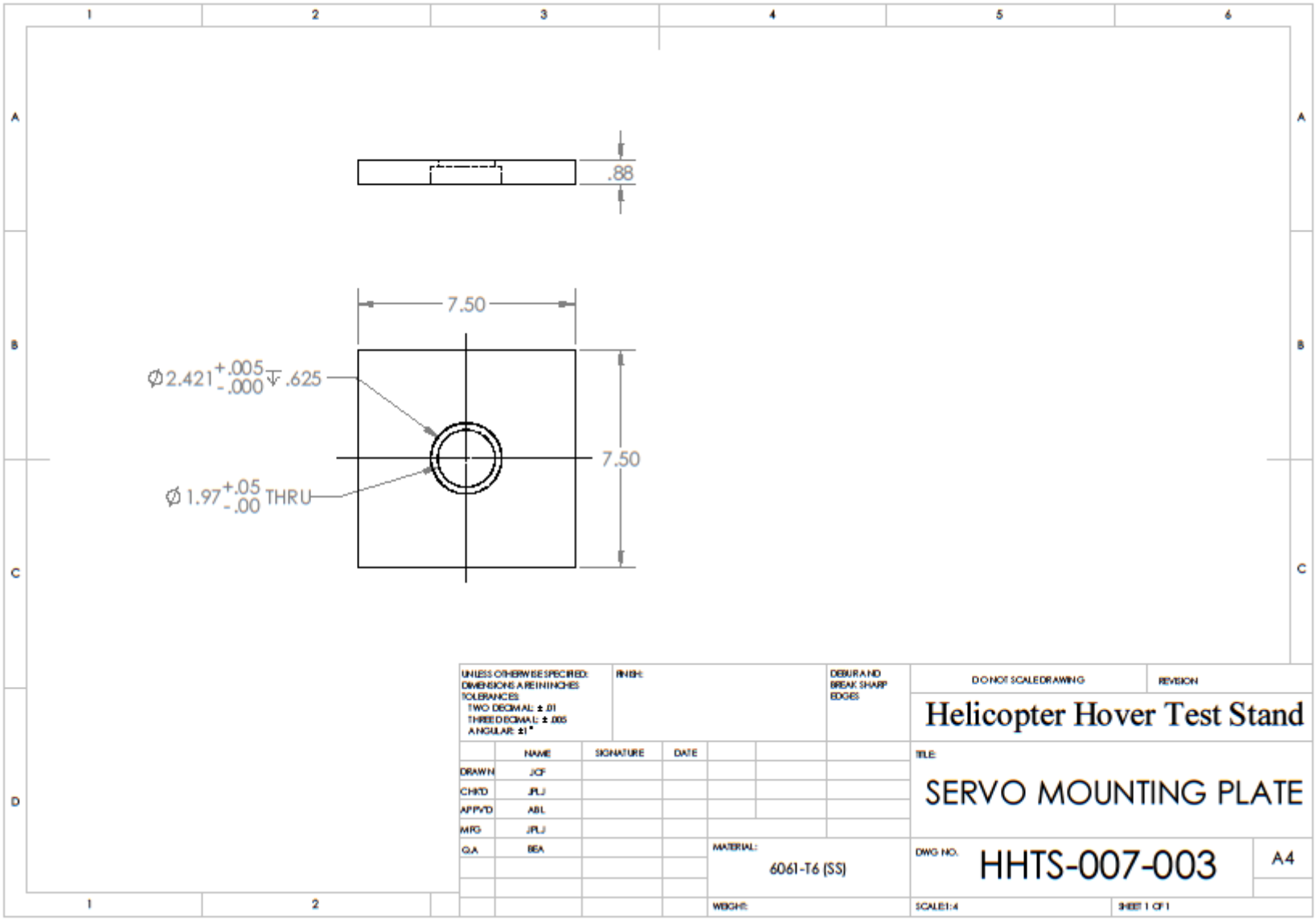
.88
7.50
Ø2.421 +.005 -.000 ↧ .625
Ø 1.97 +.05 -.00 THRU
7.50
UNLESS OTHERWISE SPECIFIED:
DIMENSIONS ARE IN INCHES
TOLERANCES:
TWO DECIMAL ± .01
THREE DECIMAL: ± .005
ANGULAR: ±1°
FINISH:
DEBUR AND BREAK SHARP EDGES
DO NOT SCALE DRAWING
REVISION
Helicopter Hover Test Stand
NAME
SIGNATURE
DATE
DRAWN JCF
CHK'D JPLJ
APP'VD ABL
MFG JPLJ
Q.A BEA
MATERIAL:
6061-T6 (SS)
TITLE:
SERVO MOUNTING PLATE
DWG NO.
HHTS-007-003
A4
WEIGHT:
SCALE:1:4
SHEET 1 OF 1

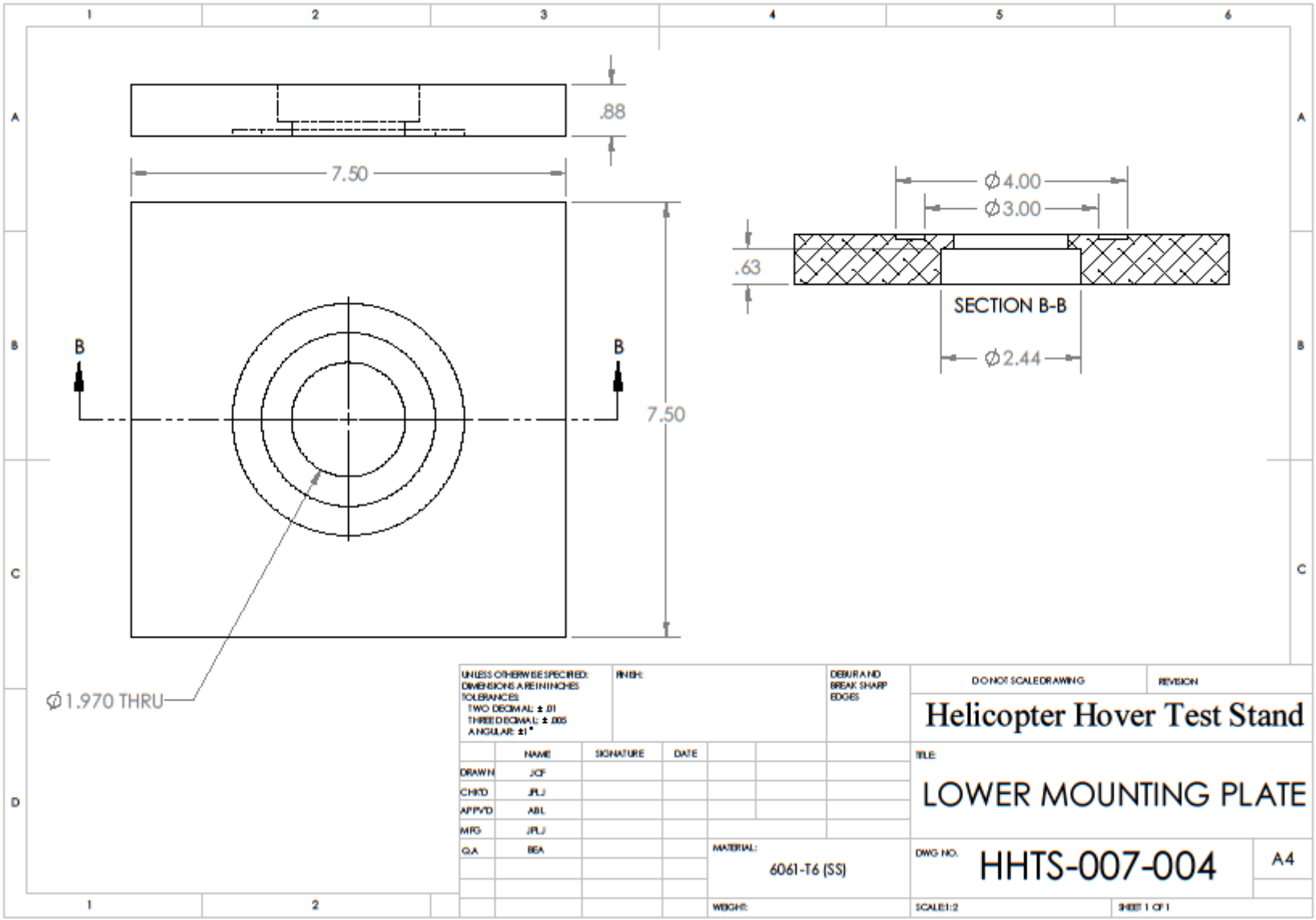
.88
7.50
7.50
B
B
Ø1.970 THRU
Ø4.00
Ø3.00
.63
SECTION B-B
Ø2.44
UNLESS OTHERWISE SPECIFIED:
DIMENSIONS ARE IN INCHES
TOLERANCES:
TWO DECIMAL ± .01
THREE DECIMAL ± .005
ANGULAR: ±1°
FINISH:
DEBUR AND BREAK SHARP EDGES
DO NOT SCALE DRAWING
REVISION
Helicopter Hover Test Stand
NAME
SIGNATURE
DATE
DRAWN JCF
CHKD JPLJ
APPVD ABL
MFG JPLJ
Q.A BEA
MATERIAL:
6061-T6 (SS)
WEIGHT:
TITLE:
LOWER MOUNTING PLATE
DWG NO.
HHTS-007-004
A4
SCALE:1:2
SHEET 1 OF 1

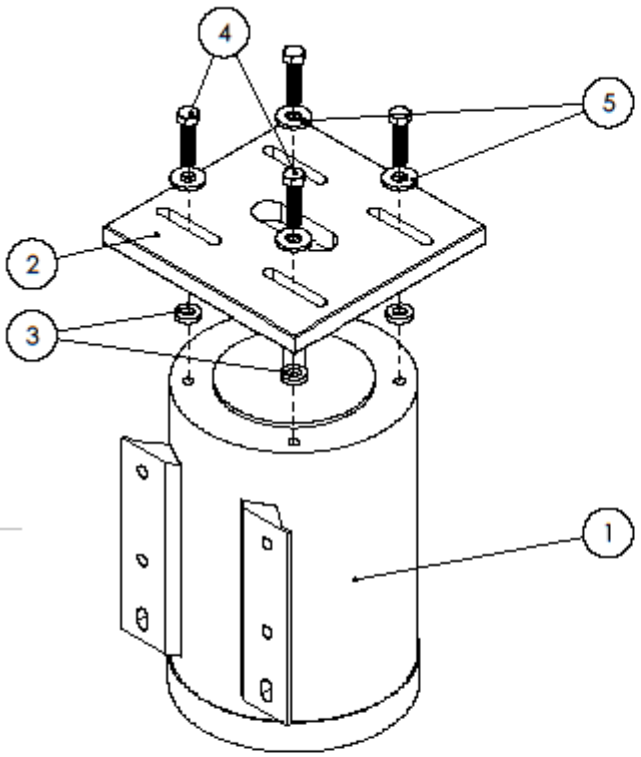

ITEM NO.	PartNo	DESCRIPTION	QTY.
1	HHTS-009-001	MOTOR	1
2	HHTS-009-002	MOTOR MOUNTING PLATE	1
3	HHTS-009-003	MOTOR MOUNT STANDOFF	4
4	HHTS-009-005	MOTOR MOUNT BOLT	4
5	HHTS-009-004	MOTOR MOUNT WASHER	4

UNLESS OTHERWISE SPECIFIED:
DIMENSIONS ARE IN INCHES
TOLERANCES:
TWO DECIMAL: ± .01
THREE DECIMAL: ± .005
ANGULAR: ±1°

FINISH:

DEBUR AND BREAK SHARP EDGES

DO NOT SCALE DRAWING

REVISION

	NAME	SIGNATURE	DATE
DRAWN	JCF		
CHK'D	JPLJ		
APP'VD	ABL		
MFG	JPLJ		
Q.A	BEA		

MATERIAL:

WEIGHT: 17.59

Helicopter Hover Test Stand

TITLE:

MOTOR MOUNT ASSEMBLY

DWG NO. HHTS-009

A4

SCALE: 1:4

SHEET 1 OF 1

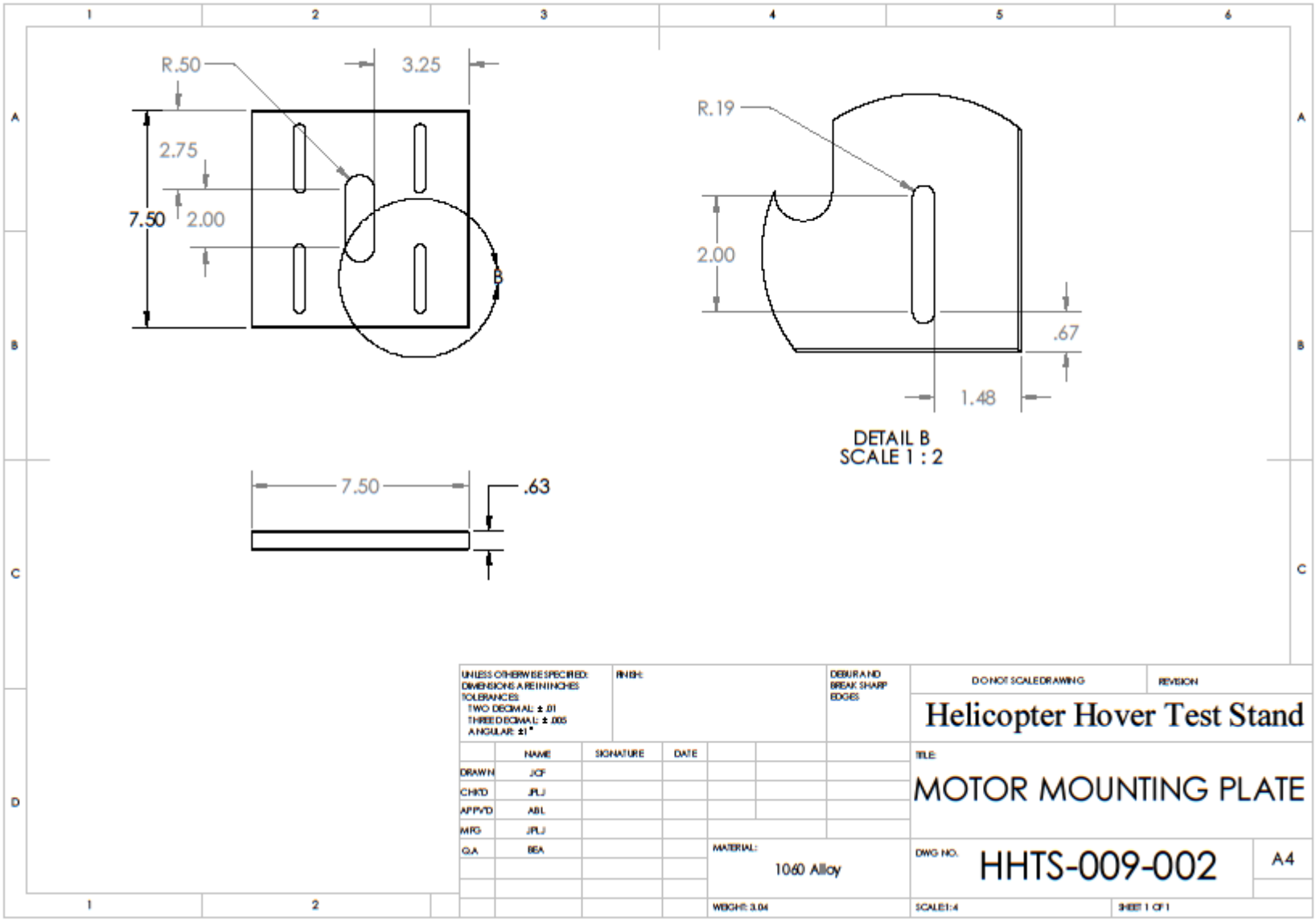
R.50
3.25
2.75
7.50
2.00
B
R.19
2.00
.67
1.48
DETAIL B
SCALE 1 : 2
7.50
.63
UNLESS OTHERWISE SPECIFIED:
DIMENSIONS ARE IN INCHES
TOLERANCES:
TWO DECIMAL ± .01
THREE DECIMAL ± .005
ANGULAR: ±1°
FINISH:
DEBUR AND BREAK SHARP EDGES
DO NOT SCALE DRAWING
REVISION
Helicopter Hover Test Stand
NAME
SIGNATURE
DATE
DRAWN
JCF
CHKD
JPLJ
APPVD
ABL
MFG
JPLJ
Q.A
BEA
MATERIAL:
1060 Alloy
TITLE:
MOTOR MOUNTING PLATE
DWG NO.
HHTS-009-002
A4
WEIGHT: 3.04
SCALE:1:4
SHEET 1 OF 1

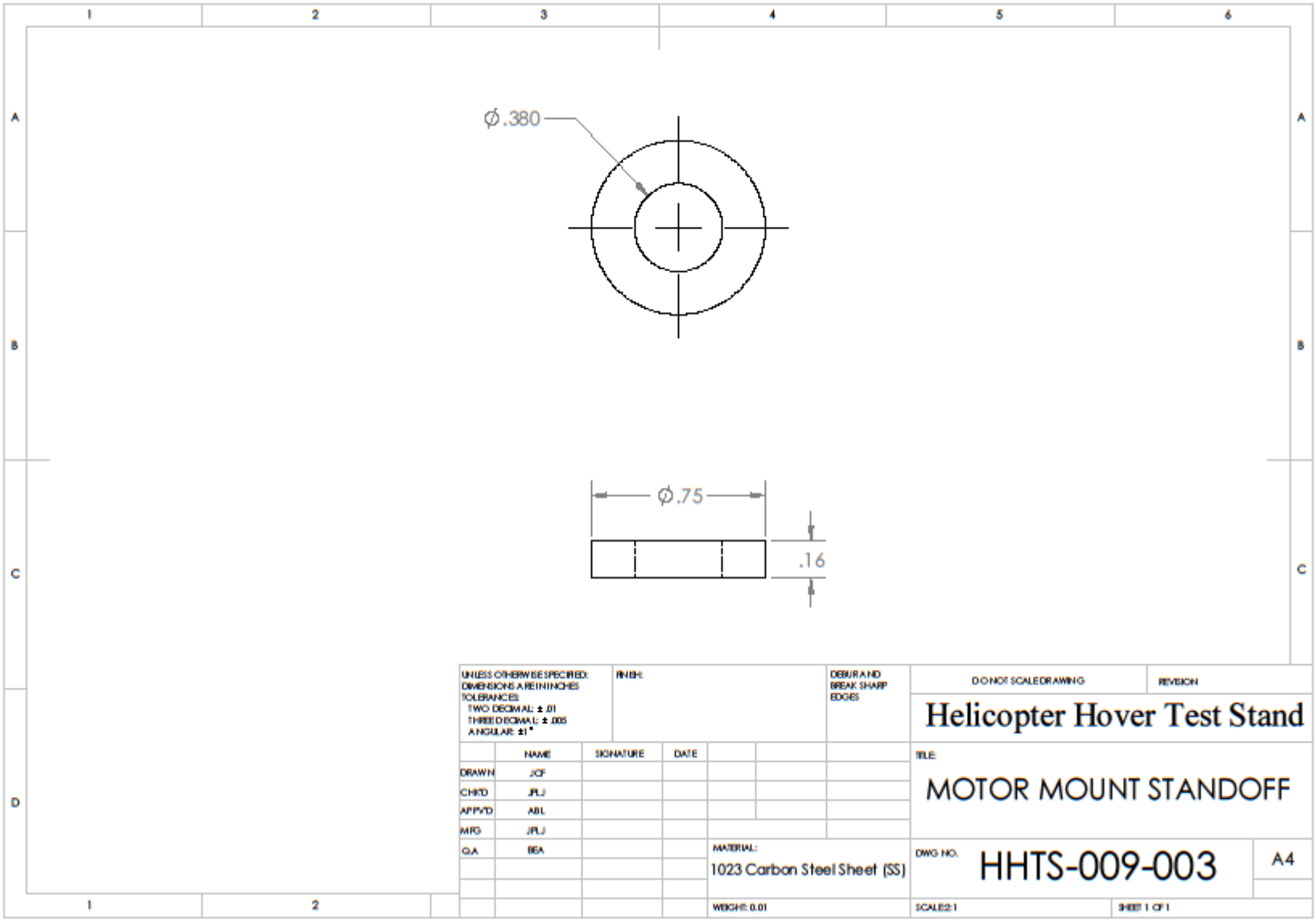
1
2
3
4
5
6
A
B
C
D
Ø.380
Ø.75
.16
UNLESS OTHERWISE SPECIFIED:
DIMENSIONS ARE IN INCHES
TOLERANCES:
TWO DECIMAL: ± .01
THREE DECIMAL: ± .005
ANGULAR: ±1°
FINISH:
DEBUR AND BREAK SHARP EDGES
DO NOT SCALE DRAWING
REVISION
Helicopter Hover Test Stand
NAME
SIGNATURE
DATE
DRAWN JCF
CHKD JPLJ
APPVD ABL
MFG JPLJ
Q.A BEA
TITLE:
MOTOR MOUNT STANDOFF
MATERIAL:
1023 Carbon Steel Sheet (SS)
DWG NO.
HHTS-009-003
A4
WEIGHT: 0.01
SCALE: 2:1
SHEET 1 OF 1

Appendix B

Process Documentation Sheets

Helicopter Hover Test Stand 2015: Manufacturing Plan						
Created by	Jonathan Labrie			Name	Bearing Housing Assembly	
Date	10/13/2014					
Material	Al 6061 T6			Part #	HHTS-001	
Document Rev.	A			Qty	4	
OP #	Operation	Accept	Pending	NCR #	Completed Date	Initial
10	Assembly, Bearings					
	Part #	Part Name		Qty		
	HTTS-001-001	Bearing Housing		4		
	HTTS-001-003	Roller Bearing		8		
	HTTS-001-003	Thrust Bearing		4		
	HTTS-001-003	Bearing Washer		12		
OP #	Operation	Accept	Pending	NCR #	Release Date	Initial
20	Assembly, Control					
	Part #	Part Name		Qty		
	HTTS-001-002	Control Arm		4		
	HTTS-001-006	#4-40, 3/4"		8		
	HTTS-001-007	Ball Linkage		4		
	HTTS-001-008	Expoxy Bond Coat		A/R		
OP #	Operation	Accept	Pending	NCR #	Release Date	Initial
30	QA RELEASE					
Notes						

Helicopter Hover Test Stand 2015: Manufacturing Plan						
Created by	Jonathan Labrie			Name	Bearing Housing	
Date	10/28/2014					
Material	Al 6061 T6			Part #	HHTS-001-001	
Stock	2.5" OD x 24"					
Document Rev.	A			Qty	1	
OP #	Operation	Accept	Pending	NCR #	Completed Date	Initial
10	Manual Lathe	5	0	-	10/31/2014	JPL
OP #	Operation	Accept	Pending	NCR #	Completed Date	Initial
20	Manual Lathe	5	0	-	10/31/2014	JPL
OP #	Operation	Accept	Pending	NCR #	Completed Date	Initial
30	CNC Mill	5	0	-	11/12/2014	JPLJ
OP #	Operation	Accept	Pending	NCR #	Completed Date	Initial
40	CNC Mill					
OP #	Operation	Accept	Pending	NCR #	Completed Date	Initial
50	Tapping					
OP #	Operation	Accept	Pending	NCR #	Completed Date	Initial
60	Deburring/Finishing					
OP #	Operation	Accept	Pending	NCR #	Completed Date	Initial
70	Component					
Notes						

Manufacturing Operation Sheets

Helicopter Hover Test Stand 2015: Operation Sheet			OP# 10 Manual Lathe
Created by	Jonathan Labrie	Name	Bearing Housing
Date	10/26/2014		
Material	Al 6061 T6	Part #	HHTS-001-001
Stock	2.25 Dia. x 24"		
Part Rev.	A	Machine	Manual Lathe (Chuck)

Manually turn OD, Drill thru, Bore pocket, cutoff

Tool #	Description	Notes
-	OD turning insert	Face end, Finish OD
-	Spot drill	Spot .500 hole
-	1/2" Drill	Drill Thru
-	7/8" SQ EndMill	Bore .875 diameter .600 deep
-	Cut off tool	Cut part to rough length

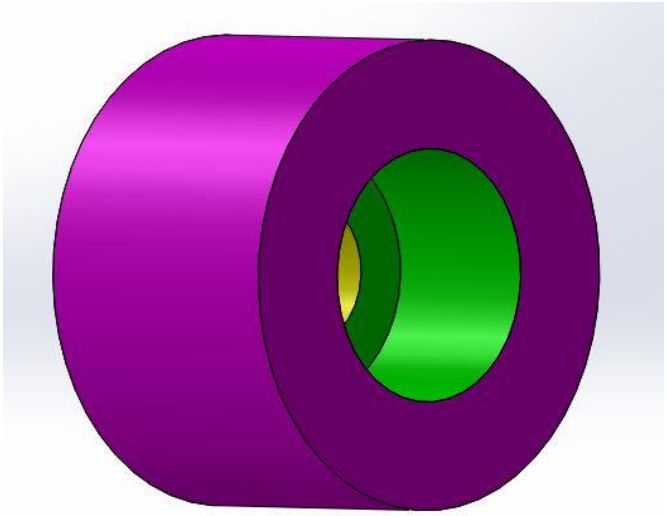

Notes	

Helicopter Hover Test Stand 2015: Operation Sheet			OP# 20 Manual Lathe
Created by	Jonathan Labrie	Name	Bearing Housing
Date	10/26/2014		
Material	Al 6061 T6	Part #	HHTS-001-001
Stock	In Process		
Part Rev.	A	Machine	Manual Lathe (Chuck)

Manually face end, Bore pocket.

Tool #	Description	Notes
-	OD turning insert	Face end, Finish OD
-	7/8" SQ EndMill	Bore .875 diameter .300 deep

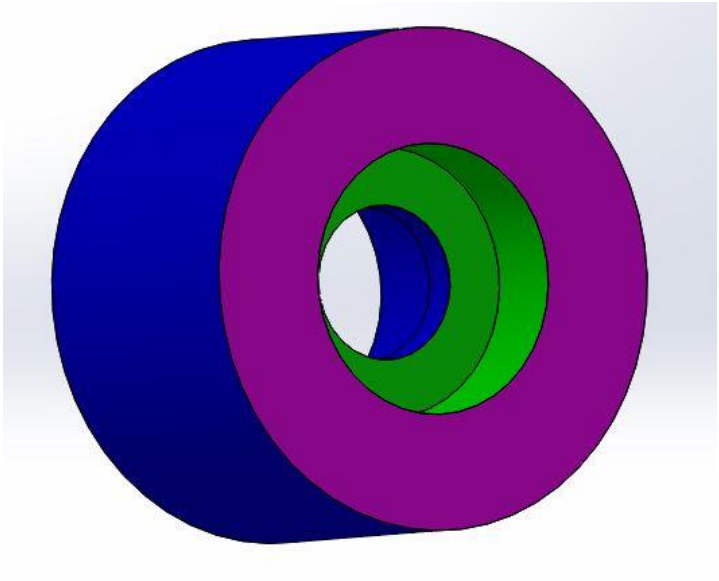

Notes	

Helicopter Hover Test Stand 2015: Operation Sheet			OP# 30 Manual Mill
Created by	Jonathan Labrie	Name	Bearing Housing
Date	10/31/2014		
Material	Al 6061 T6	Part #	HHTS-001-001
Stock	In Process		
Part Rev.	A	Machine	Manual Mill

Program number	O3014	Programmed by	Jonathan Labrie
Work coordinate	G54	File Name	HHTS-001-001 OP 30.esp
Set up	Set origin x center, y positive, z0 Top. Deep bore toward y negative		

Tool #	Description	min LOC	min OOH	Comp	Notes
1	3/8" Drill Mill, 90 deg, 2 fl	0.18	1.00	yes	Spot Holes, 8 places
2	#43 Drill (.089)	1.25	2.00	no	Drill for 4-40 tap, 8 places
3	3/8 SQ End Mill	0.5	1.00	yes	Mill flat

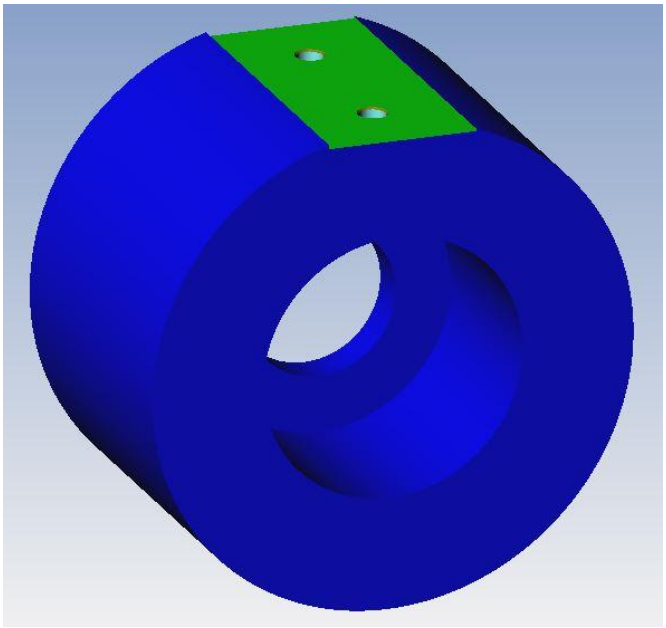

Notes	

Helicopter Hover Test Stand 2015: Operation Sheet			OP# 40 CNC Mill
Created by	Jonathan Labrie	Name	Bearing Housing
Date	10/31/2014		
Material	Al 6061 T6	Part #	HHTS-001-001
Stock	In Process		
Part Rev.	A	Machine	Haas MiniMill

Program number	O3015	Programmed by	Jonathan Labrie
Work coordinate	G54	File Name	HHTS-001-001 OP 40.esp
Set up	Set origin x y center, z0 Top. Hold with flat facing y positive. Will tap manually in OP#50		

Tool #	Description	min LOC	min OOH	Comp	Notes
1	3/8" Drill Mill, 90 deg, 2 fl	0.18	1.00	yes	Spot Holes, 8 places
2	#43 Drill (.089)	1.25	2.00	no	Drill for 4-40 tap, 8 places

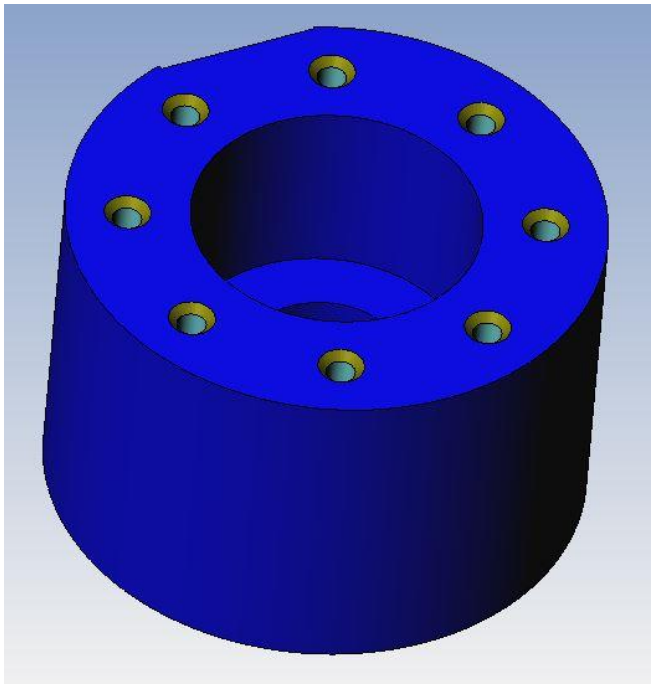

Notes	

Appendix C

Operation Manual

Safety

Operator Requirements:

If proper precaution and preventative safety measures are not taken, this device may cause serious injury or death. Any operator of the device must meet the following criteria:

1. Must have read and understood the operator manual
2. Must wear safety glasses
3. Must have completed operator checklist before operation

Operator Responsibilities:

1. Follow and enforce all safety procedures and precautions
2. Contact WPI campus police/EMS immediately in the event of any serious injury
3. Leave the device in a safe, secure, and unpowered situation when leaving the device unattended

Second user:

A second person must accompany the operator whenever power to the Helicopter Hover Test Stand is turned on. This second person must meet the following criteria:

1. Must give a verbal exchange that they are the second for the operator
2. Must remain in sight of the Helicopter Hover Test Stand at all times
3. Must read and understood the Helicopter Hover Test Stand operator manual
4. Must wear safety glasses

Structural Safety Inspection

Without taking proper safety precautions, operation of this device may cause serious injury or death. The structural integrity of the system plays a large role in the system. Should a component fail, it may eject itself at high speed, possibly causing serious injury. Any such failure may also cause a large imbalance of the rotating system, leading to catastrophic damage. The Structural Safety Inspection is designed to detect and prevent serious structural failures and deficiencies. IMPORTANT: Ensure that power to the test stand has been disconnected before inspection.

In order to ensure safe operation inspect the following items BEFORE EACH USE:

1. Blades
    a. Inspect for cracks or damage
    b. Ensure proper installation in blade grip
2. Rotor Hub
    a. Pins are installed correctly and secured with lock wire
    b. Hinges move freely and are clear of obstructions
3. Drive shaft
    a. Inspect for cracks or other damage
    b. Position of nut on top of rotor hub
4. Safety Enclosure
    a. Inspect for cracks or other damage
    b. Ensure proper installation, no gaps or holes

In order to ensure safe operation inspect the following items once per academic quarter:

1. Warnings and labels
    a. All warnings and labels have not been removed, are intact and legible
2. Drive system
    a. Belt is correctly tensioned
    b. Belt is not cracked or hardened
    c. Motor fan is clear of dust and debris
3. Frame and support
    a. Stand welds are intact with no cracks
    b. Drive shaft support bearings spin freely
    c. Frame is level and base has not shifted
4. Electrical
    a. Wiring is properly shielded: no cuts or abrasions in protective coverings
    b. Variable frequency drive is clear of dust and debris

Appendix D

Stress Concentration Graphs

Stress concentration factor graphs are used for the calculation of the stress on the drive shaft base fillet. The following graphs are taken from Peterson's Stress Concentration Factors, Second Edition. Walter D. Pilkey, 1997, John Wiley & Sons, Inc., New York, pgs 157, 164, 166, 168.

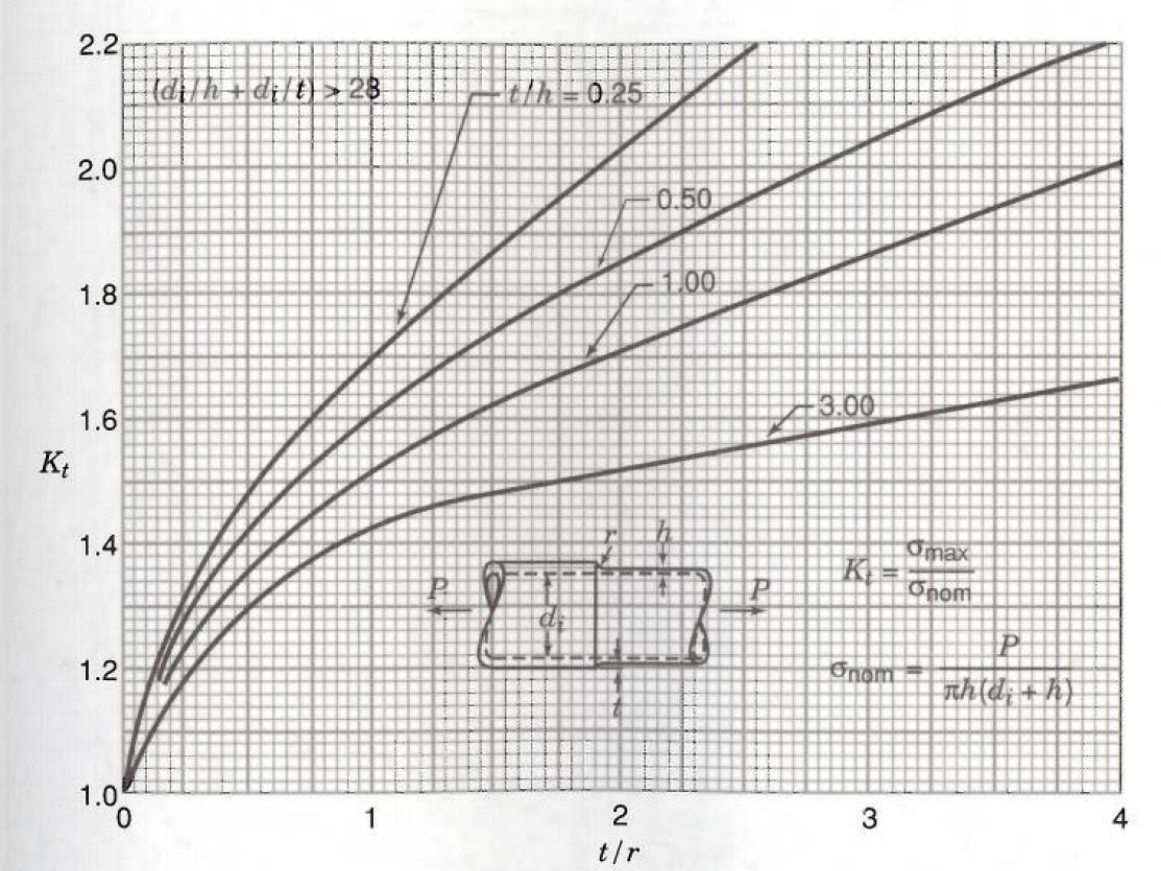

Chart 3.5 Stress concentration factors K_t for a tube in tension with fillet (Lee and Ades 1956; ESDU 1981).

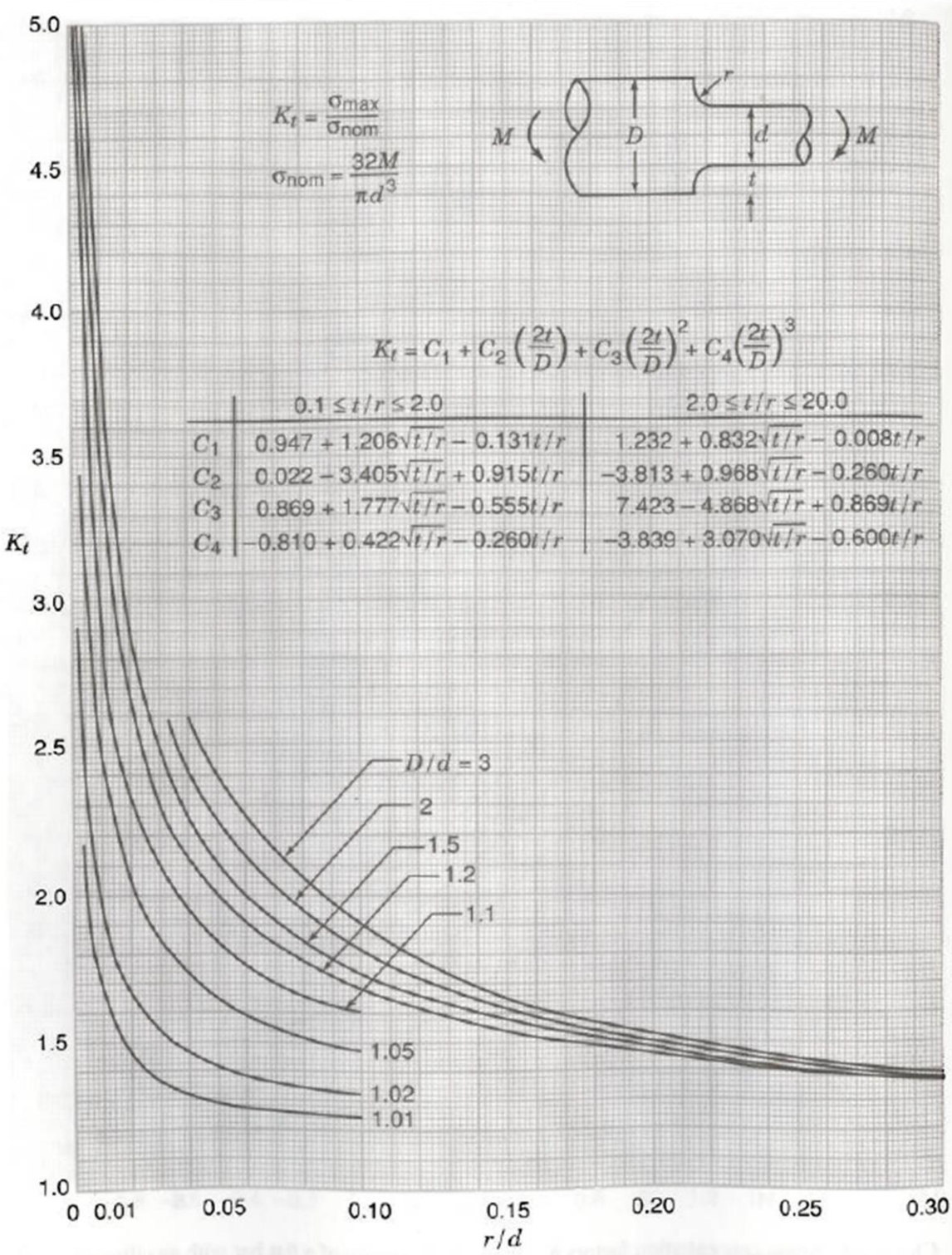

Chart 3.10 Stress concentration factors K_t for bending of a stepped bar of circular cross section with a shoulder fillet (based on photoelastic tests of Leven and Hartman 1951; Wilson and White 1973).

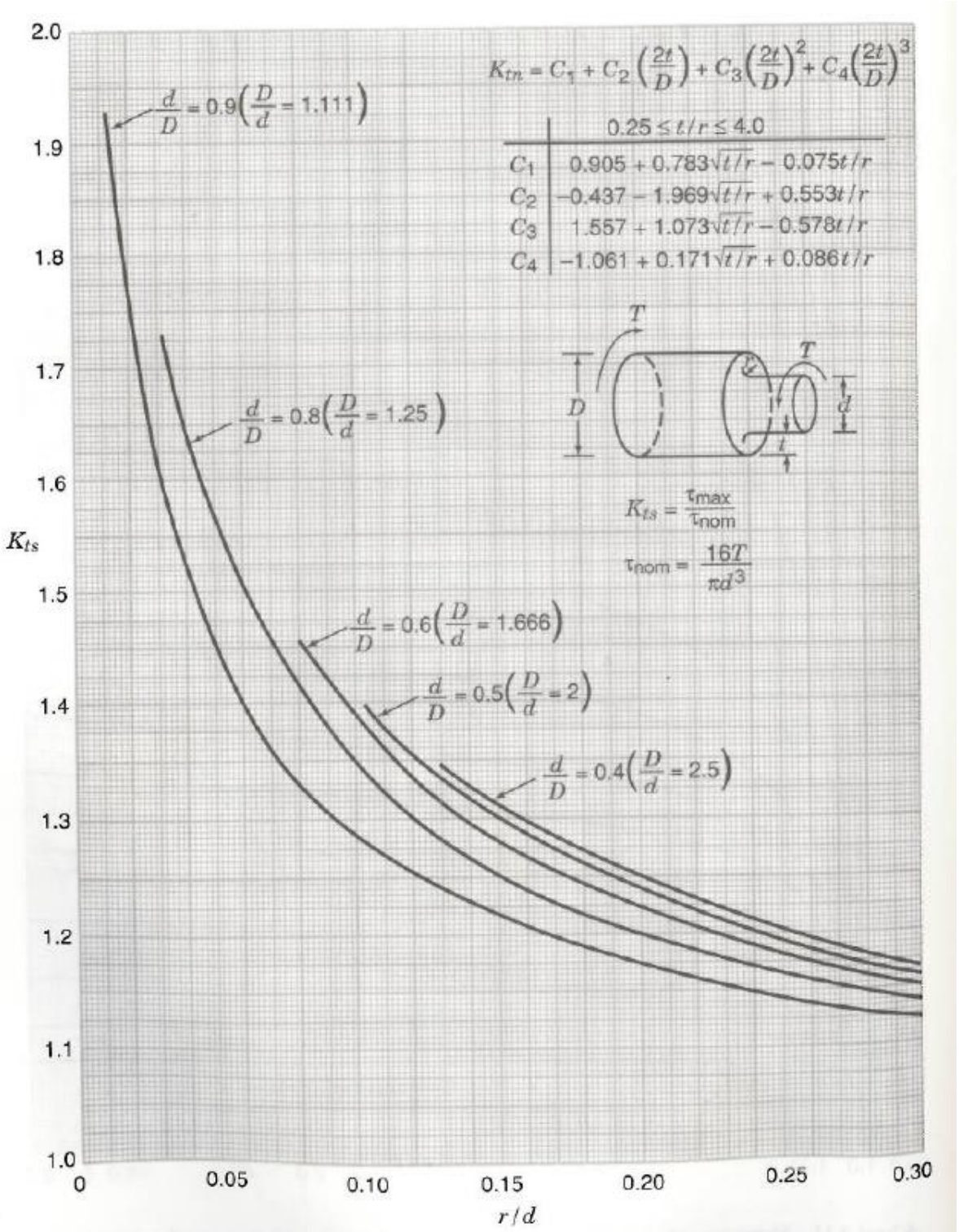

Chart 3.12 Stress concentration factors K_{ts} for torsion of a shaft with a shoulder fillet (data from Matthews and Hooke 1971).

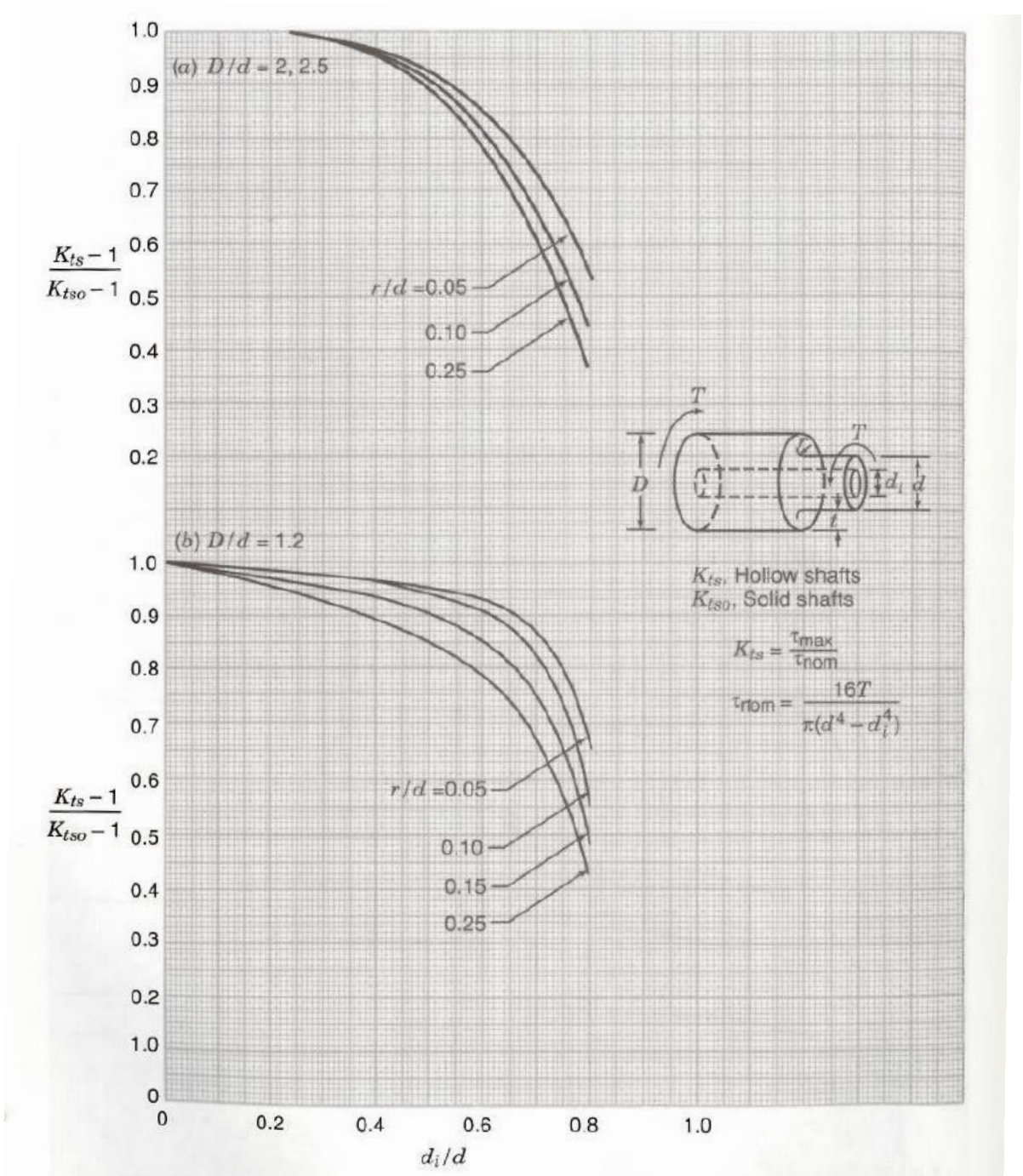

Chart 3.14 Effect of axial hole on stress concentration factors of a torsion shaft with a shoulder fillet (from data of Rushton 1964). (*a*) $D/d = 2, 2.5$; (*b*) $D/d = 1.2$.

1.2

Appendix E

Power Calculation using Momentum Theory

```
% NACA 0012 Airfoil

clc, clear all, close all

% Blade characteristics
R = 0.6;     % rotor radius, m
er = 0.1211;   % dist from axis to blade, m
c = 0.06;    % chord length, m

% Constants (NACA 0012 Airfoil)
alpha_max = 12           ;% Degrees
Cl_al_max = 2*pi*alpha_max*pi/180 ;% Coefficient of lift at max alpha
C_d    = 0.02          ;% Blade drag coefficient at zero lift
k     = 1.25          ;% Induced power factor (1.15-1.25)
rho    = 1.2           ;% Flow density, kg/m^3

% Design Parameters
V = 1250;    %RPM
N = 4;      %number of blades

% Efficiencies
EF_sys = .95;
```

Calculations

```
sigma = (N.*(R-er).*c)/(pi.*(R^2)); %rotor solidarity
A = (pi.*R^2)           ; %disk area, m^2
ohm = V.*(2.*pi)/60        ; %angular velocity, rad/s

% Thrust calculations

Lpb = 0.5*rho*Cl_al_max*ohm^2*c*(1/4*(R^4-er^4)-1/3*er*(R^3-er^3));

T_tot = N*Lpb           ; %total thrust, N

Watts = ((k.*T_tot.^(3/2))/sqrt(2.*rho.*A) + rho.*A.*((ohm.*R).^3).*(.125.*sigma.*C_d)); %watts
Ideal_Horsepower = Watts/746;

%Efficiency Losses
Min_Horsepower = Ideal_Horsepower/EF_sys;


disp('Ideal Horsepower')
disp(Ideal_Horsepower)
```

```
disp('Minimum Horsepower')
disp(Min_Horsepower)
```

```
Ideal Horsepower
  0.9104

Minimum Horsepower
  0.9584
```

Published with MATLAB® R2014a

Matlab Code for Calculating Stress on Rotor Hub

```
clc, clear, close
```

Stress and Strain on Helicopter Test Stand

Setting Parameters

Setting Material Parameters

```
tens_al       = 255e6;              % MPa
shear_al      = 131e6;              % MPa
tens_steel    = 248e6;              % MPa
shear_steel   = .6*tens_steel;      % MPa

 % Rotor Head Parameters %

Rpms    = 1500;             % rev/min
disp('Rpms'), disp(Rpms)
Omega   = Rpms*(2*pi/60);   %rads/s
r       = .6;               % m
er_flap = 0.028575;         % m
er_lead = .1127;            % m
m_blade = .200;             % Kg
m_flap  = .234;             % Kg
```

```
Rpms
        1500
```

Calculating Forces

Calculating Lift Force

```
L = (5*9.81)/4;                                     % Newtons
disp('Lift Force in Newtons'), disp(L)

 % Calculating Centrpital Force %
Fcf_fh = .5*(m_flap+m_blade)*Omega^2*(r^2-er_flap^2); % Newtons
disp('Centripital Force at Flapping Hinge in Newtons'), disp(Fcf_fh)

Fcf_blade = .5*(m_blade)*Omega^2*(r^2-.06);

 % Coning Angle %
 betao = 2;                                         % degrees
```

```
Lift Force in Newtons
   12.2625
```

```
Centripital Force at Flapping Hinge in Newtons
   1.9232e+03
```

Calculating force on the flapping hinge

Force on HHTS-003-002

```
 Fmax_HHTS_003_002 = 2*pi*(0.003175^2)*shear_steel;
    disp('Max force on HHTS-003-002 in Newtons'), disp(Fmax_HHTS_003_002)
 F_on_HHTS_003_002 = sqrt(Fcf_fh^2+L^2);
    disp('Force on HHTS-003-002 in Newtons'), disp(F_on_HHTS_003_002)
 SF_HHTS_003_002 = Fmax_HHTS_003_002/F_on_HHTS_003_002;
    % disp('Safety factor for HHTS-003-002'), disp(SF_HHTS_003_002)

 % Force on HHTS-003-001
 Fmax_HHTS_003_001 = 2*tens_al*.00635*.01016;
    disp('Max force on HHTS-003-001 in Newtons'), disp(Fmax_HHTS_003_001)
 F_on_HHTS_003_001 = F_on_HHTS_003_002;
   % disp('Force on HHTS-003-001 in Newtons'), disp(F_on_HHTS_003_001)
 SF_HHTS_003_001 = Fmax_HHTS_003_001/F_on_HHTS_003_001;
   % disp('Safety factor for HHTS-003-001'), disp(SF_HHTS_003_001)

% Force on HHTS-002-001 at HHTS-003-002
Fmax_HHTS_002_001 = tens_al*.003175*.0127;
    disp('Max force on HHTS-002-001 in Newtons'), disp(Fmax_HHTS_002_001)
F_on_HHTS_002_001 = F_on_HHTS_003_002;
   % disp('Force on HHTS-002-001 in Newtons at HHTS-003-002'), disp(F_on_HHTS_002_001)
SF_HHTS_002_001 = Fmax_HHTS_002_001/F_on_HHTS_002_001;
   % disp('Safety factor for HHTS-002-001 at HHTS-003-002'), disp(SF_HHTS_002_001)
```

```
Max force on HHTS-003-002 in Newtons
   9.4248e+03

Force on HHTS-003-002 in Newtons
   1.9232e+03

Max force on HHTS-003-001 in Newtons
   3.2903e+04

Max force on HHTS-002-001 in Newtons
   1.0282e+04
```

Calculating Force on HHTS_002_006

Force on HHTS-002-006

```
Fmax_HHTS_002_006 = tens_steel*2*pi*.00198^2;
    disp('Max force on HHTS-002-006 in Newtons'), disp(Fmax_HHTS_002_006)
F_on_HHTS_002_006 = F_on_HHTS_003_002;
   % disp('Force on HHTS-002-006 in Newtons'), disp(F_on_HHTS_002_006)
```

```
SF_HHTS_002_006 = Fmax_HHTS_002_006/F_on_HHTS_002_006;
   % disp('Safety factor for HHTS-002-006'), disp(SF_HHTS_002_006)

 % Force on HHTS_002_003 at pin hole
Fmax_HHTS_002_003_atpinhole = tens_steel*2*.00198*.0095;
    disp('Max Force on HHTS-002-003 at HHTS-002-006'), disp(Fmax_HHTS_002_003_atpinhole)
F_on_HHTS_002_003_atpinhole = F_on_HHTS_003_002;
   % disp('Force on HHTS-002-003 at HHTS-002-006'), disp(F_on_HHTS_002_003_atpinhole)
SF_HHTS_002_003_atpinhole = Fmax_HHTS_002_003_atpinhole/F_on_HHTS_002_003_atpinhole;
   % disp('Safety factor for HHTS-002-003 at HHTS-002-006'), disp(SF_HHTS_002_003_atpinhole)

 % Force on HHTS-002-001 at HHTS-002-006
Fmax_HHTS_002_001_atpinhole = tens_al*2*.00198*.00476*2;
    disp('Max Force on HHTS-002-001 at HHTS-002-006'), disp(Fmax_HHTS_002_001_atpinhole)
F_on_HHTS_002_001_atpinhole = F_on_HHTS_003_002;
   %  disp('Force on HHTS-002-001 at HHTS-002-006'), disp(F_on_HHTS_002_001_atpinhole)
SF_HHTS_002_001_atpinhole = Fmax_HHTS_002_001_atpinhole/F_on_HHTS_002_001_atpinhole;
   % disp('Safety factor for HHTS-002-001 at HHTS-002-006'), disp(SF_HHTS_002_001_atpinhole)

 % Force on HHTS-002-003 at head
Fmax_HHTS_002_003_athead = 7.1255e-5*tens_steel;
    disp('Max Force on HHTS-002-002 at its head'), disp(Fmax_HHTS_002_003_athead)
F_on_HHTS_002_003_athead = F_on_HHTS_003_002;
   % disp('Force on HHTS-002-003 at at its head'), disp(F_on_HHTS_002_003_athead)
SF_HHTS_002_003_athead = Fmax_HHTS_002_003_athead/F_on_HHTS_002_003_athead;
   % disp('Safety factor for HHTS-002-003 at its head'), disp(SF_HHTS_002_003_athead)
```

```
Max force on HHTS-002-006 in Newtons
   6.1089e+03
Max Force on HHTS-002-003 at HHTS-002-006
   9.3298e+03
Max Force on HHTS-002-001 at HHTS-002-006
  9.6133e+03
Max Force on HHTS-002-002 at its head
  1.7671e+04
```

Calculating Force on HHTS-001-006 at HTTS-002-002

Force on HHTS-001-006

```
Fmax_HHTS_001_006 = tens_steel*8*.1257/(100*100);
    disp('Max Force on HHTS-001-006 at HHTS-002-002'), disp(Fmax_HHTS_001_006)
F_on_HHTS_001_006 = F_on_HHTS_003_002;
   % disp('Force on HHTS-001-006 at HHTS-002-002'), disp(F_on_HHTS_001_006)
SF_HHTS_001_006 = Fmax_HHTS_001_006/F_on_HHTS_001_006;
   % disp('Safety factor for HHTS-001-006 at HHTS-002-002'), disp(SF_HHTS_001_006)

 % Force HHTS-002-002 at 001
Fmax_HHTS_002_002_at001 = 8*tens_al*.00556*.00635;
     disp('Max Force on HHTS-002-002 at HHTS-001-006'), disp(Fmax_HHTS_002_002_at001)
F_on_HHTS_002_002_at001 = F_on_HHTS_003_002;
```

```
   % disp('Force on HHTS-002-002 at HHTS-001-006'), disp(F_on_HHTS_002_002_at001)
SF_HHTS_002_002_at001 = Fmax_HHTS_002_002_at001/F_on_HHTS_002_002_at001;
   % disp('Safety factor for HHTS-002-002 at HHTS-001-006'), disp(SF_HHTS_002_002_at001)
```

```
Max Force on HHTS-001-006 at HHTS-002-002
   2.4939e+04

Max Force on HHTS-002-002 at HHTS-001-006
   7.2024e+04
```

Calculating interior Shear on HHTS-001-001

Force on HHTS-001-001

```
Fmax_HHTS_001_001 = .02223*.00318*shear_al;
    disp('Max Force on interior HHTS-001-001'), disp(Fmax_HHTS_001_001)
F_on_HHTS_001_001 = F_on_HHTS_003_002;
   % disp('Force on HHTS-001-001'), disp(F_on_HHTS_001_001)
SF_HHTS_001_001 = Fmax_HHTS_001_001/F_on_HHTS_001_001;
    %disp('Safety factor for HHTS-001-001'), disp(SF_HHTS_001_001)
```

```
Max Force on interior HHTS-001-001
  9.2606e+03
```

Calculating Forces on blade root pin

Force on Blade root pin

```
Fmax_Bladeroot_pin = (.0028/2)^2*pi*shear_steel*2;
    disp('Max Force on Blade Root Pin'), disp(Fmax_Bladeroot_pin)
F_Bladeroot_pin = Fcf_blade*cosd(betao)+L*sind(betao);
   % disp('Force on Blade Root Pin'), disp(F_Bladeroot_pin)
SF_Bladeroot_pin = Fmax_Bladeroot_pin/F_Bladeroot_pin;
    %disp('Safety factor for Blade Root Pin'), disp(SF_Bladeroot_pin)

 % Force on Blade grip pin hole
Fmax_Bladegrip_hole = 2*.0064*.0028*tens_al;
    disp('Max Force on Blade Grip Hole'), disp(Fmax_Bladegrip_hole)
F_Bladegrip_hole = F_on_HHTS_003_002;
   % disp('Force on Blade Grip Hole'), disp(F_Bladegrip_hole)
SF_Bladegrip_hole = Fmax_Bladegrip_hole/F_Bladegrip_hole;
   % disp('Safety factor for Blade Grip Hole'), disp(SF_Bladegrip_hole)
```

```
Max Force on Blade Root Pin
   1.8325e+03
Max Force on Blade Grip Hole
   9.1392e+03
```

Published with MATLAB® R2014a

Matlab Code for Calculating Torsion on the Shaft

```
%Matlab Code for Calculating Torsion on the Shaft
clear, close, clc

Read_Graphs_Torsion = 'no' ;
Read_Graphs_Tension = 'no' ;
Read_Graphs_Bending = 'no' ;

Display_Fatigue_Calculations = 'yes';
```

Calculating torsion on the shaft

Input Parameters

```
c1     = .009525;   % m, ID of drive shaft
c0     = .01905;    % m, OD of drive shaft
T      = 15;      % Nm, Torque generted by motor
r      = .003175;   % m, Off set distance of CG
M      = 5;      % Kg, Mass of rotor head
omega_RPM  = 1500;     % Rpm
L      = .2286;    % m, distance from shaft point to rotor head, 9in
F_Lift   = 76.9;     % N, Total lift
beta    = 3*pi/180;   % rad, coning angle

rad     = .00635    ;% radius of stress concentration fillet, m
D      = .030     ;% diameter of lower drive shaft, m
d      = 2*c0      ;
d_i     = 2*c1      ;
t      = (D-d)/2    ;% edge to edge, m
```

Direct Torsion due to Engine Torque

```
output_K_ts = Stress_concentration_torsion(D, d, d_i, rad, Read_Graphs_Torsion);
K_ts = output_K_ts(1);

J        = pi/2*(c0^4-c1^4);
tau_max     = (T*c0)/J;
tau_maxMPa   = tau_max/10^6;
tau_maxMPa_conc = tau_maxMPa*K_ts;
```

Stress due to Rotor Imbalance

```
output_K_tb = Stress_concentration_bending(D, d, rad, Read_Graphs_Bending);
K_t_bending = output_K_tb(1);

omega_RADS   = omega_RPM*2*pi/60;
V        = omega_RADS*r;
Fcent      = M*V^2/r;
Mimb      = Fcent*L;
S_imb      = Mimb*c0/J;
S_imbMPa    = S_imb/10^6;
S_imbMPa_conc  = S_imbMPa*K_t_bending;
```

Stress due to Lift Dissymmetry

```
output_K_t = Stress_concentration_tension(D, d, d_i, rad, Read_Graphs_Tension);
K_t_tension = output_K_t(1);

F_Liftz       = F_Lift*cos(beta);
M_Liftx       = F_Lift*sin(beta)*L;
A          = pi*(c0^2-c1^2);
S_Liftmax      = M_Liftx*c0/J;
S_LiftmaxMPa    = S_Liftmax/10^6;
S_LiftmaxMPa_conc  = S_LiftmaxMPa*K_t_bending;

S_Liftz     = F_Liftz/A;
S_LiftzMPa   = S_Liftz/10^6;
S_LiftzMPa_conc = S_LiftzMPa*K_t_tension;
```

Overall Stress

```
S_Max = S_imbMPa_conc + S_LiftzMPa_conc + S_LiftmaxMPa_conc;
S_Min = S_imbMPa_conc + S_LiftzMPa_conc - S_LiftmaxMPa_conc;

SzMax      = S_Max;
SzMin      = S_Min;
Sy       = 0;
tauyz      = tau_maxMPa_conc;

Princ_Max    = (SzMax+Sy)/2+sqrt(((SzMax-Sy)/2)^2+tauyz);
Princ_Min    = (SzMin+Sy)/2+sqrt(((SzMin-Sy)/2)^2+tauyz);

tau_max_in_plane = sqrt(((SzMax/2)^2)-tauyz);

S_rest      = -((M*9.8)/A)*10^-6;
```

Overall

```
clc
disp('Max Torsion due to motor torque in (MPa)'), disp(tau_maxMPa_conc)

disp('Stress due to imbalance on rotor head (MPa)'), disp(S_imbMPa_conc)

disp('Stress in x direction due to lift disymmetry (MPa)'), disp(S_LiftmaxMPa_conc)
disp('Stress in z direction due to lift disymmetry (MPa)'), disp(S_LiftzMPa_conc)

disp('Tau_max_in_plane'), disp(tau_max_in_plane)

disp('Total Max Stress (MPa)'), disp(Princ_Max)
disp('Total Min Stress (MPa)'), disp(Princ_Min)

%Fatigue Calcualations

if strcmp(Display_Fatigue_Calculations,'yes')
  Mean_Stress   = (Princ_Max+Princ_Min)/2;
  disp('Mean Stress (MPa)'), disp(Mean_Stress)

  Stress_Amp   = (Princ_Max-Princ_Min)/2;
  disp('Stress Amplitude (MPa)'), disp(Stress_Amp)

  Stress_Amp_start_stop   = (Mean_Stress-S_rest)/2;
  disp('Stress Amplitude Start/Stop(MPa)'), disp(Stress_Amp_start_stop)

  Stress_range = Princ_Max-Princ_Min;
  disp('Stress_range'), disp(Stress_range)

  Stress_ratio = Princ_Min/Princ_Max;
  disp('Stress_ratio'), disp(Stress_ratio)

  Stress_range_start_stop = Mean_Stress-S_rest;
  disp('Stress_range_start_stop'), disp(Stress_range_start_stop)

  Stress_ratio_start_stop = S_rest/Mean_Stress;
  disp('Stress_ratio_start_stop'), disp(Stress_ratio_start_stop)
end
```

```
Max Torsion due to motor torque in (MPa)
  1.6119

Stress due to imbalance on rotor head (MPa)
  11.4340

Stress in x direction due to lift disymmetry (MPa)
  0.1175

Stress in z direction due to lift disymmetry (MPa)
  0.1347
```

```
Tau_max_in_plane
  5.7035

Total Max Stress (MPa)
  11.8225

Total Min Stress (MPa)
  11.5903

Mean Stress (MPa)
  11.7064

Stress Amplitude (MPa)
  0.1161

Stress Amplitude Start/Stop(MPa)
  5.8818

Stress_range
  0.2322

Stress_ratio
  0.9804

Stress_range_start_stop
  11.7637

Stress_ratio_start_stop
  -0.0049
```

Published with MATLAB® R2014a

Torsion Stress Concentration at base fillet of small drive shaft section

```
function [output_K_ts] = Stress_concentration_torsion(D, d, d_i, rad, Read_Graphs_Torsion)
```

```
% Find K_tso
Graph_read_1 = D/d;
Graph_read_2 = rad/d;

if strcmp(Read_Graphs_Torsion, 'yes')
  disp('------  Values for  ------')
  disp('------  Chart 3.12  ------')
  disp('D/d')
  disp(Graph_read_1)
  disp('r/d')
  disp(Graph_read_2)
  disp('------  Read K_ts   ------')
  disp('------  Chart 3.12  ------')
  K_tso = input('K_ts  =  ');
```

```
else
  K_tso = 1.1  ;
end

% Find K_ts
clc
Graph_read_1 = D/d;
Graph_read_2 = rad/d;
Graph_read_3 = d_i/d;

if strcmp(Read_Graphs_Torsion, 'yes')
  disp('------  Values for  ------')
  disp('------  Chart 3.14  ------')
  disp('D/d')
  disp(Graph_read_1)
  disp('r/d')
  disp(Graph_read_2)
  disp('d_i/d')
  disp(Graph_read_3)
  disp('--  Read K_ts-1/K_tso-1 --')
  disp('------  Chart 3.14  ------')
  K_tso_1__K_tso_1 = input('K_ts-1/K_tso-1  =  ');

else
  K_tso_1__K_tso_1 = .94  ;
end
```

Final Calculation and Output

```
K_ts = K_tso_1__K_tso_1*(K_tso-1)+1;
output_K_ts = K_ts;

end
```

Published with MATLAB® R2014a

Tension Stress Concentration at base fillet of small drive shaft section

```
function [output_K_ts] = Stress_concentration_tension(D, d, d_i, rad, Read_Graphs_Tension)

% Find K_t
t = (D-d)/2;
h = (d-d_i)/2;
Graph_read_1 = t/h;
Graph_read_2 = t/rad;

if strcmp(Read_Graphs_Tension, 'yes')
  disp('------  Values for  ------')
  disp('------  Chart 3.5  ------')
  disp('t/h')
```

```
  disp(Graph_read_1)
  disp('t/r')
  disp(Graph_read_2)
  disp('------  Read K_t   ------')
  disp('------  Chart 3.5  ------')
  K_t_tension = input('K_ts  =  ');

else
  K_t_tension = 1.5  ;
end
```

Final Calculation and Output

```
output_K_ts = K_t_tension;

end
```

Published with MATLAB® R2014a

Bending Stress Concentration at base fillet of small drive shaft section

```
function [output_K_tb] = Stress_concentration_bending(D, d, rad, Read_Graphs_Bending)

% Find K_tso
Graph_read_1 = D/d;
Graph_read_2 = rad/d;

if strcmp(Read_Graphs_Bending, 'yes')
  disp('------  Values for  ------')
  disp('------  Chart 3.10  ------')
  disp('D/d')
  disp(Graph_read_1)
  disp('r/d')
  disp(Graph_read_2)
  disp('------  Read K_ts   ------')
  disp('------  Chart 3.10  ------')
  K_t_bending = input('K_ts  =  ');

else
  K_t_bending = 1.3  ;
end

% Area Correction
```

Final Calculation and Output

```
output_K_tb = K_t_bending;

end
```

Published with MATLAB® R2014a

Appendix F

Budget Sheet for the Helicopter Hover Test Stand					
Date of Purchase	**Items Purchased**	**Company**	**Order Number**	**Price**	**Balance**
				Budget	$480.00
10/29/2014	Roller Bearings, Thrust Bearings, Feathering Spindle Clevis Pin, Flapping Hinge Clevis Pin	McMaster-Carr	01	$65.32	$414.68
11/6/2014	Swashplate, Follower Arms	Heli-World	02	$73.06	$341.62
2/23/2015	Retaining Ring Scews	MSC	03	$3.28	$338.34
2/17/2015	Spherical Bearing, Jesus Nut, Ball Links	McMaster-Carr	04	$87.42	$250.92
2/27/2015	Threaded Control Rod, Control Arm Screws	MSc	05	$11.84	$239.08
				Budget Remaining	$239.08